PREPARATION, STRUCTURE, AND PROPERTIES OF ADVANCED POLYMER COMPOSITES WITH LONG FIBERS AND NANOPARTICLES

DISSERTATION

Presented in Partial Fulfillment of the Requirements for
the Degree of Doctor of Philosophy in
the Graduate School of The Ohio State University

By
Gang Zhou, M.S.

* * * * *

The Ohio State University
2007

Dissertation Committee:

Professor L. James Lee, Advisor

Professor Kurt W. Koelling

Professor Jose M. Castro

Approved by

_____
Advisor

Graduate Program in Chemical Engineering

ABSTRACT

Fiber-reinforced plastics have been widely used in many civil and military applications. In this research, the relationship of processing, structure, and property of carbon or glass fiber reinforced epoxy composites were studied. It is found that humidity has great impacts on the glass transition temperature, resin viscosity, curing kinetics, and tack property of epoxy prepregs, which may significantly affect the processing and the structure of products. The mechanism of marcel formation (fiber buckling) during compression molding was also investigated. Based on the experimental data, a statistic model was build to estimate the marcel size in the epoxy composites. The model can be also used to determine the proper processing parameters, such as mold temperature and pressure rate, to eliminate the fiber waviness. In addition, the ultrasonic consolidation of epoxy prepregs was compared with ordinary vacuum debulking at room temperature or high temperature. The results shows the ultrasonic consolidation is a promising method to lower the void content in the composites, and may replace the common debulking process in production.

Polymer nanocomposites have become one of the frontiers of materials sciences since the 1990s. In this study, epoxy, phenolic, and unsaturated polyester nanocomposites were prepared. Mechanical, thermal, and/or barrier properties of these nanocomposites

were compared to neat resins. It is found that the addition of nanoparticles, such as nanoclays or carbon nanofibers, into polymer matrix can improve the strength and modulus, enhance the thermal stability, and lower the water absorption rate. Furthermore, great efforts have been made to combine the advantages of both fiber-reinforced plastics and polymer nanocomposites to produce a superior composite: long fibers and nanoparticles reinforced polymer composites. According to the characteristics of different polymer resins (epoxy, phenolic, and unsaturated polyester resins) and long fibers (glass or carbon fibers), several processes were selected to prepare various hybrid composites, such as compression molding and vacuum assisted resin transfer molding. The mechanical and thermal properties of these long fiber-nanoparticle reinforced composites were also measured. The significant improvement of these properties can be attributed to the synergic effects of long fiber and nanoparticles. In addition, nanoparticles brought some other properties to polymer materials, such as enhanced barrier properties.

Dedicated to My Dear Parents

ACKNOWLEDGMENTS

First, I would like to thank my advisor, Professor L. James Lee, for his guidance, discussions, supports, and encouragements throughout my study at the Ohio State University.

I would also like to acknowledge Professor Kurt Koelling and Professor Jose Castro for serving on my dissertation committee and their invaluable comments and suggestions.

I am grateful for Dr. Paula Stevenson, Mrs. Alice Shi, and Mrs. Martha Leming. They gave me lots of help and support when I was doing research in Center for Advanced Polymer and Composite Engineering.

I am also grateful for the help from Dr. Hongyan He, Dr. Shengnian Wang, Dr. Xia Cao, Siva Movva, Dante Guerra, and all the other members in Dr. Lee's group.

Finally, I wish to thank my dear parents and sister for their constant support on my study and endless care in my life. I also want to express my great appreciations to my wife, Chuan Chen, for her love, accompany, encouragement, and support.

VITA

January 1974	Born in Beijing, P. R. CHINA
July 1997	B. E. in Polymer Sciences and Chemical Engineering, Tsinghua University, Beijing, P. R. CHINA
July 2000	M. S. in Polymer Chemistry and Physics, Institute of Chemistry, Chinese Academy of Sciences, Beijing, P. R. CHINA
December 2006	M. S. in Chemical Engineering, The Ohio State University, Columbus, Ohio, USA
Present	Ph. D. Candidate, Center for Advanced Polymer and Composite Engineering, The Ohio State University, Columbus, Ohio, USA

PUBLICATIONS

1. **G. Zhou**, S. Movva, D. Guerra, and L. J. Lee, Analysis of the Effect of Nanoparticles on Mold Filling in a Vacuum Assisted Resin Transfer Molding System, *Proceedings of the 65th Annual Technical Conference of the Society of Plastics Engineers*, Cincinnati, Ohio, USA (2007).

2. **G. Zhou**, D. Guerra, S. Movva, and L. J. Lee, Preparation and Properties of Nanoparticles and Long Fibers Reinforced Thermoset Composites, *Proceedings of the 65th Annual Technical Conference of the Society of Plastics Engineers*, Cincinnati, Ohio, USA (2007).

3. **G. Zhou** and L. J. Lee, Preparation, Structure, and Properties of Nanoparticles and Long Fibers Reinforced Thermoset Composites, *Proceedings of 2006 Annual Meeting of AIChE*, San Francisco, California, USA (2006).

4. **G. Zhou** and L. J. Lee, Long Fiber/Nanoparticles Reinforced Polymer Composites, *Proceedings of 22nd Annual Meeting of the Polymer Processing Society*, Yamagata, Japan (2006).

5. **G. Zhou**, X. Cao, and L. J. Lee, Nanoparticles and Long Fibers Reinforced Thermoset Composites, *Proceedings of 2005 Annual Meeting of AIChE*, Cincinnati, Ohio, USA (2005).

6. **G. Zhou** and L. J. Lee, Nano-clay and Long Fiber Reinforced Phenolic Composites, *Proceedings of the 63rd Annual Technical Conference of the Society of Plastics Engineers*, Boston, Massachusetts, USA (2005).

7. D. Grewell, **G. Zhou**, L. J. Lee, A. Benatar, and E. Lee, Ultrasonic Treatment of Advanced Thermoset Composites, *Proceedings of the 62nd Annual Technical Conference of the Society of Plastics Engineers*, Chicago, Illinois, USA (2004).

8. L. Xu, **G. Zhou**, L. J. Lee, Processing and Properties of Nanoparticle Reinforced Long-fiber Thermoset Composites, *Proceedings of 2003 Annual Meeting of AIChE*, San Francisco, California, USA (2003).

9. **G. Zhou** and L. J. Lee, Nano-clay and Long Fiber Reinforced Composites Based on Epoxy and Phenolic Resin, *Proceedings of the 61st Annual Technical Conference of the Society of Plastics Engineers*, Nashville, Tennai, USA (2003).

10. T. Zhao, **G. Zhou**, L. Zhi, M. Yang, Thermoplastic Phenolic Resin/Clay Nanocomposites and Its Preparation process, *Fa Ming Zhuan Li Shuo Ming Shu*, CN 1361189 (2002).

11. T. Zhao, **G. Zhou**, L. Zhi, M. Yang, Thermosetting Phenolic Resin Filled with Nanoclay and Its Preparation, *Fa Ming Zhuan Li Shuo Ming Shu*, CN 1361188 (2002).

12. **G. Zhou** and T. Zhao, Synthesis of Phenolic/Clay Nanocomposites, *Proceedings of the 6th Pacific Polymer Conference*, Guangzhou, CHINA (1999).

FIELDS OF STUDY

Major Field: Chemical Engineering

Minor Field: Polymer Engineering

TABLE OF CONTENTS

LIST OF TABLES

LIST of FIGURES

CHAPTER 1

INTRODUCTION

1.1 Polymer Composites

Since the last century, polymeric materials have been widely used in many areas, such as in civil life and military applications. Now polymers are the fastest growing materials in the world. Between 1980 and 1990, the production of plastics increased by 62% while that of steels decreased by 21%. The annual overall production of polymeric materials has exceeded that of metal materials if computed in volume [1].

A composite is a type of material that consists of two or more components with largely different chemical or physical characteristics. The preparation of a composite from two or more materials is one of the most important approaches to produce new materials, because few pure materials fulfill the strength, design, and cost requirements of modern applications. In the 1960s, polymer composites became one of the research focuses in materials science. Since then, many conventional polymer composites have been prepared. These composites possess better chemical or physical properties than pure polymeric materials, such as high strength and modulus, good dimensional stability, improved chemical and corrosion resistance, and various functionalities [2].

1.1.1 Resins

In general, polymer resins can be divided into two types: thermoplastics and thermosets [3]. These two types of polymers differ in their molecular structures and behaviors.

In a thermoplastic polymer, individual molecules have a linear structure without chemical linking between them. With the application of heat and pressure, the weak interactions between molecules can be temporarily broken and then the plastics can be softened and made to flow. Upon cooling, the molecules restore the secondary bonds between them and the plastics change from liquid to solid state. Because of their ease of fabrication and their cost efficiency, thermoplastics become more and more popular in composite products. The most common thermoplastic resins include polyethylene (PE), polypropylene (PP), polystyrene (PS), poly(vinyl chloride) (PVC), polyamide (PA), polycarbonate (PC), poly(methyl methacrylate) (PMMA), etc.

In spite of the growing popularity of thermoplastic resins, thermoset resins are still the most widely used in composite applications. In a thermoset polymer, the molecules are chemically linked together, forming a three-dimensional network structure. Once the cross-linked structure is formed, the thermoset polymer cannot be melted and reflowed by the application of heat and pressure. In general, thermoset resins offer higher thermal stability and improved heat resistance than thermoplastic resins. Therefore, thermoset composites are dominated in the applications at elevated temperatures. The most common thermoset resins are epoxy, phenolic, unsaturated polyester, vinyl ester, polyurethanes, etc. Each of them has particular advantages or limitations that direct its application.

1.1.1.1 *Phenolics*

Phenolic resins were the first thermosetting resin to be synthesized commercially in 1907. Nowadays, phenolic resins continue to be developed and used for many applications. According to the kind of catalysts and products, phenolic resins can be generally sorted into two different categories: novolak and resol resins. Novolaks are obtained by the reaction of phenol and formaldehyde (P/F molar ratio > 1) under acidic conditions. They can become cross-linked network structure and cured resin when mixed and heated with hexamethylenetetramine (HMTA) or paraformaldehyde. Resol resins, which are different from novolak resins in synthesis and cure process, are obtained by the reaction of phenol and formaldehyde (P/F molar ratio < 1) under basic conditions. Heating or acidification of resol resins causes cross-linking to take place. The typical reaction mechanisms of novolak and resol resins are shown in Figure 1.1 and 1.2 respectively [4].

Both novolak and resol resins have good chemical and thermal resistance, fine dimensional stability, excellent electrical and thermal insulation properties, outstanding fire performance, and are cost effective. These properties enable phenolics to be used in household appliances, business equipment, wiring devices, automotive electrical systems, and mass transit. However, the drawbacks of phenolic resins are their brittleness and poor weather resistance [5].

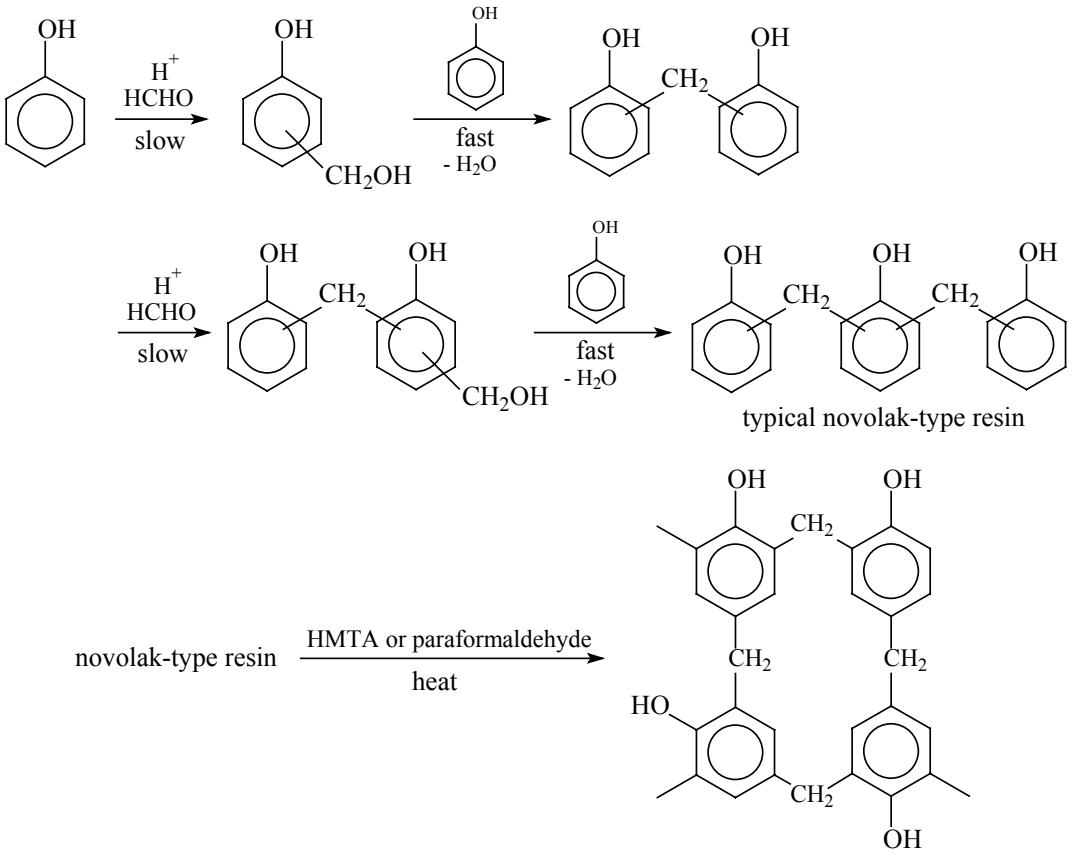

Figure 1.1 Schematic illustration of the reaction mechanism of novolak type phenolic resin [4].

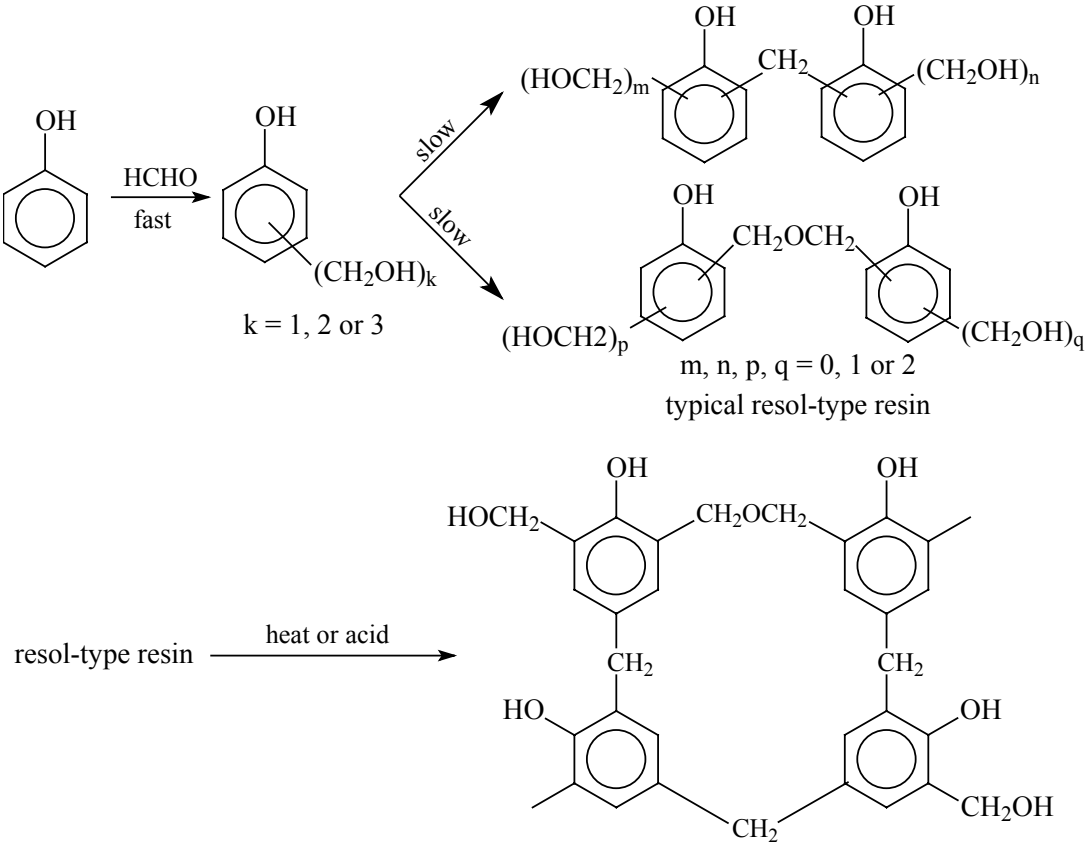

Figure 1.2 Schematic illustration of the reaction mechanism of resol type phenolic resin [4].

1.1.1.2 *Unsaturated Polyesters*

Unsaturated polyester resins are durable, resinous polymers. In general, unsaturated polyesters are step-growth products of three chemical species: unsaturated acids or anhydrides, saturated aromatic acids, and alcohols (glycols) [6-9]. A typical unsaturated acid is maleic anhydride (MA) and the alcohol is propylene glycol (PG). The unsaturated acids provide the backbone of the oligomer with unsaturated carbon-carbon (C=C) double bonds. When curing, these C=C double bonds react with monomers, such as styrene, to form the cross-links between polymer chains, and finally create a three-dimensional network structure. In the formulation of unsaturated polyester resins, the saturated acids are employed to adjust the reactivity of the resin as well as the properties of the final products. Table 1.1 presents a summary of these building blocks of unsaturated polyesters and their contributions [10]. Based on the saturated acid, unsaturated polyesters can be classified into different types: orthophthalic, isophthalic, and some specialty polyesters. The orthophthalic polyesters, in which the orthophthalic acid is used as the saturated acid, are known as general-purpose resins. They are the least expensive of the polyesters, but have relatively poor corrosive resistance. The isophthalic resins are the premium resins, which use isophthalic acid as the saturated acid. The premium resins have higher cost than the general-purpose resins, but better corrosion resistance, higher heat distortion temperature, and superior mechanical properties. Dicyclopentadienes (DCPDs) are used in some specialty polyesters, commonly in the boating building industry. DCPD polyesters cure more rapidly and completely, and have lower shrinkage and better cosmetics than general-purpose resins. A typical forming of the unsaturated polyester resin is shown in Figure 1.3 [6].

Building Blocks	Ingredients	Characteristics
Unsaturated anhydrides and dibasic acids	1. Maleic anhydride	1. Lowest cost, moderately high heat deflection temperature (HDT)
	2. Fumaric acid	2. Highest reactivity (cross-linking), higher HDT, more rigidity
Saturated anhydrides	1. Phthalic (orthophthalic) anhydride	1. Lowest cost, moderately high HDT, provides stiffness, high flex, and tensile strength
	2. Isophthalic	2. Higher tensile and flex strength better chemical and water resistance
	3. Adipic acid, azelaic acid, and sebacic acid	3. Flexibility (toughness, resilience, impact strength); adipic acid is lowest in cost of flexibility acids
	4. Chlorendic anhydride HET anhydridel	4. Flame retardance
	5. Nadic methyl anhydride	5. Very high HDT
	6. Tetrachlorophthalic anhydride	6. Flame retardance
	7. Tetrabromophthalic anhydride	7. Flame retardance
Glycols	1. Propylene glycol	1. Lowest cost, good water resistance and flexibility, compatibility with styrene
	2. Dipropylene glycol	2. Flexibility and toughness
	3. Ethylene glycol	3. High heat resistance, tensile strength, low cost
	4. Diethylene glycol	4. Greater toughness, impact strength and flexibility
	5. 2,2,4-Trimethyl-1,3-pentanediol glycol	5. Corrosion resistance with reduced density
	6. Bisphenol-A adduct	6. Corrosion resistance, high HDT, high flex and tensile strength
	7. Hydrogenated bisphenol-A adduct	7. Corrosion resistance, high HDT, high flex and tensile strength
	8. Tetrabromobisphenol-A	8. Flame resistance

Table 1.1 Unsaturated polyester building blocks [9].

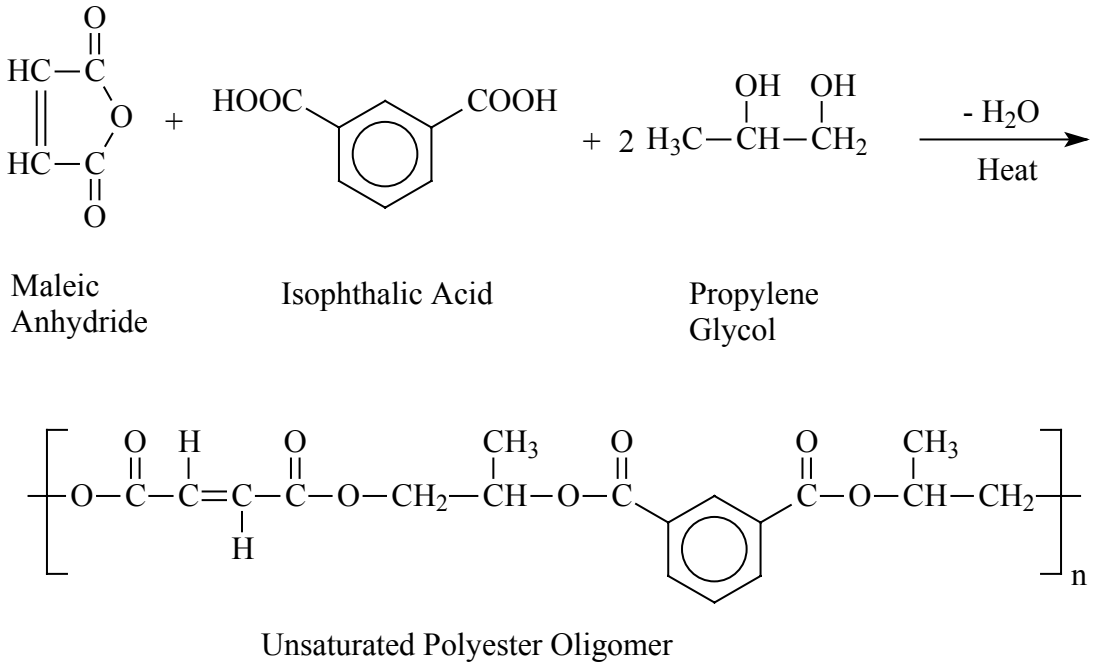

Figure 1.3 Example of the reaction mechanism of unsaturated polyester resin [6].

1.1.1.3 *Epoxies*

Epoxy resins are defined as any molecule containing more than one alpha-epoxy group, which are thermoplastic liquids or solids that may be cured to thermosets by homopolymerization with a catalyst or by copolymerization with a hardener. These resins have excellent electrical properties, low shrinkage, good adhesion to many metals, and resistance to moisture, thermal and mechanical shock. There are two main categories of epoxy resins, namely the glycidyl epoxy, and non-glycidyl epoxy resins. The glycidyl epoxies are further classified as glycidyl-ether, glycidyl-ester and glycidyl-amine. The non-glycidyl epoxies are either aliphatic or cycloaliphatic epoxy resins. According to the components, epoxy resins have many formulas. At the present time, most commercial epoxy resins are prepared by the reaction of bisphenol A (2,2-bis(4-hydroxyphenyl) propane) and epichlorohydrin [11]. A typical reaction mechanism of bisphenol A and epichlorohydrin is shown in Figure 1.4. Epoxy resins have been mass-produced since 1939, which is mainly used in reactive molding compounds and in adhesives [2].

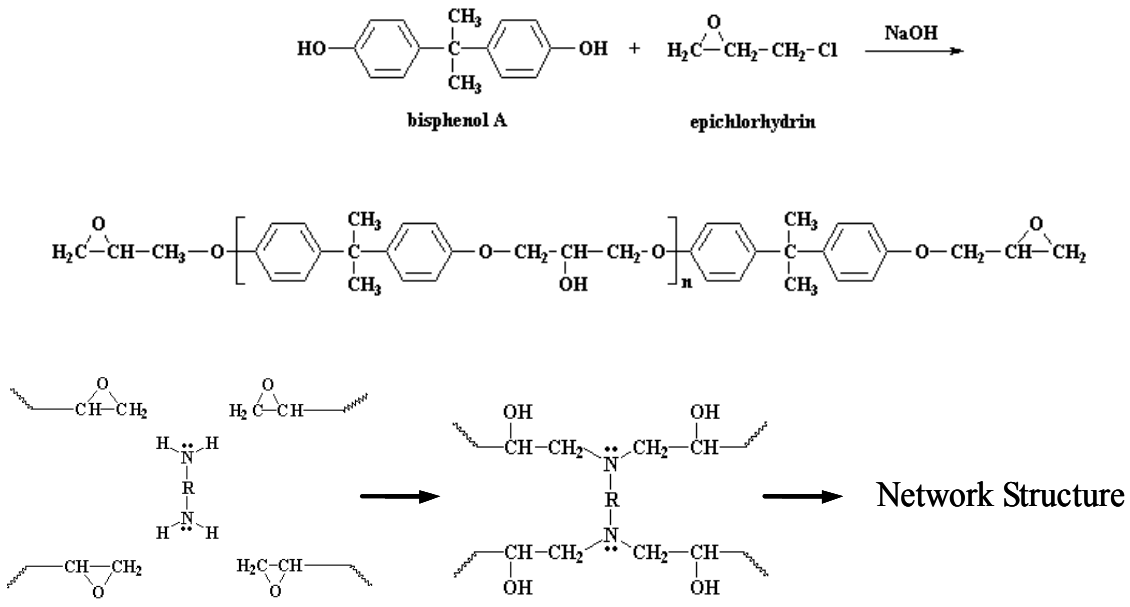

Figure 1.4 Schematic illustration of the reaction mechanism of epoxy resin.

1.1.2 Fibers

Conventional composites are materials consisting of fillers in the form of inorganic, organic, or metallic fibers or powders of relatively high strength and modulus embedded in or bonded to a matrix. Fibers are the most widely used fillers, and fiber-reinforced plastics (FRPs) are the most widely used composites. In general, fibers are the principal load-carrying members, while the surrounding matrix keeps them in the desired location and orientation, acts as a load transfer medium between them and protects environmental damage due to exposure to elevated temperature and humidity.

1.1.2.1 *Glass Fibers*

Glass fiber or fiberglass is, by far, the largest reinforcement measured in quantity or in sales. The first commercial production of fiberglass was in the late 1930s by Owens-Corning Fiberglas Corporation [12]. Since then, glass fibers have become widely used as insulation materials or composite reinforcement. Based on the composition and application, glass fibers can be classified into several types. E-glass fibers predominate in polymer matrix composites because of their high electrical insulation properties, good resistance to moisture, and high mechanical properties. S-glass fibers have higher heat resistance, strength, and modulus, but higher cost. Other specialty glass fibers, such as AR- or R-glass, possess of better chemical resistance. Typical diameter of glass fibers is 10-12 μm and specific gravity is about 2.5. The elastic modulus of glass fibers is in the order of 50-90 GPa, much higher than that of polymers [13].

1.1.2.2 *Carbon Fibers*

Carbon fiber or graphite fiber is another major type of reinforcement used in polymer composites. A common method of making carbon filaments is the oxidation and thermal pyrolysis of polyacrylonitrile (PAN), so called PAN-based carbon fibers. Carbon fibers can also be manufactured using pitch as the precursor instead of PAN. But the quality of pitch-based carbon fibers is lower than that of PAN-based fibers. Typical diameter of carbon fibers is in range of 6-10 μm and specific gravity is between 1.7 and 2.1. The tensile modulus of carbon fibers is higher than 200 GPa [12]. Compared with glass fibers, carbon fibers have low density but higher modulus and strength. Therefore, they are often used in aircraft parts, high-performance vehicles, sporting equipment, wind generator blades, and other demanding mechanical applications.

In addition, fibers made from aramid, kevlar, boron, or metal materials can also be used in polymer matrix composites. However, due to the difficulties in the production and application, they are not as popular as glass or carbon fibers.

1.1.3 Fillers and additives

Except long fibers, some fillers are added into polymer matrix for one or more of the following reasons [14]:

- reduce cost;
- increase modulus (stiffness);
- reduce shrinkage;
- improve crack resistance;
- control viscosity.

The most common fillers for thermoset resins are calcium carbonate, kaolin, and alumina hydrate. Examples of other commonly used fillers include clay, feldspar, mica, silica, glass micro-spheres, glass whisker, and micro-rubber balloon. In unsaturated polyester and vinyl ester resins, calcium carbonate is often used to reduce the cost as well as the mold shrinkage.

A variety of additives can be used to modify composite properties, performance, and appearance, including catalysts, inhibitors, colorants, release agents, flame retardants, and ultraviolet (UV) absorbers [14, 15]. Typically, the additives can change the performance of polymer composites in the following aspects: apparent color, resin viscosity, air release, curing rate, lubricity or mold release, electrical and thermal conductivity, surface smoothness, shrinkage, wetting and dispersion, etc.

1.1.4 Processing

Fiber-reinforced polymer composites can be manufactured by many processing methods, such as hand lay-up, spray-up, vacuum bagging and autoclave curing, compression molding, filament winding, pultrusion, and liquid composite molding (LCM). These methods have their own characteristics, and thus they are used to produce different types of composite parts. This study is primarily based on thermosetting polymer composites made of epoxy, phenolic, and unsaturated polyester resins, therefore most commonly used processes for these materials are introduced as follows.

1.1.4.1 *Hand Lay-up and Spray-up*

Hand lay-up is the simplest and oldest open molding method of the composite fabrication processes. In this method, glass fiber mat or woven fabric or roving is manually laid in the mold, and the liquid resin is poured or brushed over and into the glass piles. Entrapped air is removed with squeegees, rollers, or brush dabbing. The lay-up is made by layer upon layer to obtain to complete the desired structure [16]. Curing is usually initiated by a catalyst in the resin system at room temperature or in an oven at atmospheric pressure. The most commonly used polymer resins are the room-temperature curing polyesters and epoxies. Hand lay-up technique is a time-consuming, labor-intensive method, especially for large components, such as boat hulls. Although this process is low-cost, there are many drawbacks. It is a labor-intensive process, the quality of the parts is based on the skill of the operators, and the chemical emission of this open process is high, which may lead to safety and environmental issues.

Compared with hand lay-up, spray-up is devised to shorten processing time and lower labor cost. In this process, chopped fiberglass roving and catalyzed resin are simultaneously deposited on the mold surface from a combination chopper/spray gun. Rollers and squeegees are used to remove entrapped air and improve the mixing of the resin and the reinforcement. Woven fabric is often added in specific areas for greater strength. Usually, room-temperature curing polyesters are used in spray-up process. Gel coats may be used to form a high quality surface, such as tub and shower stalls.

1.1.4.2 *Vacuum Bag and Autoclave Molding*

Vacuum bag molding is a refinement of hand lay-up and spray-up, which uses a vacuum to eliminate entrapped air and excess resin. The fiber reinforcement, usually a unidirectional tape or a woven fabric, is impregnated with a partially cured resin. The resultant product is called a prepreg, which is usually stored in a freezer until molding. The prepregs are cut and laid into a mold to build up the desire structure. After the lay-up is complete, a non-stick film of nylon or polyvinyl alcohol is placed over the lay-up and sealed. Then, a vacuum is applied to consolidate separate prepreg plies into a solid part. Curing of the composite can be at room or elevated temperatures.

Autoclave molding is a similar to the vacuum bag molding. The difference is that the composite is cured in a heated pressure vessel usually equipped with a vacuum system. Because of higher heat and pressure are used for curing, the autoclave process produces more denser parts. Nowadays, vacuum bag and autoclave molding are used predominantly in the aerospace industry [14].

1.1.4.3 *Compression Molding*

Compression molding is used to transform sheet-molding compound (SMC), bulk-molding compound (BMC), or preform materials into finished products with matched metal molds. SMC and BMC contain all components including resin, fiber, fillers, catalyst, pigment, and other additives. After materials are placed into the mold cavity, heat and pressure is applied. Usually, the mold temperature is in the range of 60-160 °C (140-320 °F) and the pressure may vary from 1.0 to 34.5 MPa (150-3000 psi). After a reasonable degree of cure is achieved, the mold is opened and the part is removed from the cavity. Typical thermoset resins used in compression molding are unsaturated polyesters, vinyl esters, epoxies, and phenolics. The principal advantage of compression molding is its ability to produce parts of complex geometry, such as nonuniform thickness, ribs, holes, and shoulders, in a short period of time [17]. Compression molded products vary from dinnerware, trays, buttons, large containers, to vehicle body panels and bumpers.

1.1.4.4 *Filament Winding and Pultrusion*

Filament winding is a process by which resin impregnated fibers or rovings are wound uniformly and regularly on a rotating mandrel in predetermined patterns. The finished pattern is cured and the mandrel is removed. The resultant product could be something as simple as a piece of pipe or as complex as an aircraft fuselage. Typical fibers are fiberglass, carbon, and aramid. The most commonly used resins include thermoset polyesters, vinyl esters, epoxies, and phenolics. In the wet method, the fiber is wetted with resin just before winding on the mandrel; for the dry method, the reinforcement is in the preimpregnated form, such as prepregs. The advantages of

filament winding over other composite fabrication methods are its low materials and labor costs, and its reproducibility due to the robotic motions. The greatest disadvantages are the tooling limitations for removable mandrels and the inability to wind on concave surfaces [18].

Pultrusion is a continuous manufacturing process to produce various reinforced plastic shapes of uniform cross sections. The difference between pultrusion and filament winding is that filament winding has the primary reinforcement in the circumferential direction, while pultrusion places the primary reinforcement in the longitudinal direction [18]. Similar to filament winding, pultrusion process also involves passing continuous fiber reinforcement through a resin bath; but instead of winding the impregnated fibers on a mandrel, the part is formed by pulling the fibers through a heated die, in which the resin changes from a liquid to a gel, and finally into a rigid plastic. In commercial applications, polyesters, vinyl esters, and epoxies are used as the matrix materials. Among the common pultruded products are solid rods, hollow tubes, flat sheets, and various beams.

1.1.4.5 *Liquid Composite Molding*

LCM become increasingly popular because of its low production cost, short cycle time, good quality control, and the ability to manufacture high performance composites with complicated geometry. Processes in this category include resin transfer molding (RTM), structural reaction injection molding (SRIM), vacuum-assisted resin transfer molding (VARTM), et al [19].

In RTM process, pre-shaped fabric reinforcements, generally called a preform, are

placed in a prepared mold cavity. Once the mold has been closed, clamped, and then heated to a preset temperature, resin mixed with catalyst is injected into the mold cavity. The liquid mixture flows through the fibrous preform, expelling the air in the cavity and impregnating the reinforcement. When excess resin start to flow out the vent of the mold, the resin injection is stopped and the molded component begins to cure. When the cure is completed, the composite is removed from the mold. Trimming and postcure may be required for the molded components. Common matrix resins include unsaturated polyesters, vinyl esters, epoxies, and phenolics. Compared with compression molding, RTM has a very low tooling cost, simple mold clamping requirement, and short cycle time [14]. High quality parts produced by this method include automotive body parts, large water containers, and bathtubs.

SRIM is similar to RTM process. However, there are several key differences between SRIM and RTM. In general, SRIM resins have lower viscosity (usually in the range of 150-250 cp at room temperature for SRIM and typically in the range of 700-1000 cp for RTM). SRIM resins also have higher reactivity comparing to RTM resins, and require very fast, high-pressure impingement mixing to achieve completely mixing before entering the mold. Therefore, the curing step in SRIM is much shorter than that in RTM. But the equipment cost of SRIM is much higher than that of RTM because higher pressure is applied during molding.

One of RTM variants is VARTM. The VARTM process is quite similar to RTM except that resin is driven into the reinforcement by vacuum and the curing may take place at ambient temperature. In the 1990s, Seeman patented his methods for the manufacturing polymer composites [20-22]. These methods are called “Seeman Composite Resin Infusion Molding Process” (SCRIMP), in which a soft mold half (vacuum bag) and a rigid mold half were used and highly permeable medium and peel ply were employed. In fact, SCRIMP is a type of VARTM. Because external heating may not need and soft vacuum bag can be used as a mold, the cost of VARTM is much lower than that of RTM. Moreover, as a close-mold process, volatile organic chemical (VOC) emissions of VARTM are significantly reduced.

Currently, VARTM is becoming an important process for manufacturing very large composite parts. There are many composite products and parts made by the VARTM. For example, the Northern Star insulated railcar was produced by Hardcore-DuPont in 1995 [23]. The railcar was about 21 m (68 ft) in length, 4 m (12 ft) in height, and 3 m (10 ft) in width. The one-piece construction minimized assembly costs, reduced maintenance, and eliminated heat loss through mechanical joints and rivets resulting in superior insulating capabilities. The fiberglass composite carriage consisted of over 6.8 tons of E-glass fabric, vinyl ester resin, and polyurethane core.

In sum, different processing methods are used to produce different composite parts according to their technical and economic characteristics. The following table summarized some general technical and economic possibilities of various processes.

Method	*Output, units*	*Cycle time*	*Investment*	*Labor cost*
Hand lay-up	1–1000	30 min to several days	Low	High
Spray lay-up	1–1000	30 min to several days	Low	High
Liquid molding	1–1000	According to part	Low to Medium	Medium
Hot compression molding mats and preforms	Mass production	1–10 min	High	Medium
Hot compression molding prepregs	Mass production	2–5 min	High	Low
Autoclave	<5000		Medium	Medium
Filament winding	<10000	According to part	High	High
Pultrusion	Continuous	Continuous	High	Low

Table 1.2 Examples of economic characteristics of some processes [13].

1.1.5 Performance

The success of fiber-reinforced polymer composites in globally competitive market is primary due to their excellent performance compared to other materials. The advantages include [12]:

- Design flexibility;
- Low specific gravity;
- High strength-to-weight and modulus-to-weight ratios;
- Dimensional stability;
- High internal damping;
- Thermal stability;
- Improved corrosion and wear resistance.

As shown in Figure 4, fiber-reinforced epoxy composite is much stronger and stiffer than pure epoxy resin [2]. When 60 vol.% carbon fibers are added into epoxy resin, the strength of the composite is even greater than that of steel. Therefore, there are numerous applications of such fiber-reinforced composites. For example, because of the properties of low weight and dimensional stability of FRPs, fiber-reinforced epoxy resins are used for space shuttles and artificial satellites [24].

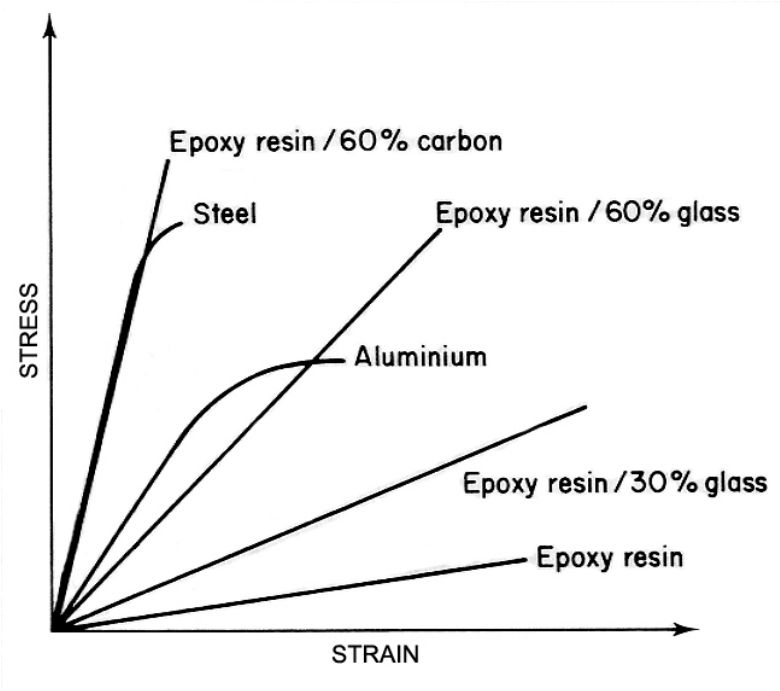

Figure 1.5 Tensile behavior of fiber-reinforced plastics and other structural materials [2].

1.2 Polymer Nanocomposites

At the beginning of the 1980s, scientists found there is a large difference between the properties of traditional materials and novel materials with nanostructures. For example, it was reported that the strength and electric conductivity of the nano-powder of copper were much higher than bulk copper [25]. Scientists attributed this change to the nano-effects of the nanoparticles. It was predicted that the nanostructured composites might show a great difference from the conventional composites. Therefore, nanocomposites have attracted great interests in the recent 20 years.

Nanocomposites are a type of composite in which the scale of the dispersed phase is within the nanometer scale at least in one dimension. Polymer nanocomposites consist of a polymeric material (thermosets or thermoplastics) and a reinforcing nanoscale material (nanoparticles). Due to the nanoscale dispersion and the high aspect ratios of the nanoparticles, polymer nanocomposites exhibit light-weight, good dimensional stability, enhanced heat and flame resistance, and improvements of strength, stiffness, and barrier properties with far less clay loading than conventional composite counterparts [25, 26]. Of course, many factors may affect the properties of polymer nanocomposites [27]:

- Type of nanoparticles and their surface treatments;
- Polymer matrix, such as molecular weight, crystallinity, and polymer chemistry;
- Synthesis methods, such as in-situ polymerization, melt compounding, and solution blending;
- Polymer nanocomposite morphology, such as nanoparticle dispersion.

1.2.1 Nanoparticles

There are different types of nanoparticles available to be incorporated into polymer matrix to form polymer nanocomposites, such as nanosilica, nano-aluminum oxide (Al_2O_3), nano-titanium oxide (TiO_2), polyhedral oligomeric silsesquioxane (POSS®), layered silicate (nanoclay), graphite, carbon nanofibers (CNFs), and carbon nanotubes (CNTs). These nanoparticles can be sorted into three categories: particulates (e.g. nanosilica), layered fillers (e.g. layered silicate and graphite), and fibrous materials (e.g. nanofibers and nanotubes).

A morphological characteristic, which is fundamentally important to understand the structure-property relationship of nanocomposites, is the surface area/volume ratio of the reinforcement materials. As illustrated in Figure 1.6, the change in particle diameter, layer thickness, or fibrous material diameter from micrometer to nanometer will change the surface area/volume ratio by three orders in magnitude [28]. For the fibrous and layered fillers, the length l is often ten to hundreds times greater than the fiber radius r or the layer thickness t. Therefore, the surface area/volume ratio is dominated by the first term and the second term is often omitted. In addition, with the remarkable increase of interfacial area, the nanocomposite performance become dominated more by the properties of the interface or interphase.

Based on the shape of the nanoparticles, the following parts will briefly introduce some common nanoplatelets and nanofibers used in polymer composites, especially nanoclays and CNFs.

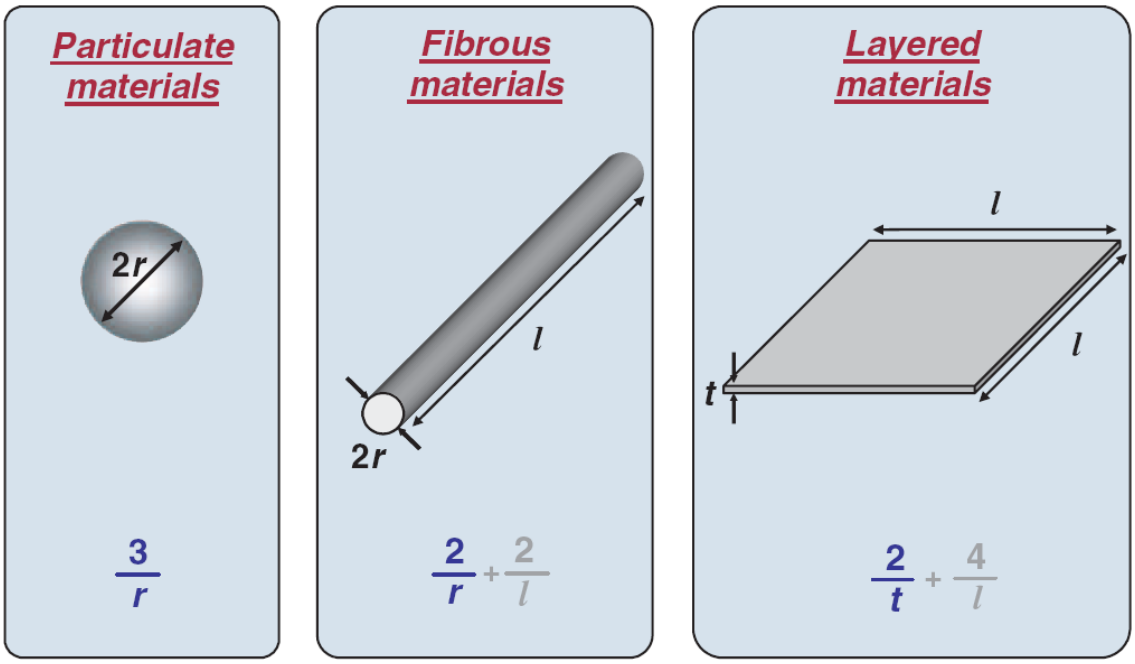

Figure 1.6 Common reinforcement geometries and their surface area/volume ratios [28].

1.2.1.1 *Nanoplatelets*

Two types of nanoplatelets particles are often used to form polymer nanocomposites: layered silicate clay and graphite.

Layered silicates, commonly known as clay minerals, are part of the large family of phyllosilicates. Every clay mineral contains two types of sheets, tetrahedral and octahedral [29]. The stacking of silicate layers leads to a regular van der Waals gap between the layers called the interlayer or gallery. Isomorphic substitution (e.g. tetrahedral Si^{4+} replaced by Al^{3+}, octahedral Al^{3+} replaced by Mg^{2+} or Mg^{2+} replaced by Li^{+}) within the layers originates negative charges that are counterbalanced by alkali and alkaline earth cations (e.g. Na^{+} or Ca^{2+}) inside the galleries [30]. This type of layered silicate is characterized by a moderate surface charge known as the cation exchange capacity (CEC). Montmorillonite (MMT), hectorite, and saponite are the most commonly used layered silicates, in which one octahedral sheet is sandwiched between two tetrahedral sheets [29], so called 2:1 layered silicates. For these clay minerals, the layer thickness is around 1 nm, and the lateral dimensions of these layers may vary from 30 nm to several microns. For example, sodium MMT clays are available as micro-size tactoids, which consists of several hundreds of individual plate-like structures with dimensions of 1000 nm × 1000 nm × 1 nm. The gap between two adjacent platelets is about 0.3 nm. Details regarding the structure and chemistry for these layered silicates are provided in Figures 1.7 and 1.8 as well as Table 1.3 [30].

Pristine layered silicates usually contain hydrated Na^{+} or K^{+} ions [29], so the layered silicates in the pristine state are only miscible with hydrophilic polymers, such as

poly(ethylene oxide) (PEO) or poly(vinyl alcohol) (PVA). It becomes very difficult to achieve nano-scale dispersion of these unmodified clays in most hydrophobic polymer matrices. In order to obtain better compatibility between layered silicates and polymer materials, the hydrophilic silicate surface must be modified to an organophilic one. Generally, this can be done by ion-exchange reactions with cationic surfactants, including primary, secondary, tertiary, and quaternary alkylammonium or alkylphosphonium cations. These organic cations lower the surface energy of the inorganic host and lead to a larger interlayer spacing. In addition, the alkylammonium or alkylphosphonium cations can provide functional groups that can react with the polymer matrix or initiate the polymerization of monomers, resulting in the improvement of the interfacial strength between the layered silicates and the polymer matrix [31].

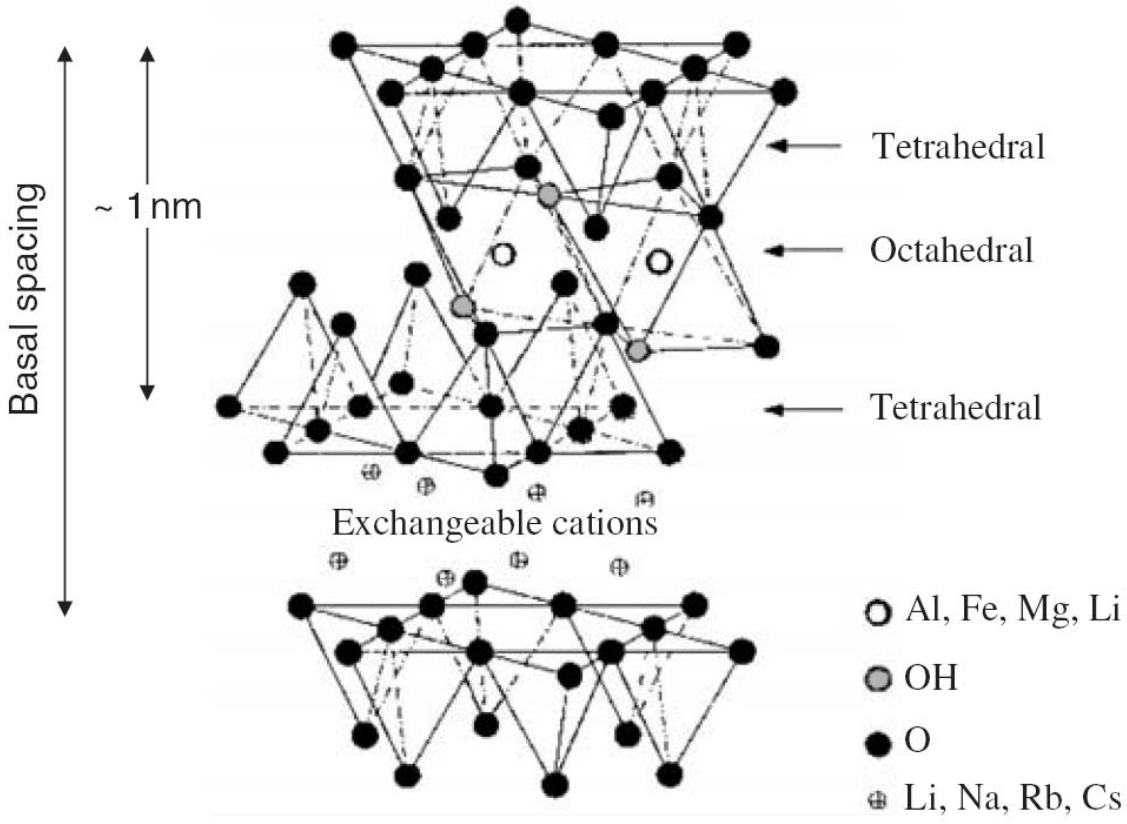

Figure 1.7 Structure of 2:1 clay minerals [30].

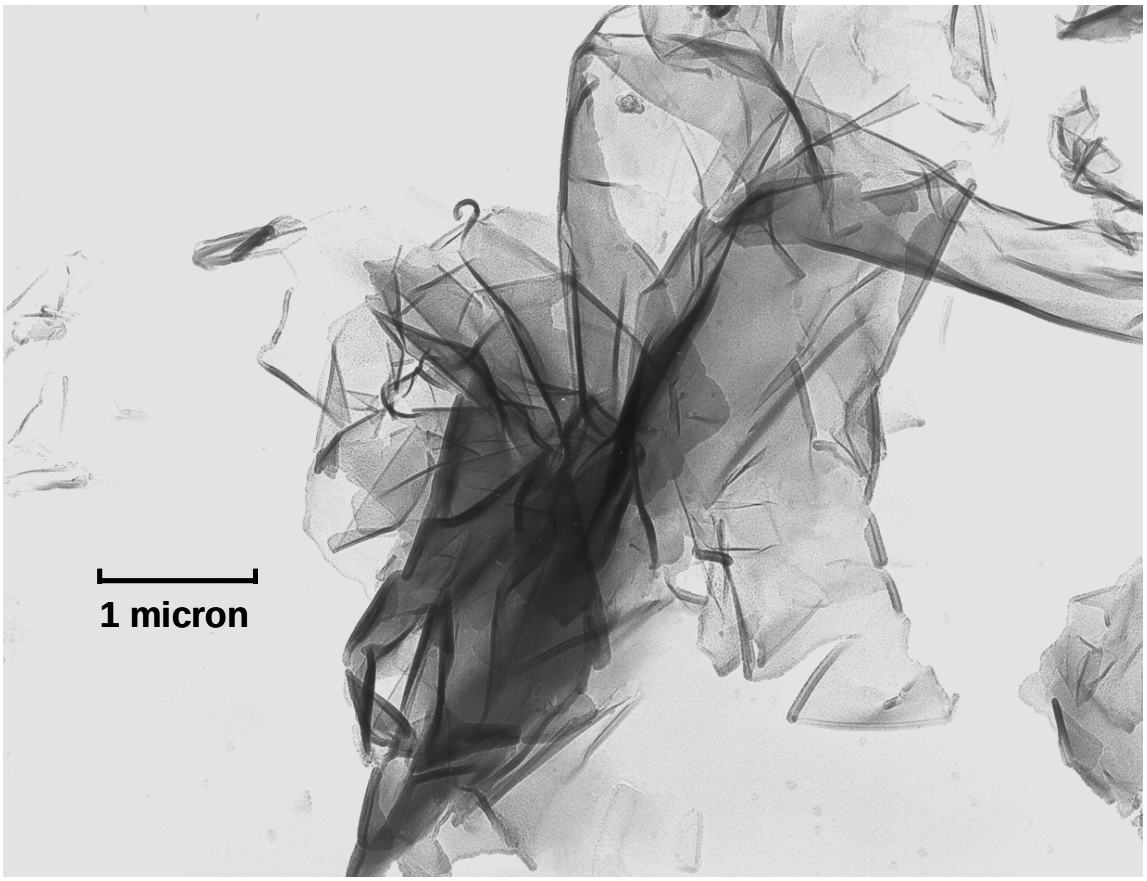

Figure 1.8 TEM image of refined montmorillonite. (Courtesy of Southern Clay Products)

2:1 phyllosilicates	Chemical formula	CEC (mequiv/100 g)	Particle length (nm)
Montmorillonite	$Mx(Al_{4-x}Mg_x)Si_8O_{20}(OH)_4$	110	100–150
Hectorite	$Mx(Mg_{6-x}Li_x)Si_8O_{20}(OH)_4$	120	200–300
Saponite	$MxMg_6(Si_{8-x}Al_x)Si_8O_{20}(OH)_4$	86.6	50–60

M, monovalent cation; *x*, degree of isomorphous substitution (between 0.5 and 1.3).

Table 1.3 Chemical formula and characteristic parameters of commonly used 2:1 clay minerals [30].

In general, the morphology of polymer-clay composites can be divided into three categories: conventional miscible composites, intercalated nanocomposites, and exfoliated nanocomposites [27, 28, 32, 33]. The structures of clay particles in polymer matrices are shown in Figure 1.9. In the conventional miscible state, the clay particles keep their crystal structure and the particle size is of micro-scale. In an intercalated nanocomposite, a few polymer molecules are inserted into the silicate galleries with fixed interlayer spacing. In contrast, an exfoliated nanocomposite is formed when the silicate nanolayers are delaminated and individually dispersed in the continuous polymer matrix. Whereas, only the exfoliated state may maximize interfacial contact between the organic and inorganic phases and lead to homogeneous dispersion, and as a result, the nanocomposites with optimum performance properties can be obtained. Therefore, the most desirable morphological state for the polymer-clay nanocomposites is exfoliation (delamination) [27].

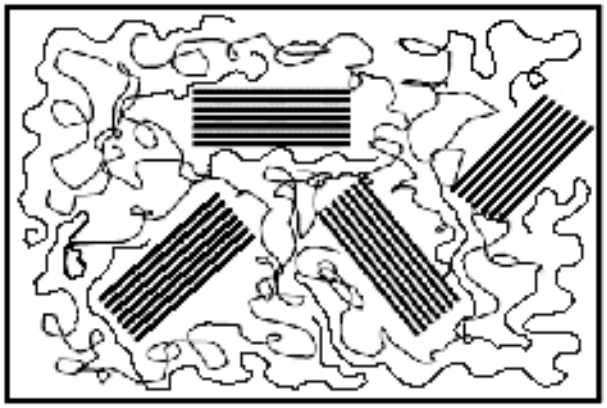

(a)

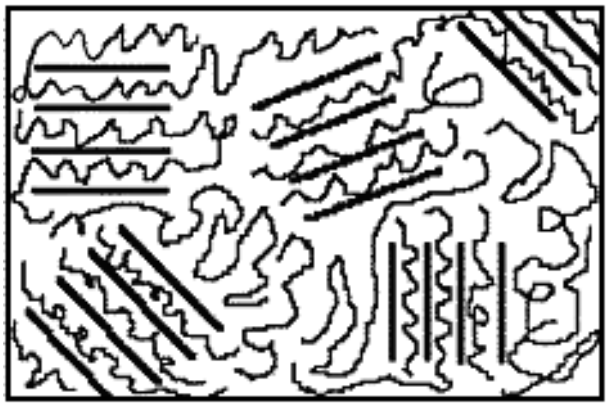

(b)

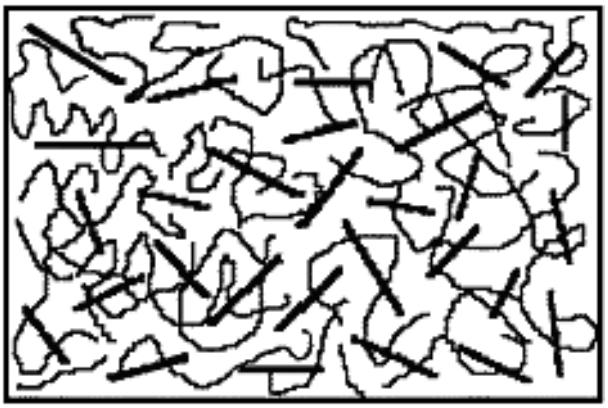

(c)

Figure 1.9 Schematic of morphologies of polymer-clay composites: (a) conventional miscible, (b) intercalated and dispersed, and (c) fully exfoliated and dispersed.

Natural flake graphite (NFG) is also composed of layered nanosheets, where carbon atoms positioned on the graphite layer are tightened by covalent bonds, while those positioned in adjacent planes are bound by much weaker van der Waals forces [34]. Certain atoms, ions, and molecules can intercalate into the interlayer spacing of the graphite. The original graphite flakes with a thickness of 0.4-60 mm may separate down to 1-nm sheets, which have a high aspect ratio (200-1500) and high modulus (~ 1 TPa). Moreover, these nanosheets expose an enormous surface area (2630 m^2/g) and play a key role in the improvement of physical and mechanical properties of the polymer nanocomposites [35].

Unlike the layered silicate, intercalation of graphite cannot be carried out by ion exchange reactions because it does not bear any net charge. One approach to prepare expanded graphite is to soap NFG in a 4:1 mixture of concentrated sulfuric acid and nitric acid. Then the treated graphite flakes are put into an oven at 900 °C for rapid expansion. The expansion ratio in thickness can be as high as 300 [34].

1.2.1.2 *Nanofibers*

The most commonly used fibrous nanoparticles in polymer materials are carbon nanotubes (CNTs) and carbon nanofibers (CNFs).

CNTs are rolled graphitic sheets into seamless tubes and have diameters ranging from 1 nanometer to tens of nanometers with length up to centimeters [36]. There are two types of CNTs: single-walled (SWNTs) and multi-walled (MWNTs). The discovery of CNTs can be traced back to as early as the early-1950s. Radushkevich and Lukyanovich published a paper with TEM images of hollow carbon filaments in the *Journal of*

Physical Chemistry of Russia in 1952 [37]. The diameter of these carbon filaments was about 50 nm [38]. However, CNTs did not catch enough attentions until the early-1990s, when Iijima et al reported their discovery of CNTs [39, 40]. Since then, the synthesis and characterization of CNTs has become one of the frontiers in materials science [41-56]. Figure 1.10 shows the TEM images of CNTs by Radushkevich and Iijima [38, 39].

The diameter of SWNTs is about 1 nm [40], while the diameters of MWNTs are in the range of ten to one hundred nanometers [39]. The structures of CNTs are illustrated in Figure 1.11. Because of the carbon-carbon sp^2 bonding, CNTs exhibit the exceptionally high stiffness and axial strength [56]. For example, it was reported Young's moduli for SWNTs and MWNTs could be as high as 1.8 TPa [48] and 1.2 TPa [52] respectively. Therefore, CNTs have been incorporated into polymers to improve modulus and strength [58-65]. In addition, CNTs are also used to enhance the electric and thermal conductivities of polymer materials [63-68]. However, low volume production and extremely high cost of the CNTs severely limit product development and applications.

Another type of fibrous material, CNFs, may serve as a substitute for CNTs. Recent studies show that polymer-CNF composites have similar properties to polymer-CNT composites [69-71]. These CNF nanocomposites can be used to make conductive paints, coatings, films, tubes, sheets, and parts for electrostatic painting, electro-magnetic interference (EMI) and electro-static discharge (ESD) applications. In addition, these composites also provide improved strength, stiffness, dimensional stability, and thermal conductivity. Moreover, the price of CNFs is much lower than that of SWNTs or MWNTs, making CNFs more promising than CNTs as reinforcement materials for a wide range of applications in automotive, aerospace, electronic and chemical industries.

CNFs can be produced by vapor-grown techniques [72, 73] or polymer carbonization process [74, 75]. In general, the diameters of CNFs are between CNTs (1-50 nm) and conventional carbon fibers (5-10 μm). Vapor-grown CNFs have diameters of 70-300 nm and lengths of 1-100 μm, while carbonized CNFs are arbitrarily long with a diameter from 100 nm to several microns. The electron microscopy images of vapor-grown CNFs are shown in Figure 1.12. The structures of CNFs have been studied by high-resolution TEM. Most vapor-grown CNFs have either parallel type or fishbone type structures [76]. Figure 1.13 shows the TEM images and schematic structure of CNFs.

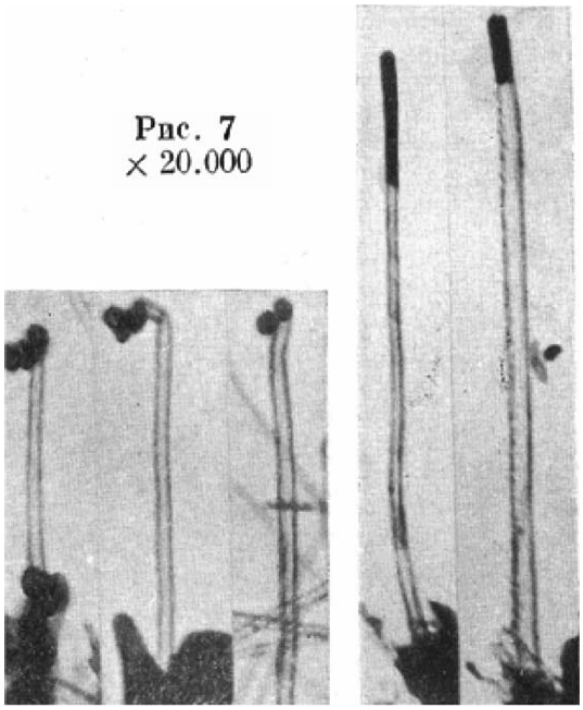

(a)

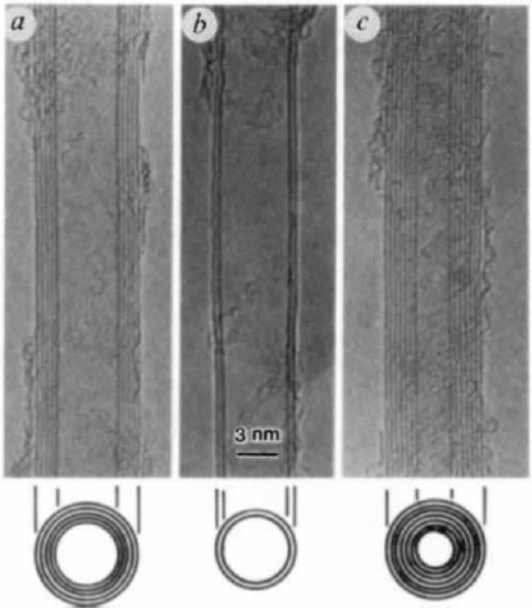

(b)

Figure 1.10 TEM images of MWNTs: (a) by Radushkevich and Lukyanovich in 1952 [38], and (b) by Iijima in 1991 [39].

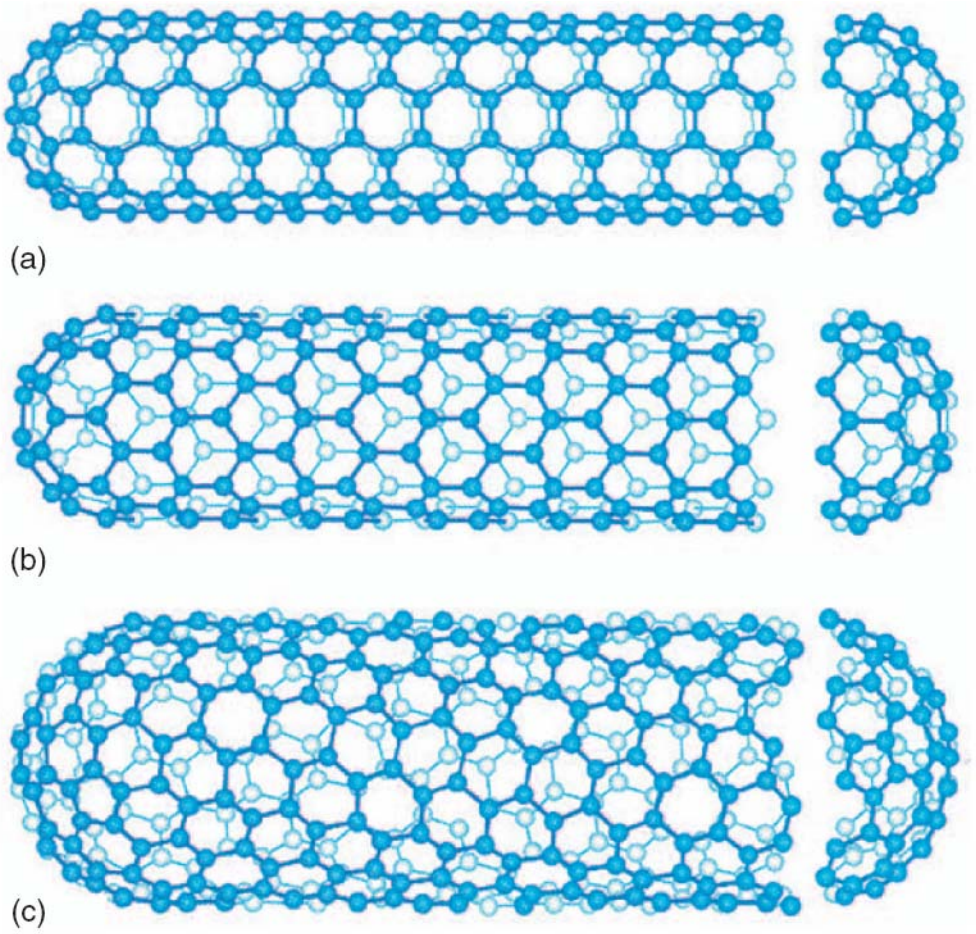

Figure 1.11 Schematic of carbon nanotube structure: (a) armchair, (b) zig-zag, and (c) chiral [36].

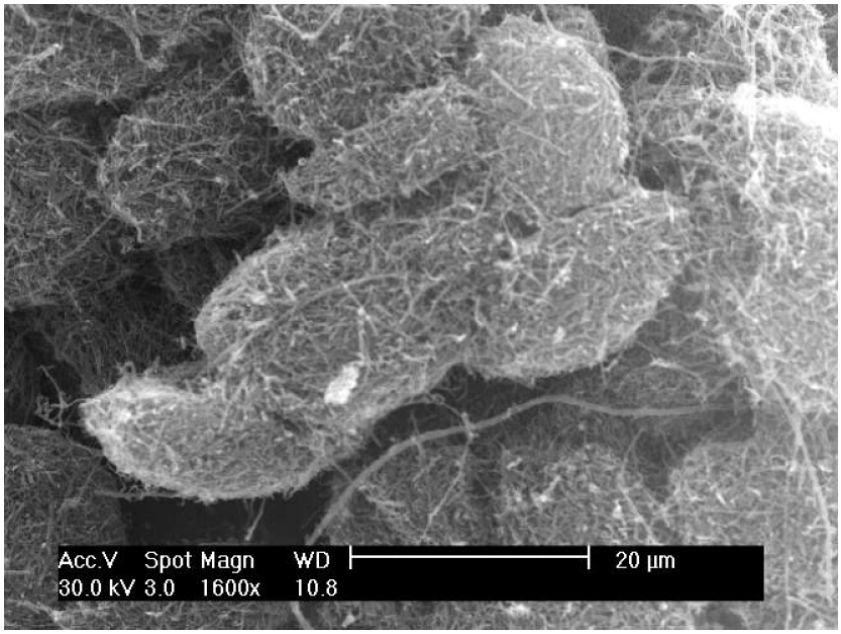

(a)

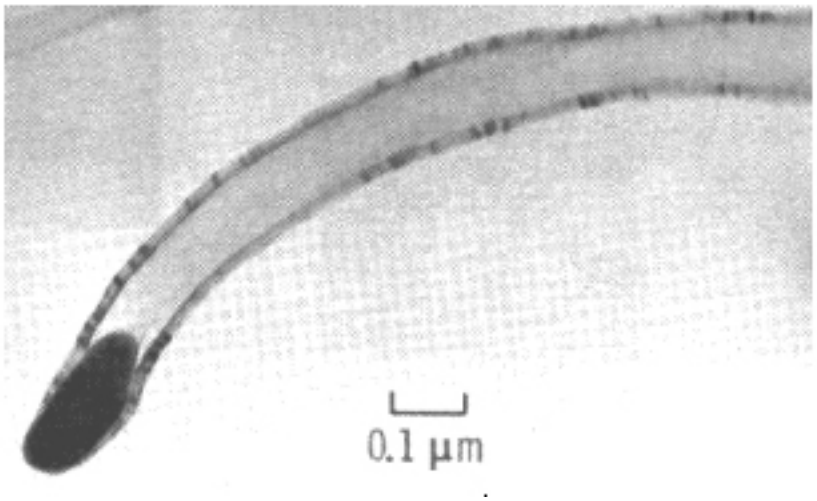

(b)

Figure 1.12 Electron microscopy images of vapor-grown CNFs: (a) SEM photo of as-received CNFs [71], and (b) TEM photo of single CNF with catalyst particle inside. (Courtesy of Applied Sciences Inc.)

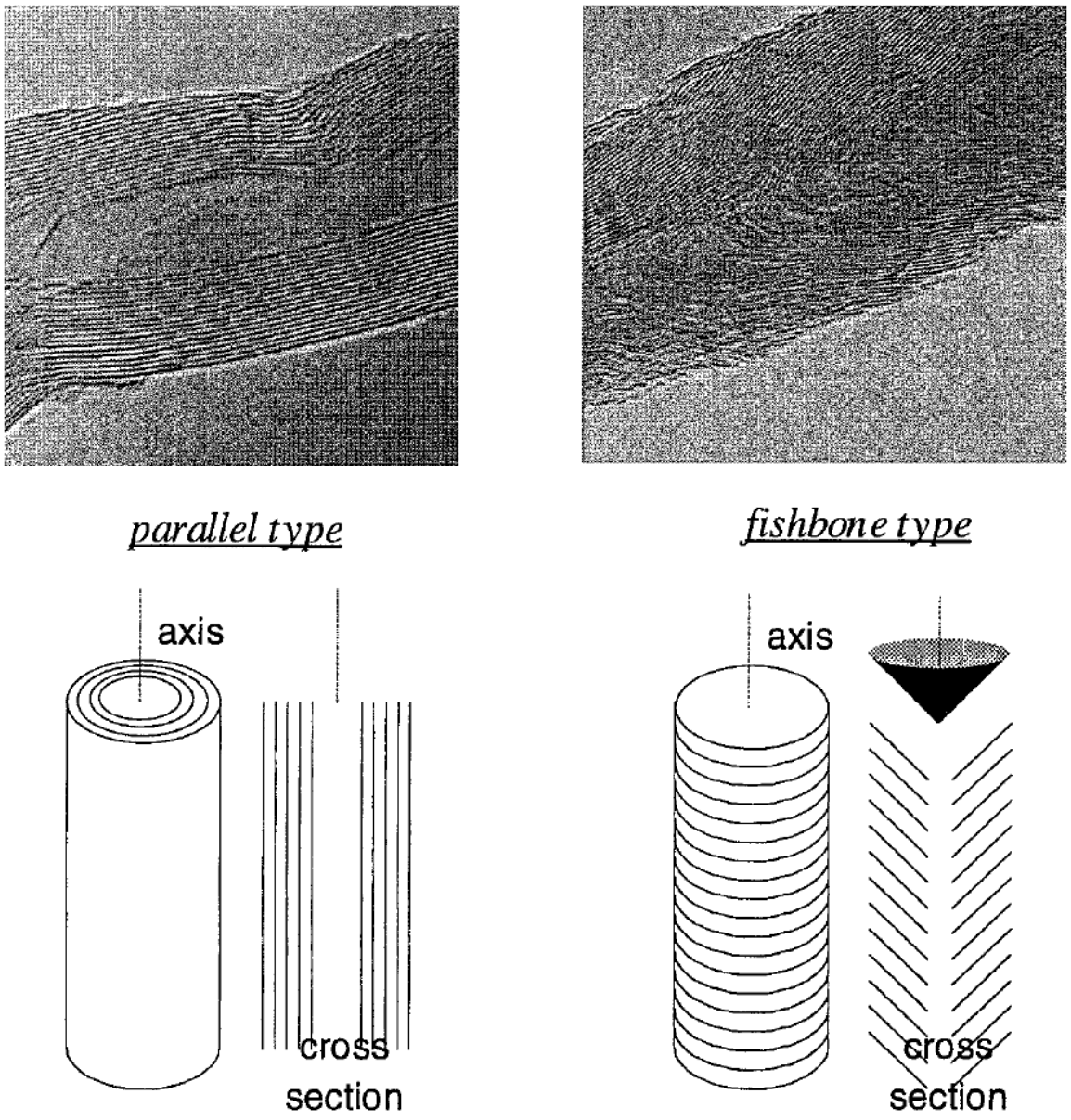

Figure 1.13 High-resolution TEM images and schematic structures of parallel and fishbone CNFs [76].

1.2.2 Preparation

Because the structure of polymer nanocomposites is usually determined during the preparation, it becomes the most crucial step to achieve good properties of the nanocomposites. Generally, there are four common methods to fabricate polymer nanocomposites: high-share mixing, solution blending, melt blending, and in-situ polymerization.

1.2.2.1 *High-share mixing*

The solid nanoparticles can be mixed with the liquid polymer resin using high-shear equipment [27]. If the surface untreated or treated nanoparticles are compatible with the selected polymer, the high-shear mixing may break the nanoparticle aggregates and disperse the polymer matrix around the nanoparticles. Fröhlich et al used high share mixer to prepare high-performance epoxy nanocomposites containing organophilic layered silicate and compatibilized liquid rubber [77]. They claimed that the intercalated structure of nanoclay was obtained in the cured epoxy sample. Koo and coworkers have successfully used high-shear mixing techniques to incorporate layered silicates, nanosilicas, carbon nanofibers, and POSS into epoxy, phenolic, and cyanate ester matrices [78-82].

High share mixing is an easy approach to prepare polymer nanocomposites. However, the disadvantage of this method is that the fibrous nanoparticles may break under high shearing and then the aspect ratio becomes smaller. In addition, nanoclays is difficult to achieve exfoliated state with high-share mixing.

1.2.2.2 *Solution Blending*

In solution blending, the polymer material is dissolved in a solvent or solvent mixture and the nanoparticles are mixed into the solution. Depending on the interactions between the nanoparticles and the solvent molecules, the van der Waals force among the nanoparticles can be reduced, and thus the aggregates may break. When the solvent evaporates under vacuum, the macromolecules will diffuse into the spacing between the nanoparticles. The driving force in this process is the entropy gained by desorption of solvent molecules, which compensates for the entropy decrease of the confined, intercalated polymer chains [83]. The advantage of this process is that it is capable to orient those anisotropic nanoparticles (e.g. nanoclays) with the aid of a magnetic or electric field. The major disadvantage of this method is that if a large amount of organic solvent is used, it may result in high cost as well as environmental and safety issues.

This technique has been widely applied with water-soluble polymers, such as poly(vinyl alcohol) (PVOH) [84-88], poly(ethylene oxide) (PEO) [88-91], polyacrylic acid (PAA) [91], and poly(vinyl pyrrolidone) [92]. Other examples with organic solvents includes polyimide [93], polystyrene (PS) [94, 95], poly(ε-caprolactone) (PCL) [96], polylacide (PLA) [97], etc.

1.2.2.3 *Melt Blending*

Melt blending is a widely used technique to prepare polymer nanocomposites, especially for thermoplastics. The procedure of melt blending involves the mixing of a molten polymer with nanoparticles, the annealing of the compound above the glass

transition temperature (T_g), and the cooling of the molten mixture to form a resultant nanocomposite. For the melt intercalation of nanoclay, the enthalpic contribution of polymer-organoclay interactions during the blending and annealing steps are thought to be the driving force [98]. Compared with solvent blending, melt blending eliminates the use of solvent, and thus the process is more environmentally friendly. Secondly, melt blending is compatible to current polymer blending and extrusion processes, so that it offers a more attractive route to fabricate polymer nanocomposites in a fast pace and on a large scale. The disadvantage is that during blending, such as extrusion process, the fibrous nanoparticles may break under high shearing and then lose their high aspect ratio [99]. In addition, it is difficult to achieve a nano-scale dispersion of nanoparticles with high molecular weight polymers.

Examples of polymer nanocomposites include PS [99-104], PP [105-113], nylon-6 [114-118], PEO [100, 119], PC [120], etc.

1.2.2.4 *In-situ Polymerization*

Unlike solvent and melt blending, in-situ polymerization can be used to synthesis both thermoplastic and thermoset polymers nanocomposites. First, nanoparticles are mixed with monomers. After the monomers diffuse into the spacing between the nanoparticles, often with an aid of ultrasonication and/or high shear device, an initiator (for thermoplastics) or a curing agent (for thermosets) is added into the system. Subsequently, the in-situ polymerization takes place. With the growth of the polymer chains, the interparticle space can be further expanded. Finally, the polymer nanocomposite is obtained. Because of the smaller size and higher movability of the

monomer molecules, it is much easier to diffuse into the aggregated particles than polymer molecules. Moreover, with the use of surface modification, catalyst or curing agent or functional groups can be introduced on the nanoparticle surface. Then, the polymer chains may grow directly from the particle surface. Therefore, the molecular-level dispersion of the nanoparticles in the polymer matrix is often achieved and the interfacial bonding between the nanoparticles and the polymer matrix can be significantly improved.

The most successful examples of polymer nanocomposites via in-situ polymerization are nanoclay reinforced nylon-6 [121-124] and epoxy [32, 125-128], in which the exfoliated nanolayers of the clays were uniformly dispersion in the polymer matrices (see Figure 1.14). Other nanocomposites synthesized by in-situ polymerization include PS [129, 130], PMMA [129, 131, 132], poly(ethylene terephtalate) (PET) [133], unsaturated polyester [134-138], vinyl ester [139], polyurethane [140], polyimide [141-143], resol-type phenolic resin [144, 145] etc.

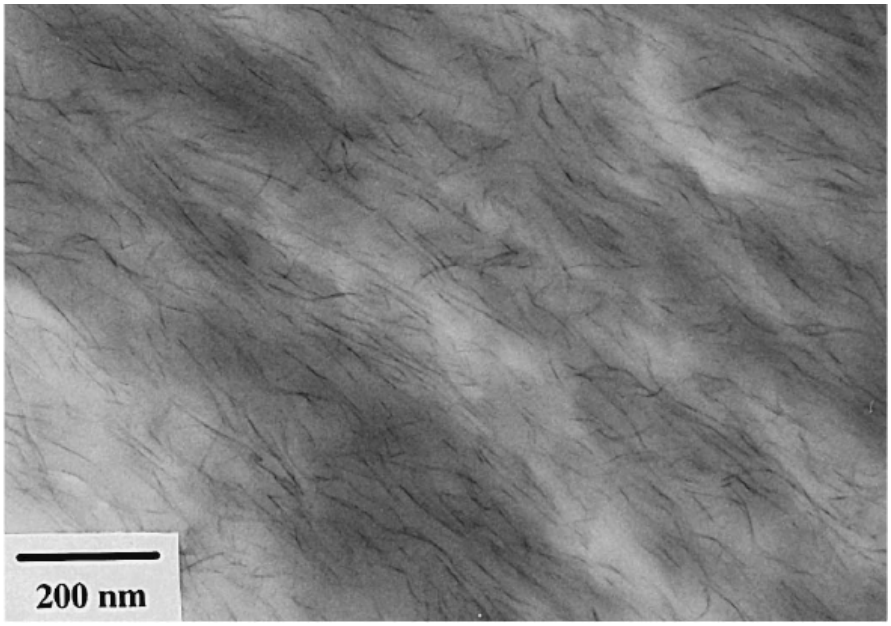

(a)

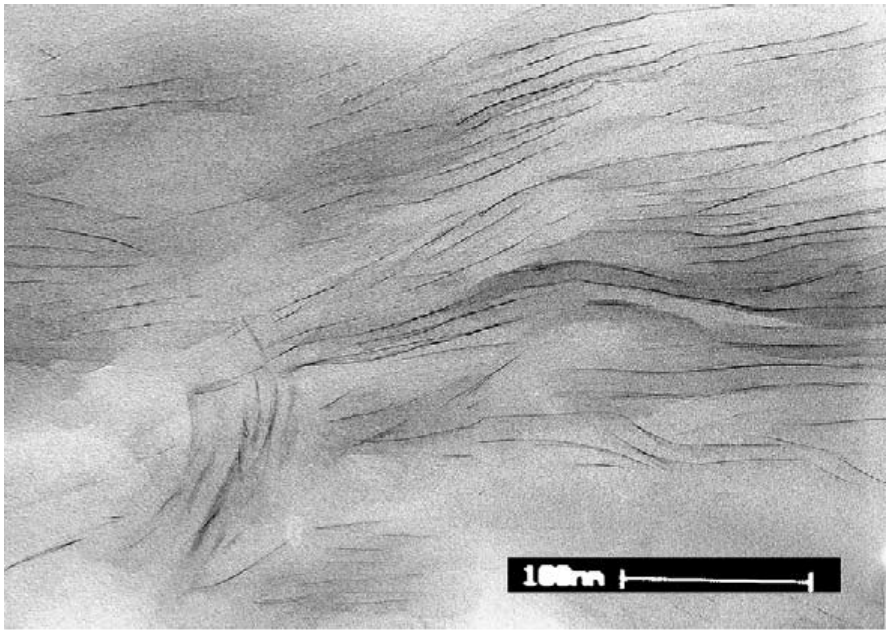

(b)

Figure 1.14 TEM pictures of polymer-organoclay nanocomposites prepared through in-situ polymerization: (a) poly(ε-caprolactam) with 5 wt.% MMT [124], and (b) epoxy resin with 3 wt.% MMT [128].

1.2.3 Properties

The nanoparticles have been incorporated into polymer materials to obtain improved general materials properties (e.g. mechanical and thermal properties) as well as unique functional properties (e.g. barrier resistance and electrical conductivity). Compared with conventional polymer composites, the main reason for these improved properties in nanocomposites is the large surface are of nanoparticles, resulting in the stronger interfacial interactions between the matrix and the nanoparticles.

1.2.3.1 *Mechanical Properties*

The tensile or flexural properties (strength and modulus) of thermoplastic polymer materials can be remarkably improved with the incorporation of nanoclays. For instance, Table 1.4 shows the tensile properties of organoclay-reinforced nylon-6 of low, medium, and high molecular weight (LMW, MMW, and HMW) grades [117]. It can be seen the improvement of tensile strength and modulus become greater with the increase of the polymer molecular weight. Another example is the PET-clay nanocomposites [146], as shown in Table 1.5. It was reported that both flexural strength and modulus of PET were improved more than 50%. Tensile properties of PP nanocomposites have also been investigated [107, 147]. From the Figure 1.15, it can be seen the Young's modulus increased more than 50%, but the yield stress only have slightly improvement. For thermoset materials, the moduli show the similar trend to those of thermoplastics, i.e. the stiffness of materials increase with the incorporation of nanoclays.

Nylon 6 $(HE)_2M_1R_1$ organoclay nanocomposites	Modulus (GPa)	Yield strength (MPa)	Strain at yield point[a] (%)	Elongation at break (%)	
				Crosshead speed 0.51 cm/min	Crosshead speed 5.1 cm/min
LMW					
0.0 wt% MMT	2.82	69.2	4.0	232	28
3.2 wt% MMT	3.65	78.9	3.5	12	11
6.4 wt% MMT	4.92	83.6	2.2	2.4	4.8
MMW					
0.0 wt% MMT	2.71	70.2	4.0	269	101
3.1 wt% MMT	3.66	85.6	3.5	81	18
7.1 wt% MMT	5.61	95.2	2.4	2.5	5
HMW					
0.0 wt% MMT	2.75	69.7	4.0	3.4	129
3.2 wt% MMT	3.92	84.9	3.3	119	27
7.2 wt% MMT	5.70	97.6	2.6	4.1	6.1

[a] Strain measured during modulus and yield strength testing using a cross speed of 0.51 cm/min.

Table 1.4 Select mechanical properties for nylon-6 organoclay nanocomposites [117].

Sample [a]	Clay content [wt.-%]	Flexural strength [kgf cm^{-2}]	Flexural modulus [kgf cm^{-2}]	HDT [c] (18.6 kgf cm^{-2}) [°C]	UV trans. [d] [%]	CO_2 Barrier
Pure PET	0	730	23 000	74	75	0.304
Exfoliated:						
PET/PK-802/Sb/SB	0.66	1200	34 069	100.5	2.23	0.04
PET/CWC/Sb/SB	1.22	1215	34 391	102	1.42	0.01
PET/PK-805/Sb/SB	2.5	1252	34 664	104	0.33	–
Intercalated						
PET/PK-805/SB	2.5	1061	30 301	82	18.6	0.225

Table 1.5 Properties of PET/Clay nanocomposites [144].

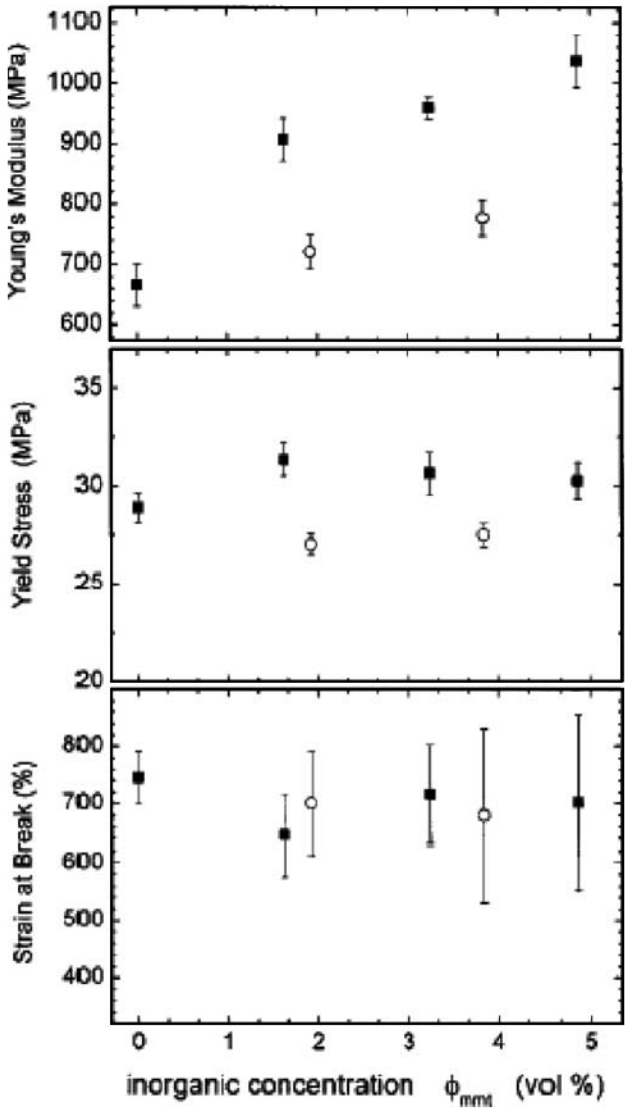

Figure 1.15 Tensile characterization of PP/f-MMT nanocomposites (■) and conventionally filled PP/2C18-MMT macro-composites (○) [145].

However, the tensile or flexural strength of thermoset nanocomposites display a completely different behavior depending on their T_g and testing temperature. In high T_g thermosets, such as unsaturated polyester [148] and epoxy resin [149, 150], neither intercalated nor exfoliated nanoclay lead to an improvement of the tensile stress at break, they rather make the materials more brittle. In contrast, nanocomposites based on both epoxy [151, 152] and polyurethane [153] matrices in the rubbery state exhibit a considerable increase in tensile strength. For instance, 7.5 vol.% of the exfoliated nanoclays improve the tensile strength and modulus of elastomeric epoxy matrix by more than 10-fold [151]. The similar trend of the tensile strength is also observed in silicon rubber nanocomposites [154]. It seems clay nanolayers are more effective in improving mechanical properties when the polymer is in its rubbery state than glassy state. Figure 1.16 shows the possible model to explain these interesting phenomena [151]. In a rubbery matrix, the clay layers may be aligned when strain is applied. Propagation of fracture across the polymer matrix containing aligned silicate layers is energy consuming, and thus the tensile strength and modulus are enhanced. In a glassy matrix, clay particle alignment upon applied strain is minimal and blocking of the facture by the clay layers is less efficient. In phenolic resin-clay nanocomposites, both tensile strength and modulus increased significantly with 2 wt.% and 3 wt.% nanoclays, but decrease steadily at higher silicate content [155].

CNFs can also improve the mechanical properties of various polymer matrices, including thermoplastics and thermosets. For example, PMMA containing 5 wt.% CNFs exhibited improvement of 60-70% in the tensile strength and 135-160% in compressive strength [156]. Finegan et al used surface-treated CNFs to improve the tensile strength

and modulus of PP [157]. It was also reported that PE-CNF composites showed extremely high toughness with moderate strength. The tensile elongation was at least 160 times higher than neat PE materials, and the increase of toughness was more than 200 times [158]. Epoxy-CNF composites were also studied. It was reported that the interaction between CNFs and epoxy was enhanced using a surfactant of polyoxyetheylene alkyl ether (AEO_9), leading to comprehensive improvement in tensile strength (~20%), elastic modulus (~35%), and ultimate strain (~60%) [159]. Koo and his coworkers used oxidized CNFs in epoxy matrix to obtain better dispersion and improved performances [82]. Patton et al prepared epoxy-CNFs composites through vacuum infusion process, and achieved the highest improvement of 37% in flexural strength and 97% in flexural modulus [160]. Table 1.6 shows the details of the experimental results. For vinyl ester resin, however, both flexural strength and modulus decrease due to the poor dispersion and void content increase with increasing nanofiber loading [161].

Other mechanical properties of polymer materials, such as fracture toughness [134, 150, 162-164], can also be improved by adding nanoparticles. The mechanism of toughening is mainly proposed to the creation of rough fracture surface by the incorporation of nanoparticles, which lead to need more energy for the generation of new surface area [134]. Another factor that affects the fracture toughness is the interactions between polymer matrix and nanoparticles [148]. A way to improve the toughness of polymer nanocomposites is to strength the bonding of the polymer-nanoparticle interface [164].

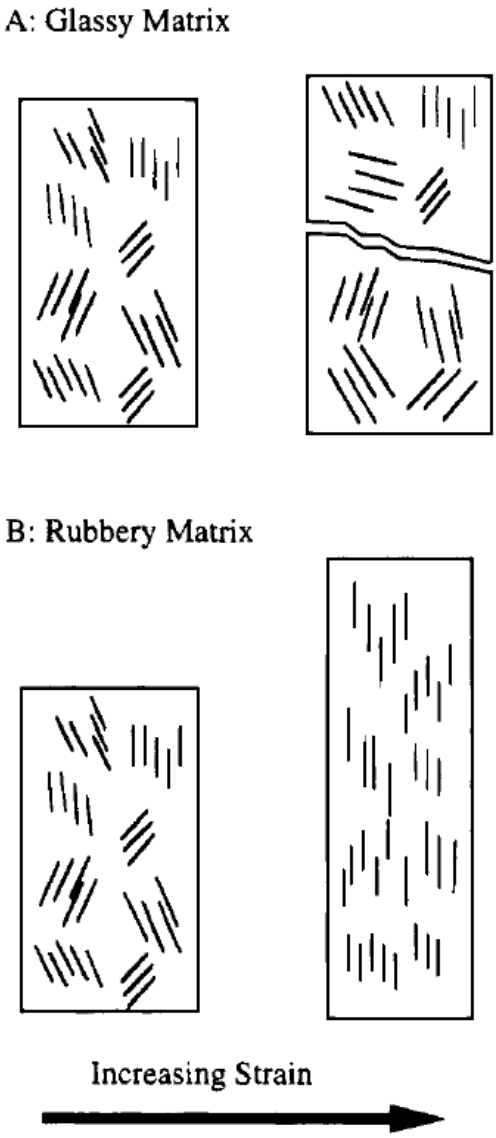

Figure 1.16 Proposed model for the fracture of (A) a glassy and (B) a rubbery polymer-clay exfoliated nanocomposites with increasing strain [149].

Entry	Pressure (psi)	Oil removed	Fib. volume (%)	Ground fiber	Plasma treated	Void content (%)	Flexural modulus (Gpa)	Flexural strength (MPa)
1	14.7	n/a	0	n/a	n/a	n/a	3.98	90
2	1000	No	18.2	Ground[d]	No	1.71	5.33	111
3	500	No	18.2	Ground[d]	No	1.86	5.34	120
4	250	No	18.2	Ground[d]	No	2.31	6.05	121
5	14.7	No	18.2	Ground[d]	No	7.59	5.75	93
6	1000	No	30.8	Unground	No	3.57	7.40	102
7	1000	No	40.0	Unground	No	13.70	7.46	74
8	500	Yes/air[b]	18.2	Unground	yes[e]	2.95	6.81	112
9	500	Yes/N_2[c]	18.2	Ground[d]	yes[e]	1.93	6.70	107
10	500	No	18.2	Ground[d]	Yes[e]	1.93	6.44	121
11	500	Yes/air[b]	18.2	Unground	No	3.27	7.85	123

Table 1.6 VGCNF/epoxy composites prepared using acetone/epoxy solution infusion [160].

1.2.3.2 *Thermal Properties*

Heat distortion temperature (HDT) of a polymeric material is an index of heat resistance towards applied load. It was reported there was a significant increase in HDT from 65 °C for the neat nylon-6 to 152 °C for 4.7 wt.% clay composites [122]. As shown in Table 1.7 [147], the HDT increases from 109 °C for the neat PP to 152 °C for 6 wt.% clay nanocomposite, after that the HDT becomes to level off. Similar trend has also been found in PLA/organoclay nanocomposites [30]. The increase of HDT can be attributed to the strong interaction between nanoparticles and polymer matrix, which provide the mechanical reinforcement to a higher temperature.

Unlike HDT, T_g of nanocomposites did not show a certain enhancement. For epoxy-clay nanocomposites, Messersmith et al [32], Brown et al [165], and Feng et al [166] studied the T_g of epoxy/organoclay nanocomposites using dynamic mechanical analysis (DMA) respectively. They found the T_g of nanocomposites was higher than that of the neat epoxy, and claimed the T_g increase could be attribute to enhanced molecular interaction at the epoxy-clay interface, resulting in restricted motions of polymer segments near the organic-inorganic interface. However, Becker et al [163] and Xu et al [167] found the T_g of epoxy/MMT nanocomposites decreased using dynamic mechanical thermal analysis (DMTA). They thought this T_g reduction might be associated with the void of crosslinking in the composites, because the organoclay could change the chemistry of the curing reaction. Zilg et al also reported the decline of T_g in epoxy nanocomposites [150, 168]. Other researchers found the T_g is almost unchanged with the addition of nanoclays [169]. Due to the complexity of thermoset system, it is very difficult to determine the governing factors, which increase or decrease the T_g [163].

Organically modified mmt (wt%)	HDT (°C)	
	PP/f-MMT	PP/alkyl-MMT
0	109 ± 3	109 ± 3
3	144 ± 5	130 ± 7[a]
6	152 ± 5	141 ± 7[b]
9	153 ± 5	

Table 1.7 HDT of PP/MMT nanocomposites and unfilled PP [147].

1.2.3.3 *Barrier Properties*

Nanoparticles, especially nanoclays, are more effective to enhance the barrier properties of polymer matrix than conventional macro-fillers. The mechanism is believed to the tortuous path generated by nanoplatelets, which retards the progress of the small molecules through the polymer resin (see Figure 1.17) [93, 170]. For instance, the addition of 2 wt.% nanoclay in polyimide can reduce the permeability coefficient of water vapor about ten-fold [93]. Another example is the epoxy/layered silicate nanocomposites. With 3-5 wt.% clay loading, the moisture permeability was decreased significantly [171]. It was also reported that the incorporation of 5 wt.% nanoclay in PS foams could slow down the CO_2 diffusion rate [172].

The diffusion and permeability coefficients of polymer nanocomposites has been modeled based on the particle shape, concentration, orientation, and degree of exfoliation [173-175]. The effects of nanoparticle orientation and incomplete exfoliation on the relative permeability in polymer nanocomposites are shown in Figure 1.18. In this study [173], the volume fraction Φ_s of the nanoparticles is 0.05. It can be seen the relative permeability will decrease with the increasing of the nanosheet length, and the complete exfoliation of nanoparticles will lead to the lowest permeability. In addition, the study showed plate-like morphology is particularly efficient at maximizing the diffusion path when compared to other filler shapes, such as spheres or cubes.

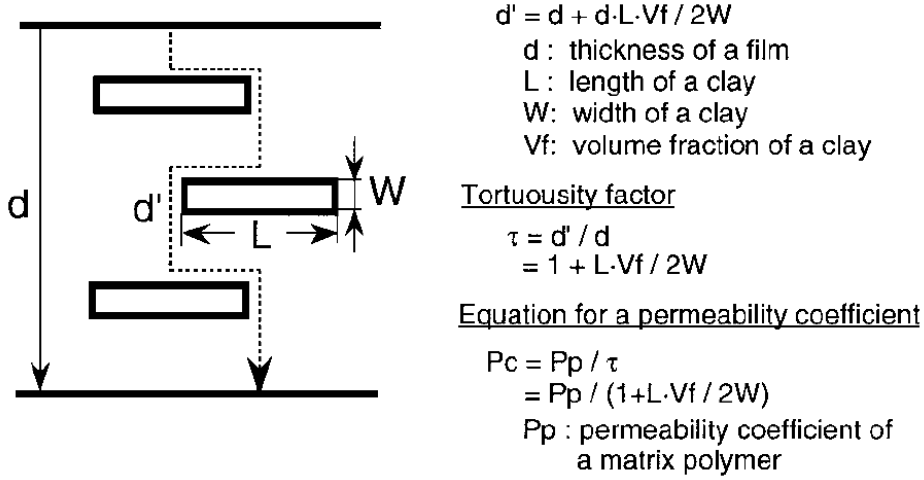

Figure 1.17 A model for the path of a diffusing molecule through polymer-clay nanocomposite [170].

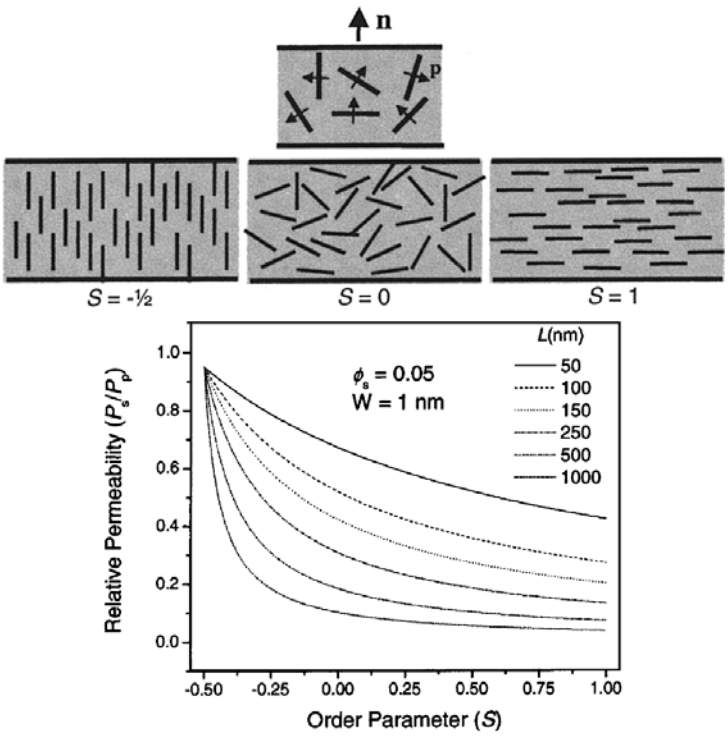

(a)

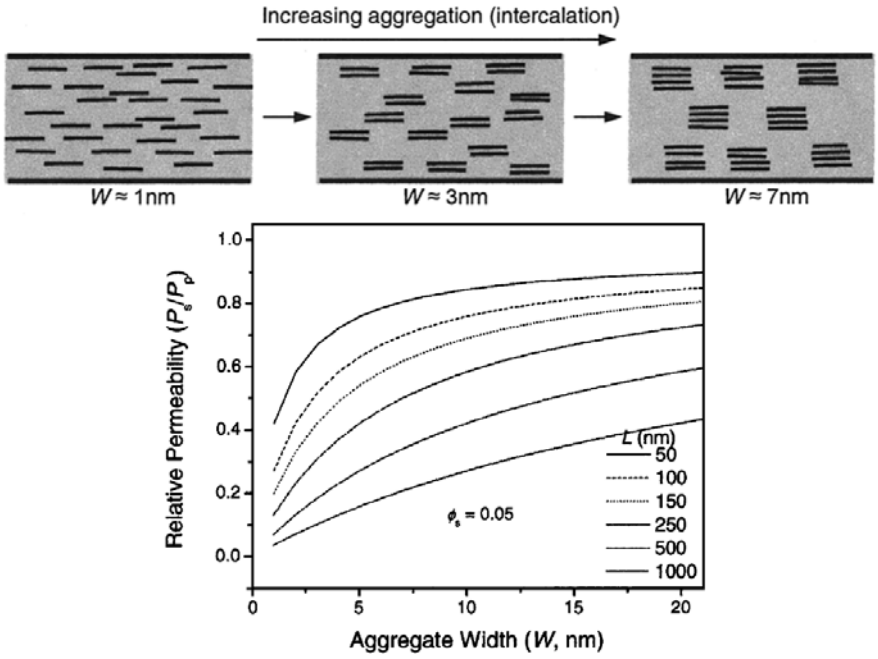

(b)

Figure 1.18 Relative permeability in polymer nanocomposites with (a) various nanoparticle orientation and (b) various degree of exfoliation [173].

1.2.3.4 *Flame Retardance and Thermal Stability*

Polymer nanocomposites have been found to exhibit excellent thermal stability and flame retardance. The cone calorimeter is one of the most effective methods for studying the flammability of materials [176], which can measure fire-relevant properties such as heat release rate (HRR), mass loss rate (MLR), and time to ignition. The thermal stability is usually characterized by thermogravimetric analysis (TGA).

Morgan et al [177] studied the flammability of two polymer nanocomposites made from polycarprolactam (PA-6) and polyethylene-co-vinylacetate (EVA) with nanoclays. As shown in Figure 1.19, the average and peak HRRs are significantly reduced for intercalated and delaminated nanocomposites with low clay content. The similar behaviors were reported in other thermoplastic nanocomposites, such as PP [108], PS [108, 178], and Nylon-12 [179]. For thermoset resins, epoxy [180, 181], unsaturated polyester [182], and vinyl ester [181] systems have been investigated. For example, compared to neat epoxy or vinyl ester resins, the peak HRRs and mean MLRs of 6 wt.% MMT nanocomposites declined about 40% and 35%, respectively [181].

Not only nanoclay, but also CNTs and CNFs can also bring the flame retardance to polymeric materials. Kasiwagi et al [183] investigated the effects of carbon particles, including SWNT, MWNTs, CNFs, and carbon black powders (CBPs), on the flammability of PMMA. As shown in Figure 1.20, a small amount of nanoparticles (0.5 wt.% SWNTs, 1 wt.% MWNTs, or 4 wt.% CNFs) could form a network protective layer of char during the tests and decrease HRRs and MLRs dramatically.

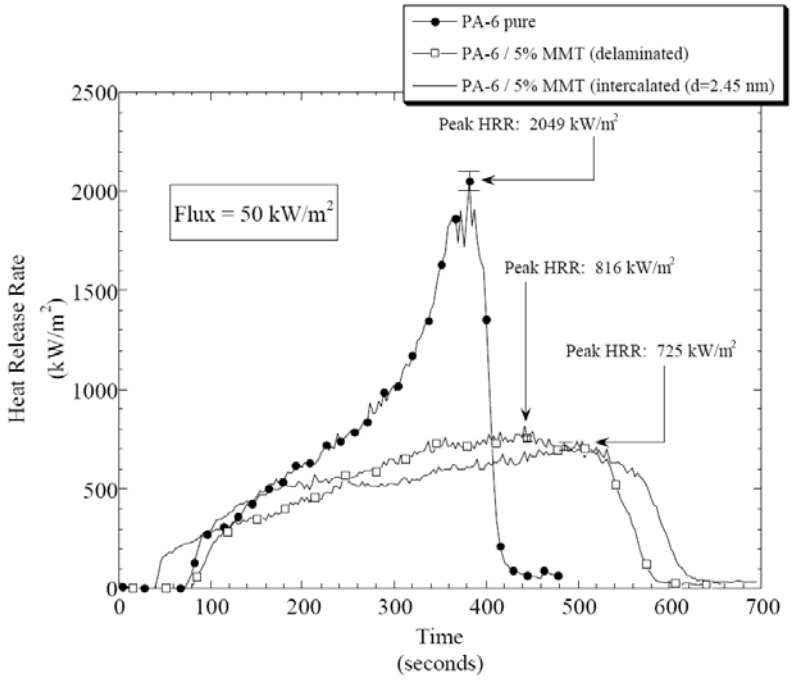

(a)

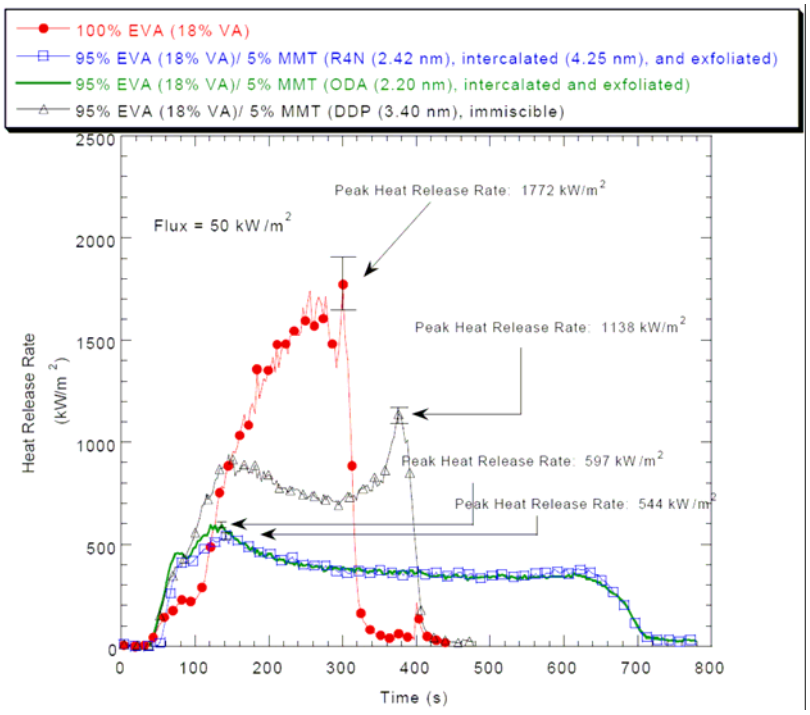

(b)

Figure 1.19 Heat release rate data for (a) pure PA-6, intercalated and delaminated PA-6/MMT nanocomposites, and (b) pure EVA and EVA/MMT nanocomposites [177].

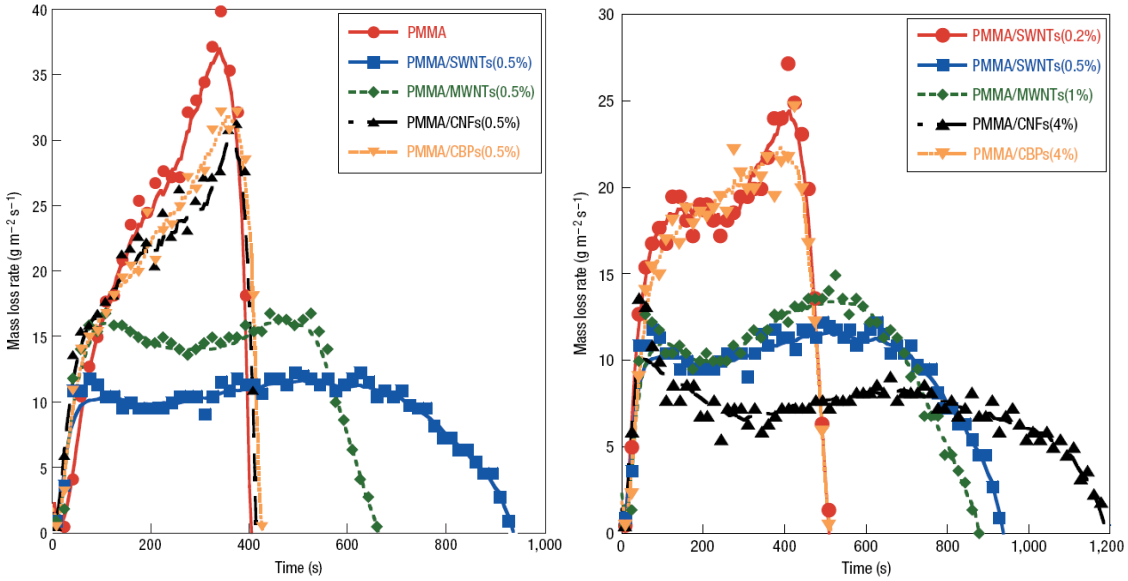

(a)

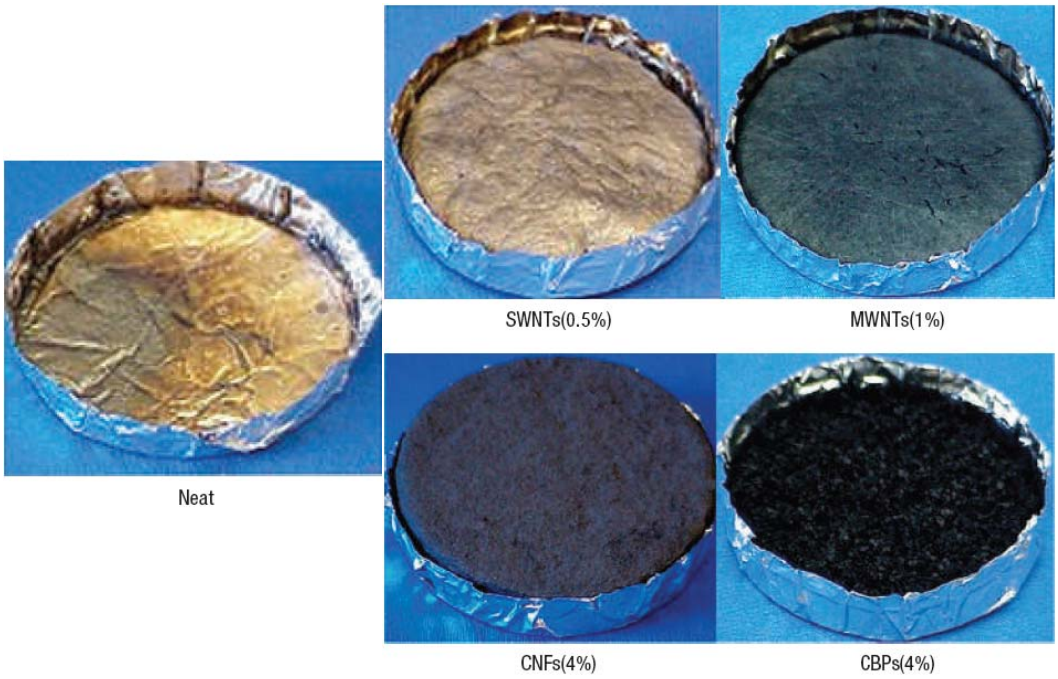

(b)

Figure 1.20 Effects of the nanoparticle type and concentration on (a) mass loss rate and (b) the configuration of the residues (reproduced from [183]).

All these improvement has been attributed to the large surface area of nanoparticles, resulting in strong interactions between the polymer molecules and nanoparticles during combustion. These lead to form continuous char layer, which protect inner polymer materials from flame, restrict the thermal motion of polymer in a confined space, and delay the emission of volatile decomposed products. The similar arguments can be also applied to the significant increase of thermal decomposition temperature of polymer nanocomposites [30, 176, 178, 181, 184].

1.2.3.5 *Other properties*

Nanoparticles can not only improve the mechanical and thermal properties of polymers, but also may provide some functional features to polymeric materials. For instance, the addition of flake graphite [34], CNTs [64-68, 185], and CNFs [63, 161, 186-188] can enhance the electrical conductivity and/or thermal conductivity of polymer matrices. Nano-TiO_2 powders can be used as a UV light absorber to improve the weather stability of polymer products [27]. Another example is the chemical stability and solvent resistance of epoxy resin can be enhanced by adding nanoclays [169].

1.3 Current Challenges in Polymer Composites and Nanocomposites

In a conventional fiber-reinforced polymer composite, the system can be divided into three parts, i.e. fiber, polymer matrix, and the interface between the fiber and the polymer matrix. Generally, the mechanical properties of polymers are much lower than those of long fibers. Moreover, the distance between fibers can be as large as several millimeters. Therefore, the polymer matrix between the long fibers becomes the weak part in the composites [189]. Under tension, compression, shear, or impact, failure of the polymer matrix may take place. In addition, water or other small molecules may diffuse onto the interface between polymer matrix and long fibers, leading to substantially decrease of interfacial strength and adhesive failure between polymer matrix and long fibers. These will affect the performance of the polymer composites in applications.

There are also some problems with the steps of composite processing, such as the moisture effects on composite prepregs [190], and the undesirable fiber buckling during molding [19].

For polymer nanocomposites, excellent properties (e.g. thermal stability and barrier property) exhibit great potential in civil and military applications. Although some polymer nanocomposites have been used in automobile industry, such as Toyota Motor [191] and General Motor Company [28], but there are still many challenges for us to solve. One of them is the dispersion of nanoparticles. Uniform dispersion of nanoparticles against the agglomeration due to van der Waals bonding is the most important step in the processing of nanocomposites. Beside the problems of aggregation of nanoparticles, exfoliation of clay and graphitic layers are essential. Furthermore, the loading of

nanoparticles often cannot reach high level (<10 wt%) in polymer nanocomposites due to the dispersion difficulty. Therefore, mechanical properties of polymer nanocomposites are relatively low compared with those of highly loaded FRPs (>50 wt%).

Another challenge in the processing of polymer nanocomposites is the increase of resin viscosity with the presence of nanoparticles [71, 148]. This may cause many difficulties during composite processing. For instance, high-viscosity resins lead to long mold filling time and poor wettability with between polymer matrix and reinforcement. It is also easy to trap air bubbles and difficult to remove them, resulting in poor performance of the resultant composites.

Other issues, such as low volume fabrication, high cost of nanoparticles, and safety risk, may also hinges on the application of nano-reinforcement materials. Compared with conventional fillers, the high cost rules out the use of CNFs and CNTs for large-volume applications. It is anticipated that as applications for CNFs and CNTs increase, the cost of these nanoparticles will be dramatically reduced [76]. In addition, it is reported that nanoparticles, such as CNFs and CNTs, may bring safety issue to human health. Further study on this issue is needed.

1.4 Objectives and Scope of Study

The overall goal of this project is to prepare high-performance thermoset polymer composites by using both long fibers and nano-particles. Nevertheless, in order to succeed in producing these new composites, two questions need to be answered: How to well disperse nanoparticles into FRPs? Can the resin processability be maintained with the presence of nanoparticles? To answer these questions, an in-depth understanding of the synthesis, processing, morphology, and property relationships of such composites is paramount. Within this scope, I conducted a systematic experimental and theoretical study with three tasks:

Objective I: To synthesize and prepare the thermoset polymer composites with long fibers and nanoparticles. Epoxy, phenolic, and unsaturated polyester resins are used as polymer matrix. Nanoclays and carbon nanofibers are the nano-fillers, and long glass fibers and carbon fibers are used as the conventional reinforcement.

Objective II: To determine the key factors that control the dispersion of nanoparticles and the processability of polymer resins. Then, develop efficient methods to preparing the nanoparticles and long fibers reinforced thermoset composites.

Objective III: To characterize the mechanical and thermal properties of such thermoset resin-nanoparticle-long fiber composites. Finally, find out the optimal condition of the preparing and processing to achieve the best properties of the composites.

In this work, I tried to combine the advantages of both FRP and polymer nanocomposites to produce a superior composite — long fibers and nanoparticles

reinforced polymer composites. Continuous fibers can provide good mechanical properties to the composites, while nanoparticles may strengthen the matrix between the long fibers and provide good barrier properties to protect the interface between the polymer matrix and the long fibers. These efforts will reduce the matrix and interface failure in the composites, and extend the longevity of the composites.

A detailed introduction of polymer composites and nanocomposites was presented in Chapter 1. The materials, preparation, structure, and properties of polymer composites and nanocomposites were reviewed.

In Chapter 2 and 3, the studies were focused on making conventional composites from epoxy prepregs through the process of compression molding. First, the effects of humidity on curing kinetics, glass transition temperature, and tack property of graphite/epoxy prepregs were investigated. Then, the ultrasonic consolidation and marcel formation during the processing of glass fiber/epoxy prepregs were studied.

In Chapter 4 and 5, the research was mainly on thermosetting polymer nanocomposites and long fiber-nanoparticles hybrid composites. The synthesis and properties of epoxy and phenolic composites were described in Chapter 4. The composites based on unsaturated polyester resin were introduced in Chapter 5.

Chapter 6 was about the conclusions and recommendations of my studies. The overview of the study of long fiber and/or nanoparticle reinforced polymer composites is shown in Figure 1.21.

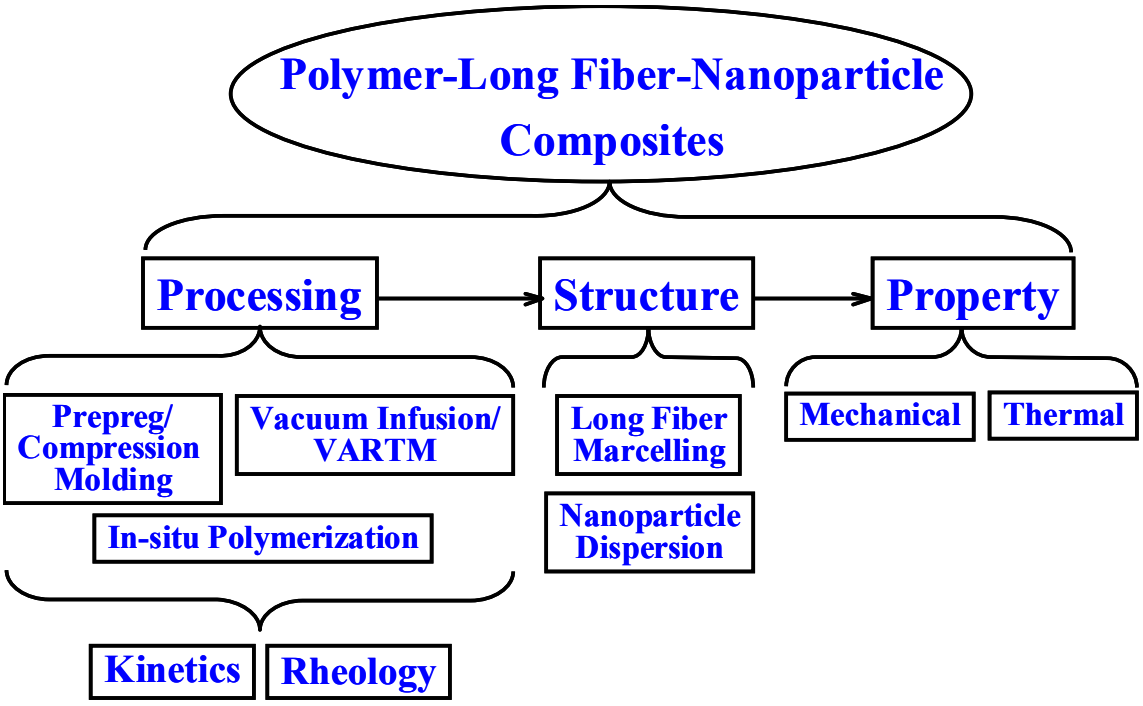

Figure 1.21 Overview of the study of long fiber and/or nanoparticle reinforced polymer composites.

References

1. L. A. Utracki, *Polym. Eng. Sci.*, **35**, 2 (1995).

2. R. P. Sheldon, *Composite Polymeric Materials*, Applied Science Publishers: London/ New York (1982).

3. M. M. Schwartz, *Composite Materials (II)*, Prentice Hall PTR: New Jersey (1996).

4. Z. Rappoport, *The Chemistry of Phenols*, John Wiley & Sons: New Jersey (2003).

5. A. Knop, W. Scheib, *Chemistry and Application of Phenolic Resins*, Springer-Verlag: Berlin/Heidelberg/New York (1979).

6. P. F. Bruins, *Unsaturated Polyester Technology*, Gordon and Breach Science Publishers: New York (1976).

7. *How ingredients influence unsaturated polyester properties*, Amoco Chemicals Corporation/Bulletin IP-70 (1980).

8. R. Burns, *Polyester Molding Compound*, Marcel Dekkar: New York (1982).

9. H. F. Mark, N. M. Bikales, C. G. Overberger, G. Menges, *Encyclopedia of Polymer Science and Engineering*, John Wiley & Sons: New York, **12** (1988).

10. B. C. Trivedi, B. M. Culbertson, *Maleic Anhydride*, Plenum Press: New York/London (1982).

11. K. Dusek, *Epoxy resins and composites,* Springer-Verlag: Berlin/New York (1986).

12. K. L. Loewenstein, *The Manufacturing Technology of Continuous Glass Fibers*, Elsevier Scientific: New York (1973).

13. M. Biron, *Thermosets and Composites – Technical Information for Plastics Users*, Elsevier: Oxford/New York/Tokyo (2004).

14. P. K. Mallick, *Fiber-Reinforced Composites*, Marcel Dekker: New York/Basel (1988).

15. *Modern Plastics Encyclopedia*, McGraw-Hill: New York (1998).

16. M. M. Schwartz, *Composite Materials Handbook*, McGraw-Hill: New York (1991).

17. B. A. Davis, P. J. Gramman, T. A. Osswald, A. C. Rios, *Compression Molding*, Hanser Gardner Publications: Cincinnati (2003).

18. P. K. Mallick, S. Newman, *Composite Materials Technology*, Hanser Publishers: Munich/Vienna/New York (1990).

19. T. G. Gutowski, *Advanced Composites Manufacturing*, John Wiley & Sons: New York (1997).

20. W. H. Seemann, *U.S. Patent 4,902,215* (1990).

21. W. H. Seemann, *U.S. Patent 5,052,906* (1991).

22. W. H. Seemann, *U.S. Patent 5,316,462* (1994).

23. A. Perrella, *Reinforced Plastics*, **39**, 48 (1995).

24. J. F. Monk, *Thermosetting Plastics 2nd Edition*, Addison Wesley Longman: Great British (1997).

25. X. Wang, Z. Qi, F. Wang, *Eng. Plast. Appl.*, **27**, 1 (1998).

26. E. P. Giannelis, *Adv. Mater.*, **8**, 29 (1996).

27. J. H. Koo, *Polymer Nanocomposites – Processing, Characterization, and Applications*, McGraw-Hill: New York/Chicago/San Francisco (2006).

28. E. T. Thostenson, C. Li, T.-W. Chou, *Compos. Sci. Technol.*, **65**, 491 (2005).

29. M. A. Scott, K. A. Carrodo, P. K. Dutta, *Handbook of Layered Materials*, Marcel Dekker: New York (2004).

30. S. S. Ray, M. Okamoto, *Prog. Polym. Sci.*, **28**, 1539 (2003).

31. R. Krishnamoorti, R. A. Vaia, E. P. Giannelis, *Chem. Mater.*, **8**, 1728 (1996).

32. P. B. Messersmith, E. P. Giannelis, *Chem. Mater.*, **6**, 1719 (1994).

33. Z. Wang, T. Lan, T. J. Pinnavaia, *Chem. Mater.*, **8**, 2200 (1996).

34. Y.-X. Pan, Z.-Z. Yu, Y.-C. Ou, G.-H. Hu, *J. Polym. Sci. Part B: Polym. Phy.*, **38**, 1626 (2000).

35. A. Yasmin, J. Lou, I. M. Daniel, *Compos. Sci. Technol.*, **66**, 1182 (2006).

36. F. Hussain, M. Hojjati, M. Okamoto, R. E. Gorga, *J. Compos. Mater.*, **40**, 1511 (2006).

37. L. V. Radushkevich, V. M. Lukyanovich, *Zurn. Fisic. Chim.*, **26**, 88 (1952).

38. M. Monthioux, V. L. Kuznetsov, *Carbon*, **44**, 1621 (2006).

39. S. Iijima, *Nature*, **354**, 56 (1991).

40. S. Iijima, T. Ichihashi, *Nature*, **363**, 603 (1993).

41. J. W. Mintmire, B. I. Dunlap, C. T. White, *Phys. Rev. Lett.*, **68**, 631 (1992).

42. N. Hamada, S. Sawada, A. Oshiyama, *Phys. Rev. Lett.*, **68**, 1579 (1992).

43. S. Iijima, P.M. Ajayan, T. Ichihashi, *Phys. Rev. Lett.*, **69**, 3100 (1992).

44. D. S. Bethune, C. H. Kiang, M. S. de Vries, G. Gorman, R. Savoy, J. Vazquez, R. Beyers, *Nature*, **363**, 605 (1993).

45. M. J. Yacaman, M. M. Yoshida, L. Rendon, J. G. Santiesteban, *Appl. Phys. Lett.*, **62**, 202 (1993).

46. T. Guo, B. Nikolaev, A. G. Rinzler, D. Tomanek, D. T. Colbert, R. E. Smalley, *J. Phys. Chem.*, **99**, 10694 (1995).

47. H. Dai, E. W. Wong, C. M. Lieber, *Science*, **272**, 523 (1996).

48. M. M. J. Treacy, T. W. Ebbesen, J. M. Gilson, *Nature*, **381**, 678 (1996).

49. A. Thess, R. Lee, P. Nikolaev, H. Dai, P. Petit, J. Robert, C. Xu, Y. H. Lee, S. G. Kim, A. G. Rinzler, D. T. Colbert, G. E. Scuseria, D. Tomanek, J. E. Fischer, R. E. Smalley,

Science, **273**, 483 (1996).

50. L. X Benedict, S. G. Louie, M. L. Cohen, *Solid State Comm.*, **100**, 177 (1996).

51. C. Journet, W. K. Maser, P. Bernier, A. Loiseau, M. Lamy de la Chapelle, S. Lefrant, P. Deniard, R. Lee, J. E. Fischer, *Nature*, **388**, 756 (1997).

52. E. W. Wong, P. E. Sheehan, C. M. Lieber, *Science*, **277**, 1971 (1997).

53. M. Tian, F. Li, L. Chen, Z. Mao, *Phys. Rev. B*, **58**, 1166 (1998).

54. Y.-K. Kwon, S. Saito, D. Tomanek, *Phys. Rev. B*, **58**, R13314 (1998).

55. W. Yi, L. Lu, D.-L. Zhang, Z.-W. Pan, S.-S. Xie, *Phys. Rev. B*, **59**, R9015 (1999).

56. M. F. Yu, O. Lourie, M. J. Dyer, K. Moloni, T. F. Kelly, R. S. Ruoff, *Science*, **287**, 637 (2000).

57. V. N. Popov, *Mater. Sci. Eng. R*, **43**, 61 (2004).

58. L. S. Schadler, S. C. Giannaris, P. M. Ajayan, *Appl. Phys. Lett.*, **73**, 3842 (1998).

59. C. Bower, R. Rosen, L. Jin, J. Han, O. Zhou, *Appl. Phys. Lett.*, **74**, 3317 (1999).

60. R. Haggenmueller, H. H. Gommans, A. G. Rinzler, J. E. Fischer, K. I. Winey, *Chem. Phys. Lett.*, **330**, 219 (2000).

61. Z. Jin, K. P. Pramoda, G. Xu, S. H. Goh, *Chem. Phys. Lett.*, **337**, 43 (2001).

62. J. C. Kearns, R. L. Shambaugh, *J. Appl. Polym. Sci.*, **86**, 2079 (2002).

63. K. Lozano, E. V. Barrera, *J. Appl. Polym. Sci.*, **79**, 125 (2001).

64. A. Allaoui, S. Bai, H.M. Cheng, J.B. Bai, *Compos. Sci. Technol.*, **62**, 1993 (2002).

65. K.-T. Lau, M. Lu, C.-K. Lam, H.-Y. Cheung, F.-L. Sheng, H.-L. Li, *Compos. Sci. Technol.*, **65**, 719 (2005).

66. J. Sandler, M. S. P. Shaffer, T. Prasse, W. Bauhofer, K. Schulte, A. H. Windle, *Polymer*, **40**, 5967 (1999).

67. B. Safadi, R. Andrews, E. A. Grulke, *J. Appl. Polym. Sci.*, **84**, 2660 (2002).

68. L. Valentini, D. Puglia, E. Frulloni, I. Armentano, J. M. Kenny, S. Santucci, *Compos. Sci. Technol.*, **64**(1), 23 (2004).

69. H. Ma, J. Zeng, M. L. Realff, S. Kumar, D. A. Schiraldi, *Polym. Mater. Sci. Eng.*, **86**, 411 (2002).

70. J. Sandler, A. H. Windle, P. Werner, V. Altstadt, M. V. Es, M. S. P. Shaffer, *J. Mater. Sci.*, **38**, 2135 (2003).

71. J. Xu, *Rheology of Polymeric Suspensions: Polymer Nanocomposites and Waterborne Coatings*, Doctorial Dissertation, The Ohio State University (2005).

72. N. M. Rodriguez, *J. Mater. Res.*, **8**, 3233 (1993).

73. A. Oberlin, M. Endo, T. Koyama, *J. Cryst. Growth*, **32**, 335 (1976).

74. I. Chun, D. H. Reneker, H. Fong, X. Fang, J. Deitzel, N. B. Tan, K. Kearns, *J. Adv. Mater.*, **31**, 36 (1999).

75. Y. A. Dzenis, Y. K. Wen, *Mater. Res. Soc. Symp. Proc.*, **702**, 173 (2002).

76. K. P. De Jong, J. W. Geus, *Catal. Rev. Sci. Eng.*, **42**, 481 (2000).

77. J. Fröhlich, R. Thomann, O. Gryshchuk, J. Karger-Kocsis, R. Mülhaupt, *J. Appl. Polym. Sci.*, **92**, 3088 (2004).

78. J. H. Koo, H. Stretz, A. Bray, W. Wootan, S. Mulich, B. Powell, J. Weispfenning, T. Grupa, *Proc. SAMPE 2002 ISSE*, SAMPE, Long Beach, California (2002).

79. J. H. Koo, H. Stretz, A. Bray, J. Weispfenning, Z. P. Luo, W. Wootan, *Proc. SAMPE 2003 ISSE*, SAMPE, Long Beach, California (2003).

80. J. H. Koo, C. U. Pittman, Jr., K. Liang, H. Cho, L. A. Pilato, Z. P. Luo, G. Pruett, P. Winzek, *Proc. SAMPE 2003 ISTC*, SAMPE, Dayton, Ohio (2003).

81. J. H. Koo, L. A. Pilato, P. Winzek, S. Shivakumar, C. U. Pittman, Z. P. Luo, *Proc. SAMPE 2004 ISSE*, SAMPE, Long Beach, California (2004).

82. J. H. Koo, L. A. Pilato, G. Wissler, A. Abusafieh, J. Weispfenning, *Proc. SAMPE 2005 ISSE*, SAMPE, Long Beach, California (2005).

83. B. K. G. Theng, *Formation and properties of clay-polymer complexes*, Elsevier: New York (1979).

84. D. J. Greenland, *J. Colloid Sci.*, **18**, 647 (1963).

85. K. E. Strawhecker, E. Manias, *Chem. Mater.*, **12**, 2943 (2000).

86. M. S. P. Shaffer, A. H. Windle, *Adv. Mater.*, **11**, 937 (1999).

87. B. O. Lee, W. J. Woo, M.-S. Kim, *Macromol. Mater. Eng.*, **286**, 114 (2001).

88. N. Ogata, S. Kawakage, T. Orgihara, *J. Appl. Polym. Sci.*, **66**, 573 (1997).

89. X. Zhao, K. Urano, S. Ogasawara, *Colloid Polym. Sci.*, **267**, 899 (1989).

90. E. Ruiz-Hitzky, P. Aranda, B. Casal, J. C. Galvan, *Adv. Mater.*, **7**, 180 (1995).

91. J. Billingham, C. Breen, J. Yarwood, *Vibr. Spectosc.*, **14**, 19 (1997).

92. R. Levy, C. W. Francis, *J. Colloid Interface Sci.*, **50**, 442 (1975).

93. K. Yano, A. Usuki, A. Okada, T. Kurauchi, O. Kamigaito, *J. Polym. Sci. Part A: Polym. Chem.*, **31**, 2493 (1993).

94. C. A. Mitchell, J. L. Bahr, S. Arepalli, J. M. Tour, R. Krishnamoorti, *Macromolecules*, **35**, 8825 (2002).

95. B. Safadi, R. Andrews, E. A. Grulke, *J. Appl. Polym. Sci.*, **84**, 2660 (2002).

96. G. Jimenez, N. Ogata, H. Kawai, T. Ogihara, *J. Appl. Polym. Sci.*, **64**, 2211 (1997).

97. N. Ogata, G. Jimenez, H. Kawai, T. Ogihara, *J. Polym. Sci. Part B: Polym. Phys.*, **35**, 389 (1997).

98. R. A. Vaia, E. P. Giannelis, *Macromolecules*, **30**, 7990 (1997).

99. J. Shen, X. Han, L. J. Lee, *J. Cellular Plastics*, **42**, 105 (2006).

100. R. A. Vaia, S. Vasudevan, W. Krawiec, E. P. Giannelis, *Adv. Mater.*, **7**, 154 (1995).

101. R. A. Vaia, K. D. Jandt, E. J. Kramer, E. P. Giannelis, *Macromolecules*, **28**, 8080 (1995).

102. R. A. Vaia, K. D. Jandt, E. J. Kramer, E. P. Giannelis, *Chem. Mater.*, **8**, 2628 (1996).

103. R. A. Vaia, E. P. Giannelis, *Macromolecules*, **30**, 8000 (1997).

104. E. Manias, W. J. Han, K. D. Jandt, E. J. Kramer, E. P. Giannelis, *Macromolecules*, **33**, 7955 (2000).

105. M. Kato, A. Usuki, A. Okada., *J. Appl. Polym. Sci.*, **66**, 1781 (1997).

106. M. Kawasumi, N. Hasegawa, M. Kato, A. Usuki, A. Okada., *Macromolecules*, **30**, 6333 (1997).

107. N. Hasegawa, M. Kawasumi, M. Kato, A. Usuki, A. Okada., *J. Appl. Polym. Sci.*, **67**, 87 (1998).

108. J. W. Gilman, C. L. Jackson, A. B. Morgan, R. Harris, Jr., E. Manias, E. P. Giannelis, M. Wuthenow, D. Hilton, S. H. Phillips, *Chem. Mater.*, **12**, 1866 (2000).

109. P. H. Nam, P. Maiti, M. Okamoto, T. Kotaka, N. Hasegawa, A. Usuki, *Polymer*, **42**, 9633 (2001).

110. P. Svoboda, C. Zeng, H. Wang, L. J. Lee, D. L. Tomasko, *J. Appl. Polym. Sci.*, **85**, 1562 (2002).

111. K. Lozano, J. Bonilla-Rios, E. V. Barrera, *J. Appl. Polym. Sci.*, **80**: 1162 (2001).

112. H. Ma, J. Zeng, M. L. Realff, S. Kumar, D. A. Schiraldi, *Compos. Sci. Technol.*, **63**, 1617 (2003).

113. P. Cortes, K. Lozano, E. V. Barrera, J. Bonilla-Rios, *J. Appl. Polym. Sci.*, **89**, 2527 (2003).

114. L. Liu, Z. Qi, X. Zhu, *J. Appl. Polym. Sci.*, **71**, 1133 (1999).

115. D. M. Lincoln, R. A. Vaia, Z. G. Wang, B. S. Hsiao, *Polymer*, **42**, 1621 (2001).

116. H. R. Dennis, D. L. Hunter, D. Chang, S. Kim, J. L. White, J. W. Cho, D. R. Paul, *Polymer*, **42**, 9513 (2001).

117. T. D. Fornes, P. J. Yoon, H. Keskkula, D. R. Paul, *Polymer*, **42**, 9929 (2001).

118. T. D. Fornes, D. L. Hunter, D. R. Paul, *Macromolecules*, **37**, 1793 (2004).

119. R. A. Vaia, B. B. Sauer, O. K. Tse, E. P. Giannelis, *J. Polym. Sci. Part B: Polym. Phys.*, **35**, 59 (1997).

120. E. Hammel, X. Tang, M. Trampert, T. Schmitt, K. Mauthner, A. Eder, P. Potschke, *Carbon*, **42**, 1153 (2004).

121. A. Usuki, M. Kawasumi, Y. Kojima, A. Okada, T. Kurauchi, O. Kamigaito, *J. Mater. Res.*, **8**, 1174 (1993).

122. A. Usuki, Y. Kojima, M. Kawasumi, A. Okada, Y. Fukushima, T. Kurauchi, O. Kamigaito, *J. Mater. Res.*, **8**, 1179 (1993).

123. P. B. Messersmith, E. P. Giannelis, *J. Polym. Sci. Part A: Polym. Chem.*, **33**, 1047 (1995).

124. R. A. Vaia, G. Price, P. N. Ruth, H. T. Nguyen, J. Lichtenhan, *Appl. Clay Sci.*, **15**, 67 (1999).

125. K. H. Chen, S. M. Yang, *J. Appl. Polym. Sci.*, **86**, 414 (2001).

126. I.-J. Chin, T. Thurn-Albrecht, H.-C. Kim, T. P. Russell, J. Wang, *Polymer*, **42**, 5947 (2001).

127. C. S. Triantafillidis, P. C. LeBaron, T. J. Pinnavaia, *Chem. Mater.*, **14**, 4088 (2002).

128. C. Chen, M. Khobaib, D. Curliss, *Prog. Org. Coat.*, **47**, 376 (2003).

129. C. Zeng, L. J. Lee, *Macromolecules*, **34**, 4098 (2001).

130. M. S. P. Shaffer, K. Koziol, *Chem. Commun.*, (18), 2074 (2002).

131. Z. Jia, Z. Wang, C. Xu, J. Liang, B. Wei, D. Wu, S. Zhu, *Mater. Sci. Eng. A*, **A271**, 395 (1999).

132. C. Velasco-Santos, A. L. Martinez-Hernandez, F. T. Fisher, R. Ruoff, V. M. Castano, *Chem. Mater.*, **15**, 4470 (2003).

133. Y. Ke, C. Long, Z. Qi, *J. Appl. Polym. Sci.*, **71**, 1139 (1999).

134. X. Kornmann, L. A. Berglund, J. Skerte, E. P. Giannelis, *Polym. Eng. Sci.*, **38**, 1351 (1998).

135. D. J. Suh, Y. T. Lim, O. O. Park, *Polymer*, **41**, 8857 (2000).

136. X.-A. Fu, S. Qutubuddin, *Polym. Eng. Sci.*, **44**, 345 (2004).

137. L. Xu, L. J. Lee, *Polymer*, **45**, 7325 (2004).

138. I. Mironi-Harpaz, M. Narkis, A. Siegmann, *Polym. Eng. Sci.*, **45**, 174 (2005).

139. A. P. Shah, R. K. Gupta, *2002 ANTEC Proc. – SPE*, **60**, 2270 (2002).

140. C. Zilg, R. Thomann, R. Muelhaupt, J. Finter, *Adv. Mater.*, **11**, 49 (1999).

141. Y. Yang, Z. Zhu, J. Yin, X. Wang, Z. Qi, *Polymer*, **40**, 4407 (1999).

142. A. Gu, S.-W. Kuo, F.-C. Chang, *J. Appl. Polym. Sci.*, **79**, 1902 (2001).

143. C. Park, Z. Ounaies, K. A. Watson, R. E. Crooks, J. Smith Jr., S. E. Lowther, J. W. Connell, E. J. Siochi, J. S. Harrison, T. L. St. Clair, *Chem. Phys. Lett.*, **364**, 303 (2002).

144. H. Y. Byun, M. H. Choi, I. J. Chung, *Chem. Mater.*, **1**3, 4221 (2001).

145. L. Zhi, T. Zhao, Y. Yu, *Scripta Mater.*, **47**, 875 (2002).

146. T.-Y. Tsai, C.-H. Li, C.-H. Chang, W.-H. Cheng, C.-L. Hwang, R.-J. Wu, *Adv. Mater.*, **17**, 1769 (2005).

147. P. H. Nam, P. Maiti, M. Okamoto, T. Kotaka, *Proc. Nanocomposites*, Chicago, Illinois, USA (2001).

148. L. Xu, *Integrated Analysis of Liquid Composite Molding (LCM) Process*, Doctorial Dissertation, The Ohio State University (2004).

149. T. Lan, P. D. Kaviratna, T. J. Pinnavaia, *Chem. Mater.*, **7**, 2144 (1995).

150. C. Zilg, R. Mülhaupt, J. Finter, *Macromol. Chem. Phys.*, **200**, 661 (1999).

151. T. Lan, T. J. Pinnavaia, *Chem. Mater.*, **6**, 2216 (1994).

152. Z. Wang, T. J. Pinnavaia, *Chem. Mater.*, **10**, 1820 (1998).

153. Z. Wang, T. J. Pinnavaia, *Chem. Mater.*, **10**, 3769 (1998).

154. S.-J. Wang, C.-F. Long, X.-Y. Wang, Q. Li, Z.-N. Qi, *J. Appl. Polym. Sci.*, **69**, 1557 (1998).

155. M. H. Choi, I. J. Chung, *J. Appl. Polym. Sci.*, **90**, 2316 (2003).

156. J. Zeng, B. Saltysiak, W. S. Johnson, D. A. Schiraldi, S. Kumar, *Compos. Part B,* **35B**, 245 (2004).

157. I. C. Finegan, G. G. Tibbetts, D. G. Glasgow, J.-M. Ting, M. L. Lake, *J. Mater. Sci.*, **38**, 3485 (2003).

158. K. Lozano, S. Yang, R. E. Jones, *Carbon*, **42**, 2329 (2004).

159. Z. Ying, J.-H. Du, S. Bai, F. Li, C. Liu, H.-M. Cheng, *Int. J. Nanoscience*, **1**, 425 (2002).

160. R. D. Patton, C. U. Pittman Jr., L. Wang, J. R. Hill, *Compos. Part A,* **30A**, 1081 (1999).

161. J. Xu, J. P. Donohoe, C. U. Pittman Jr., *Compos. Part A,* **35A**, 693 (2004).

162. A. S. Zerda, A. J. Lesser, *J. Polym. Sci. Part B: Polym.Phys.*, **39**, 1137 (2001).

163. O. Becker, R. Varley, G. Simon, *Polymer*, **43**, 4365 (2002).

164. L. Xu, L. J. Lee, *Polym. Eng. Sci.*, **45**, 496 (2005).

165. J. M. Brown, D. Curliss, R. A. Vaia, *Chem. Mater.*, **12**, 3376 (1998).

166. W. Feng, A. Ait-Kadi, B. Riedl, *Polym. Eng. Sci.*, **42**, 1827 (2002).

167. W.-B. Xu, S.-P. Bao, P.-S. He, *J. Appl. Polym. Sci.*, **84**, 842 (2001).

168. C. Zilg, R. Thomann, J. Finter, R. Mülhaupt, *Macromol. Mater. Eng.*, **280/281**, 41 (2000).

169. J. Massam, T. J. Pinnavaia, *Mater. Res. Soc. Symp. Proc.*, **520**, 223 (1998).

170. K. Yano, A. Usuki, A. Okada, *J. Polym. Sci. Part A: Polym. Chem.*, **35**, 2289 (1997).

171. J.-K. Kim, C. Hu, R. S. Woo, M.-L. Sham, *Compos. Sci. Technol.*, **65**, 805 (2005).

172. X. Han, C. Zeng, L. J. Lee, K. W. Koelling, D. L. Tomasko, *Polym. Eng. Sci.*, **43**, 1261 (2003).

173. R. K. Bharadwaj, *Macromolecules*, **34**, 9189 (2001).

174. A. Sorrentino, M. Tortora, V. Vittoria, *J. Polym. Sci. Part B: Polym.Phys.*, **44**, 265 (2006).

175. C. Lu, Y.-W. Mai, *Phys. Rev. Lett.*, **95**, 088303 (2005).

176. J. W. Gilman, *Appl. Clay Sci.*, **15**, 31 (1999).

177. A. B. Morgan, J. W. Gilman, T. Kashiwagi, C. L. Jackson, *Proc. Fire Retardant Chemicals Association*, Washington, DC, 25 (2000).

178. J. Zhu, A. B. Morgan, F. J. Lamelas, C. A. Wilkie, *Chem. Mater.*, **13**, 3774 (2001).

179. M. Alexandre, P. Dubois, *Mater. Sci. Eng. R*, **28**, 1 (2000).

180. J. W. Gilman, T. Kashiwagi, J. E. T. Brown, S. Lomakin, E. P. Giannelis, E. Manias, *Proc. SAMPE 1998 ISSE*, SAMPE, Anaheim, California, **43**, 1053 (1998).

181. S. Al-Malaika, A. Golovoy, C. A. Wilkie, *Chemistry and technology of polymer additives*, Blackwell Science: Oxford (1999).

182. S. Nazaré, B. K. Kandola, A. R. Horrocks, *Polym. Adv. Technol.*, **17**, 294 (2006).

183. T. Kashiwagi, F. Du, J. F. Douglas, K. I. Winey, R. H. Harris Jr, J. R. Shields, *Nature Mater.*, **4**, 928 (2005).

184. M. Zanetti, G. Camino, R. Thomann, R. Mulhaupt, *Polymer*, **42**, 4501 (2001).

185. A. Nogales, G. Broza, Z. Roslaniec, K. Schulte, I. Sics, B. S. Hsiao, A. Sanz, M. C. García-Gutiérrez, D. R. Rueda, C. Domingo, T. A. Ezquerra, *Macromolecules*, **37**, 7669 (2004).

186. T. Gibson, B. Rice, W. Ragland, *Proc. SAMPE 2005 ISSE*, SAMPE, Long Beach, California (2005).

187. S. A. Gordeyev, F. J. Macedo, J. A. Ferreira, F. W. J. Van Hattum, C. A. Bernardo, *Physica B*, **279**, 33 (2000).

188. B. A. Higgins, W. J. Brittain, *Eur. Polym. J.*, **41**, 889 (2005).

189. C. A. Harper, *Handbook of Plastics, Elastomers, and Composites, 4th Ed.*, McGraw-Hill: New York/Chicago/San Francisco (2002).

190. Z. N. Sanjana, W. H. Schaefer, J. R. Ray, *Polym. Eng. Sci.*, **21**, 474 (1981).

191. F. Gao, *Mater. Today*, **7**, 50 (2004).

CHAPTER 2

EFFECTS OF HUMIDITY ON CURING KINETICS, GLASS TRANSITION TEMPERATURE, AND TACK PROPERTY OF GRAPHITE/EPOXY PREPREGS

2.1 Introduction

Carbon fibers reinforced epoxy resins have been widely used in aerospace applications because of their excellent mechanical and thermal properties [1]. Graphite/epoxy prepreg is usually prepared first to make epoxy composites through the autoclave or compression molding process. It has been found that the curing behavior varies between the prepreg samples under dry and humid conditions, resulting in the property variation of the cured parts. Although many studies have been done on the cure kinetics and the effect of humidity exposure, most of them concentrated on either the curing kinetics of the neat epoxy resin with a constant content of moisture or impurity [2-6], or the moisture effects on the cured epoxy samples [7-10]. Sanjana and the co-workers [11] studied the effect of moisture on the reactivity of graphite/epoxy prepregs, however, their work only focused on high humidity environments. A systematic study need be carried out to explain the inconsistent cure behavior of epoxy prepregs at various humidity levels, especially the effect of humidity on the curing kinetics.

Tack is defined by the American Society for Testing and Materials (ASTM) as "the force required to separate an adherent and an adhesive at the interface shortly after they have been brought rapidly into contact under light load of short duration" [12]. The tack property of prepregs is an important factor during the preparation of polymer composites, especially for lamination and lay-up processes. Prepreg tape that has insufficient tack can result in the prepreg shifting during lay-up or lifting after being laid up or sliding out of the proper position during molding. These undesirable movements may require additional manual adjustment to put the part altogether, or lead to voids or gaps between individual prepreg tapes, or result in the part not within the desired dimensional or structural tolerances. On the other hand, too high-tack prepreg can cause difficulties to separate and reposition the misplaced prepreg ply. The tack property of epoxy prepregs is sensitive to a wide range of factors, such as the surface roughness of the samples, the chemical structure and plasticization of the resins, and the contact load and dwell time [13-15]. Some of these factors have strong affinities to environmental temperature, humidity level, and exposure time of prepregs.

Glass transition temperature (T_g) is an important characteristic of prepregs, which may be affected by the conversion of polymer resin and the moisture (plasticizer) content in materials. Because tack property is also affected by these factors and T_g is easy to be determined in practice, it is valuable to compare the tack property with the T_g of prepregs.

The purpose of this work is to investigate the moisture effects on the curing behavior and T_g of graphite/epoxy prepregs, and to establish the relationship between the tack property and the T_g of prepreg samples.

2.2 Experimental

2.2.1 Materials

The epoxy prepregs used in this study were Hexcel® IM7/8552 graphite/epoxy prepregs. The neat 8552 epoxy resin was an amine cured epoxy resin system, which was provided by Bell Helicopter. Salts used in humidity chambers were obtained from Omega Engineering Inc, including magnesium chloride ($MgCl_2$), magnesium nitrate ($Mg(NO_3)_2$), and sodium chloride (NaCl).

2.2.2 Preparation of Humidity Chambers

The desired relative humidity (RH) in three chambers was obtained by using saturated salt solutions of $MgCl_2$ (33% RH), $Mg(NO_3)_2$ (53% RH), and NaCl (75% RH) respectively [16, 17]. One desiccator with calcium chloride desiccant was used to imitate a low-humidity condition (0% RH). Another desiccator with distilled water at the bottom was to mimic 100% RH environment. All humidity chambers were placed in a room with temperature controlled at 25 ± 1 °C.

2.2.3 Test of Moisture Absorption

The samples of graphite/epoxy prepregs were placed in five humidity chambers respectively. The weights of all samples were measured by a Mettler H80 analytical balance (0.1 mg accuracy). For each sample, three specimens were tested. The equilibrium water contents in the graphite/epoxy prepreg samples were

determined by the samples that were placed in the humidity chambers at room temperature for 100 days.

The moisture content of each graphite/epoxy prepreg sample was calculated by the following equation,

$$\text{Moisture Content } \% = \frac{M_t - M_0}{M_0} \times 100\% \tag{2.1}$$

where

M_t = sample weight on the *t*-th days, g,

M_0 = sample weight at the zero day (the initial weight), g.

2.2.4 Measurement of Complex Viscosity

Rheological data were obtained using a TA ARES Rheometer with TA Orchestrator control software. Dynamic torsion tests were carried out with the frequency from 0.01 to 100 rad/s at room temperature. Two samples with different RH were chosen, one was the test sample in the 0% RH desiccator, the other was in the chamber with 100% RH. The testing samples of the graphite/epoxy prepregs were 50 mm in length and 3.2 mm in width.

The storage and loss modulus of prepreg samples were determined by dynamic torsion tests. Based on Equation (2.2), the complex viscosities were calculated as

$$\eta^* = \frac{G^*}{\omega} = \frac{\sqrt{G'^2 + G''^2}}{\omega} \tag{2.2}$$

where

G' = storage modulus in torsion, MPa,

G'' = loss modulus in torsion, MPa,

G^* = complex modulus in torsion, MPa,

ω = frequency, rad/s,

η^* = complex viscosity, Pa·s.

2.2.5 Measurement of Glass Transition Temperature and Resin Conversion

The T_g and reaction exotherm of aged prepreg samples was measured by a TA 2920 differential scanning calorimeter (DSC). About 10 mg of the graphite/epoxy prepreg sample was sealed in a hermetic aluminum sample pan. The sample was then followed by thermal scanning from -30 to 300°C at a heating rate of 5°C/min. The measured heat flow data were converted to conversion of the samples by assuming that thermal properties of the samples were independent of temperature in the test range. For each sample, three specimens were tested. The average final conversion of the epoxy resin at room temperature was determined by DSC data of the prepreg samples that were placed at room temperature for 100 days.

A typical DSC scanning curve is shown in Figure 2.1. In this work, the T_g was defined as the inflexion point of the step transition. The residual heat of the remaining reactants appeared as an exothermic peak on the DSC curve. Based on the DSC curves of prepreg samples, the conversion of each graphite/epoxy prepreg sample is calculated by

the following equation,

$$\text{Conversion } \% = 1 - \frac{A_t}{A_0} \times 100\% \tag{2.3}$$

where

A_t = peak area under the exotherm on the t-th days,

A_0 = peak area under the exotherm on the zero days.

2.2.6 Measurement of Peel Force

The testing specimens of the graphite/epoxy prepregs were 100 mm in length and 3.2 mm in width. The samples were placed in the humidity chambers for a desired period, and then were folded and compressed by an Instron 5848 micro-tester. The compression force of 111.2 N (25 lbf) was applied on each specimen for 1 min. After compression, the folded sample was pulled apart at 180° peeling angle using the Instron 5848 micro-tester. The peeling rate was set to 25.4 mm/min (1 in/min). The resistance during the peel test was recorded. For each sample, three specimens were tested.

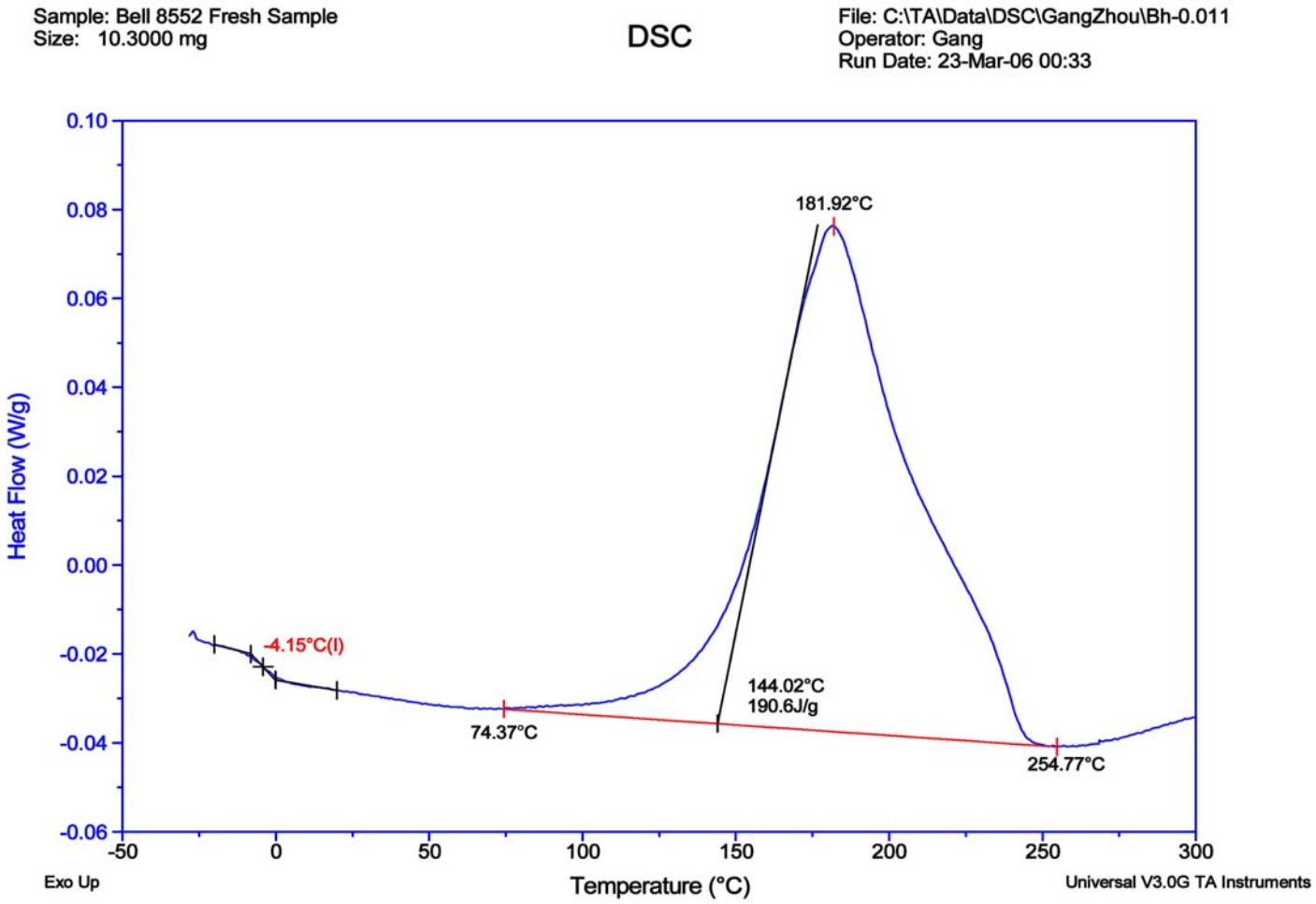

Figure 2.1 A typical DSC scanning curve of a partially cured graphite/epoxy prepreg sample.

2.3 Results and Discussion

2.3.1 Moisture Absorption

The results of moisture absorption tests are shown in Table 2.1. It can be seen that some moisture or solvent pre-existed in the fresh materials, so when the prepregs were placed in a desiccator (0% RH), the mass of samples decreased due to the desorption of water or solvent. In the 33 and 53% RH chambers, the mass of the prepregs remained almost unchanged after 1 day, meaning the absorption and desorption of moisture has reached equilibrium quickly. In the high RH environments (75 and 100%), the water uptake by the prepregs increased gradually within the 10-day period.

If we assume that the lost weight of prepreg samples in the 0% RH desiccator accounts for the moisture pre-absorbed in the epoxy resin, the total water in the graphite/epoxy prepreg samples is the sum of the pre-existed water in the epoxy matrix and the absorbed moisture by the samples. It is also assumed that the prepreg sample lost all moisture when placed in the 0% RH desiccator for 100 days. The water content in the epoxy matrix for each sample can be calculated based on the data in Table 2.1 and the weight percentage of epoxy resin in the IM7/8552 prepregs (~35.0 wt.% from the product information sheet). The calculated results are shown in Table 2.2. The equilibrium water content in the epoxy matrix is shown in Figure 2.2. It can be seen that the equilibrium water content in the epoxy matrix increased gradually with RH from 0 to 75%. The large increment of the equilibrium water content at 100% RH might result from moisture condensation on the sample surface in the saturated humid condition. The relationship between the equilibrium water content and the RH can be expressed as [18, 19]:

Time (days)	Relative Humidity in Chambers				
	0%	33%	53%	75%	100%
0	0%	0%	0%	0%	0%
1	-0.03%	0.10%	0.20%	0.34%	0.78%
4	-0.05%	0.12%	0.21%	0.36%	1.12%
7	-0.07%	0.11%	0.22%	0.40%	1.15%
10	-0.06%	0.10%	0.23%	0.39%	1.16%
100	-0.07%	0.13%	0.24%	0.48%	1.19%

Table 2.1 Percentage of moisture content of graphite/epoxy prepreg samples.

Time (days)	Relative Humidity in Chambers				
	0%	33%	53%	75%	100%
0	0.20%	0.20%	0.20%	0.20%	0.20%
1	0.11%	0.49%	0.77%	1.17%	2.43%
4	0.06%	0.54%	0.80%	1.23%	3.40%
7	0.00%	0.51%	0.83%	1.34%	3.49%
10	0.03%	0.49%	0.86%	1.31%	3.51%
100	0.00%	0.59%	0.89%	1.53%	3.60%

Table 2.2 Percentage of moisture content of epoxy matrix.

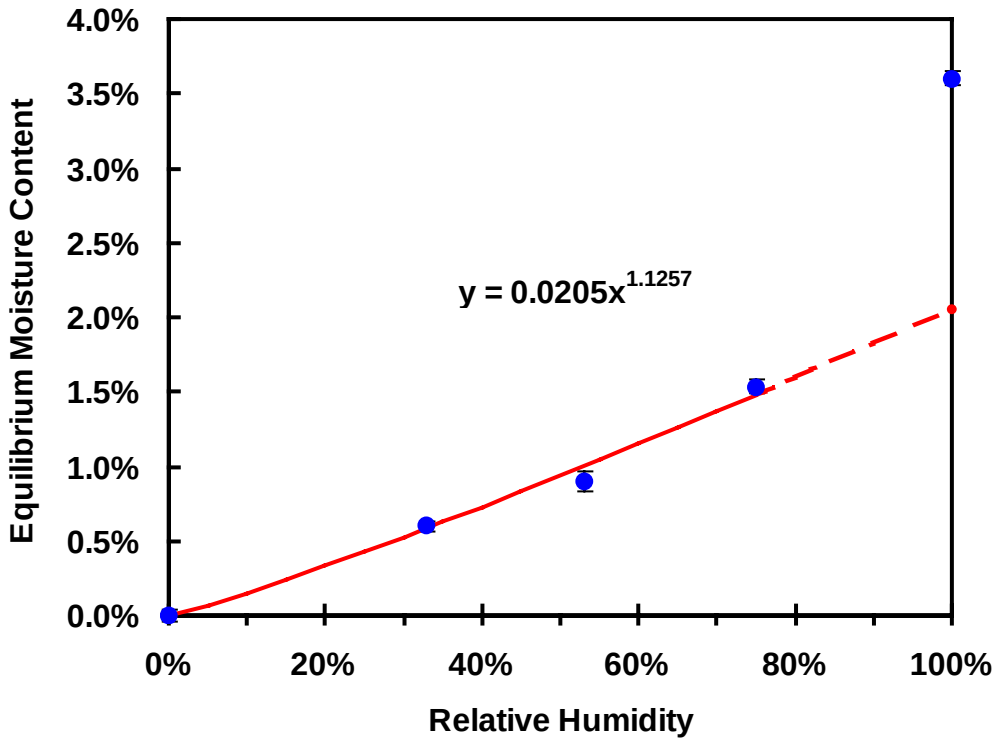

Figure 2.2 Equilibrium water content in the epoxy matrix of IM7/8552 graphite/epoxy prepregs.

$$C_\infty = a \cdot RH^b \tag{2.4}$$

where

C_∞ = equilibrium water content in the epoxy matrix,

a, b = constants.

The values of constants a and b are determined to be 0.0205 and 1.1257 respectively for the best fit of the data from 0 to 75% RH. Therefore, the equilibrium water content at 100% RH can be estimated to be around 2.05%.

2.3.2 Curing Kinetics

The epoxy-amine reaction can be described as follows [20-22]:

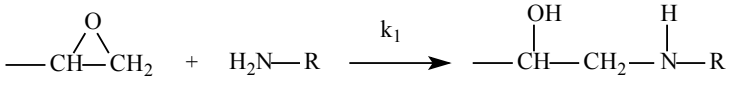

(2.5)

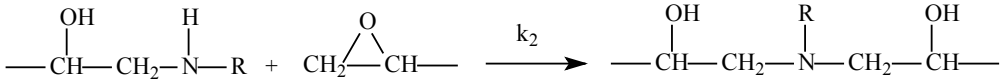

(2.6)

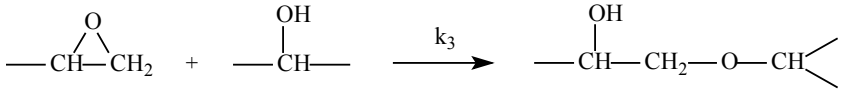

(2.7)

Equations (2.5) and (2.6) represent the reaction of primary and secondary amine with epoxy function group, respectively. Previous studies showed that these reactions could be catalyzed by hydrogen-bond donor molecules such as water, alcohols, and even the hydroxyl groups formed in the reactions [2]. The etherification reaction between epoxy and hydroxyl groups is shown in Equation (2.7). However, the etherification is

insignificant at low curing temperature [22] and is only observed for excess epoxy mixture after the amine has been depleted [23]. Therefore, the etherification was neglected in our study.

From the conversion data shown in Figure 2.3, it is obvious that moisture has a great effect on the curing of prepreg samples. A higher RH environment led to a faster reaction and higher conversion in the testing samples. This means that the moisture absorbed by the prepreg samples can accelerate the curing reaction of the epoxy resin in IM7/8552 graphite/epoxy prepregs. Equation (2.8) shows the scheme of the epoxy-amine reaction with the presence of water.

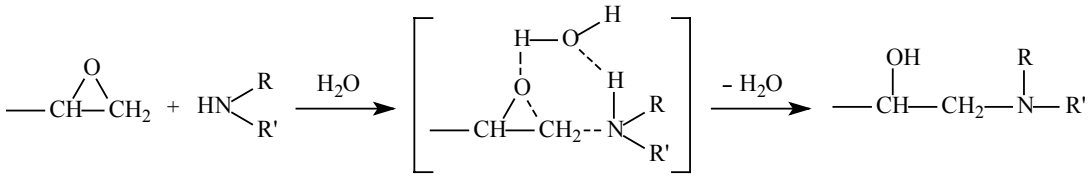

(2.8)

According to the study of Sourour and Kamal [2, 24], the following phenomenological kinetic equation was proposed to model epoxy isothermal cure kinetics.

$$\frac{d\alpha}{dt} = (K_1 + K_2\alpha)(1-\alpha)^n \tag{2.9}$$

where

α = fraction of epoxide reacted (conversion),

t = reaction time,

K_1 = reaction rate constant, for the reaction between epoxy and amine hardener,

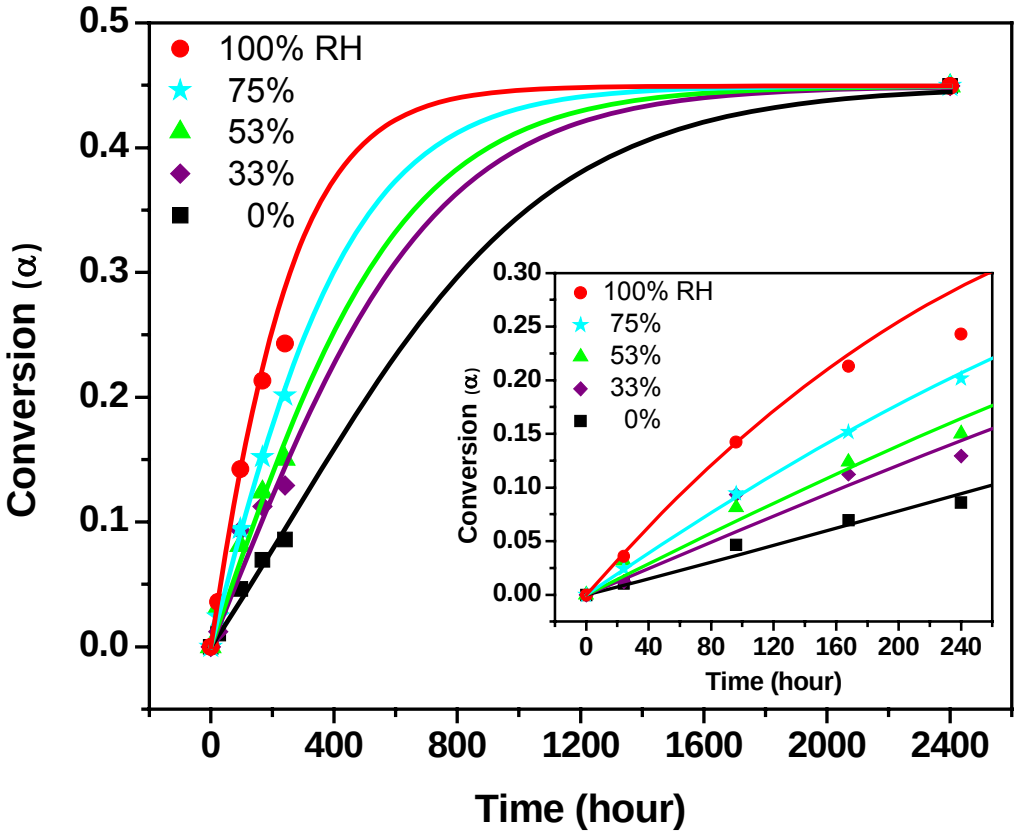

Figure 2.3 Conversion of prepreg samples in chambers with various relative humidity. (The solid lines are based on the kinetic model.)

K_2 = reaction rate constant, for the autocatalytic mechanism of epoxy-amine reaction,

n = reaction order, the overall reaction order is $n + 1$.

It was reported [25, 26] that the overall reaction order of epoxy resin is around 2.0, which meant n in the Equation (2.9) is about 1.0.

The curing reaction of the graphite/epoxy prepregs could not be completed under room temperature. A final conversion is introduced into our kinetic model. The moisture content in the epoxy matrix is also used in the kinetic model in order to consider the catalytic effect of water molecules. Therefore, the following kinetic expression is used to describe the curing mechanism of the epoxy resin in the prepreg samples at room temperature.

$$\frac{d\alpha}{dt} = (K_1 + K_2\alpha + K_3 C)(\alpha_f - \alpha) \tag{2.10}$$

where

K_3 = reaction rate constant, for the epoxy-amine reaction catalyzed by moisture,

C = moisture content in the epoxy resin, which is a function of RH as shown in Figure 2.2.

α_f = final conversion of the epoxy resin in the prepreg samples at room temperature.

The conversion expression derived from Equation (10) is:

$$\alpha = \alpha_f - \frac{K_1 + K_2\alpha_f + K_3 C}{K_2 + \exp\left[\left(K_1 + K_2\alpha_f + K_3 C\right)\cdot t + \ln\left(\frac{K_1 + K_3 C}{\alpha_f}\right)\right]} \tag{2.11}$$

From Table 2.1, it can be found that the water content in the samples did not change too much after 7 days. Therefore, the equilibrium water contents in the epoxy resin, C, were used in the calculation. As mentioned previously, the water content that catalyzes the epoxy-amine reaction is the sum of the pre-existed water in the epoxy matrix and the absorbed moisture by the prepreg sample.

All parameters used in the kinetic model are listed in Table 2.3. Based on the experimental conversion data of the prepreg samples, K_1, K_2, and K_3 were determined by the Levenberg-Marquardt least square method [27]. It can be seen that $K_3 > K_2 > K_1$, which confirms the catalytic effect of water molecules is larger than that of hydroxyl groups generated during epoxy-amine reactions. This may be attributed to the steric effect of epoxy molecules [28], making the activity of hydroxyl groups on the epoxy polymer chain much lower than that of water molecules absorbed in the epoxy matrix. The small K_1 value indicates that the epoxy-amine reaction may take place without any catalyst, but at a very low reaction rate.

From the conversion curves shown in Figure 2.3, it can be found that the kinetic model fits the experimental data very well for the samples in 0%, 33%, 53%, and 75% RH. The samples in the 100% RH chamber showed a large deviation between the experimental data and the model prediction. The aggregation of excess water molecules by hydrogen bonding in the epoxy matrix [8], resulting in less water to catalyze the epoxy-amine reaction, may be a reason for this discrepancy.

α_f	C at various RH					K_1 (h^{-1})	K_2 (h^{-1})	K_3 (h^{-1})
	0%	33%	53%	75%	100%			
44.9%	0.00%	0.59%	0.89%	1.53%	3.60%	0.000824	0.00337	0.0895

Table 2.3 Parameters in the kinetic model of epoxy-amine reaction.

2.3.3 Complex Viscosity

The changes of complex viscosity of graphite/epoxy prepregs in a chamber with 0 and 100% RH are shown in Figure 2.4. The complex viscosity of epoxy resins increased with time, especially for the sample in the 100% RH chamber. This is because the curing reaction of epoxy resin took place when the prepregs were placed at room temperature. Water molecules promoted the epoxy-amine reaction causing the complex viscosity to increase more rapidly in the environment with a higher humidity.

2.3.4 Glass Transition Temperature

Figure 2.5 shows the T_g of graphite/epoxy prepreg samples over a 10-day period. The transition temperature of the fresh prepreg sample is about –3.3 °C. At the beginning, water absorbed by the prepregs acted as a plasticizer, therefore the T_g declined with the increase of water content. However, the curing reaction of the epoxy resin would occur at room temperature, so the T_g increased gradually with time even without water. Water molecules accelerated the curing reaction of the epoxy resin, resulting in faster T_g increase in the environments with high humidity (75 and 100% RH). The trend of the T_g increase is consistent with that of the complex viscosity obtained by rheological testing.

The DiBenedetto equation [29, 30] is widely used to describe the relationship between T_g and conversion, especially for thermosetting resins [31-33]. A simplified form of the DiBenedetto equation is shown as follows:

$$\frac{T_g - T_{g0}}{T_{g\infty} - T_{g0}} = \frac{\lambda \cdot \alpha}{1-(1-\lambda)\alpha} \quad \text{or} \quad T_g = T_{g0} + \frac{\lambda \cdot \alpha}{1-(1-\lambda)\alpha}(T_{g\infty} - T_{g0}) \tag{2.12}$$

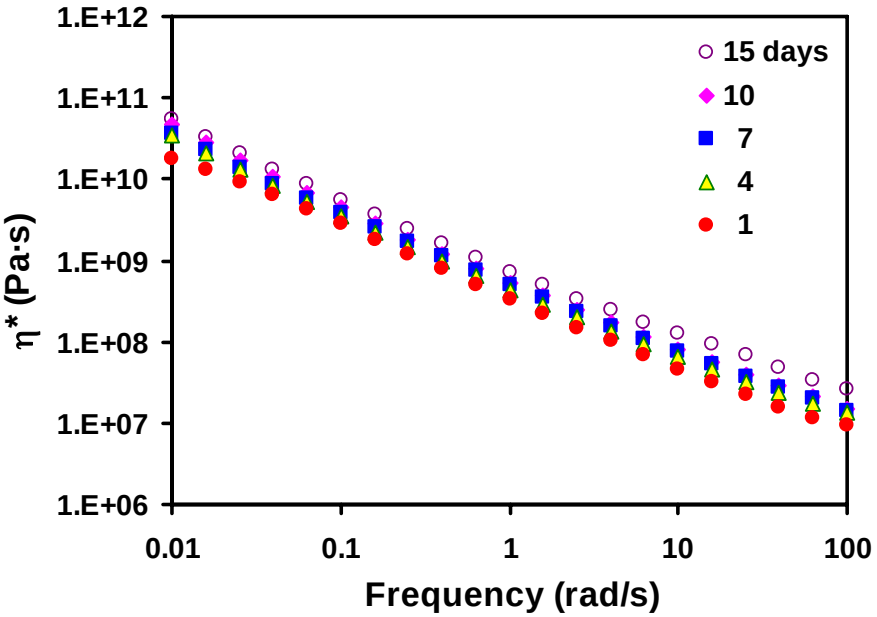

(a)

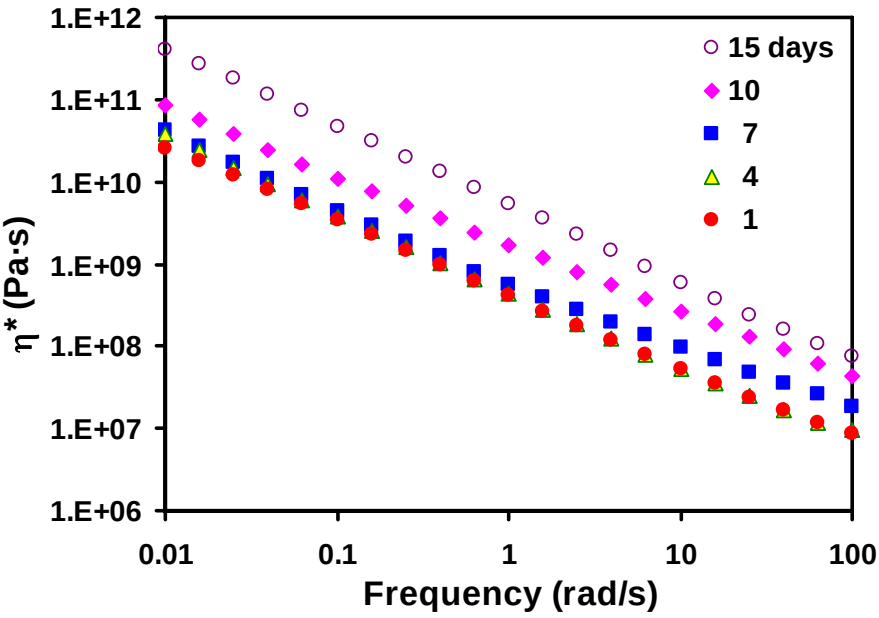

(b)

Figure 2.4 Complex viscosity of graphite/epoxy prepreg samples in (a) 0% RH and (b) 100% RH chambers.

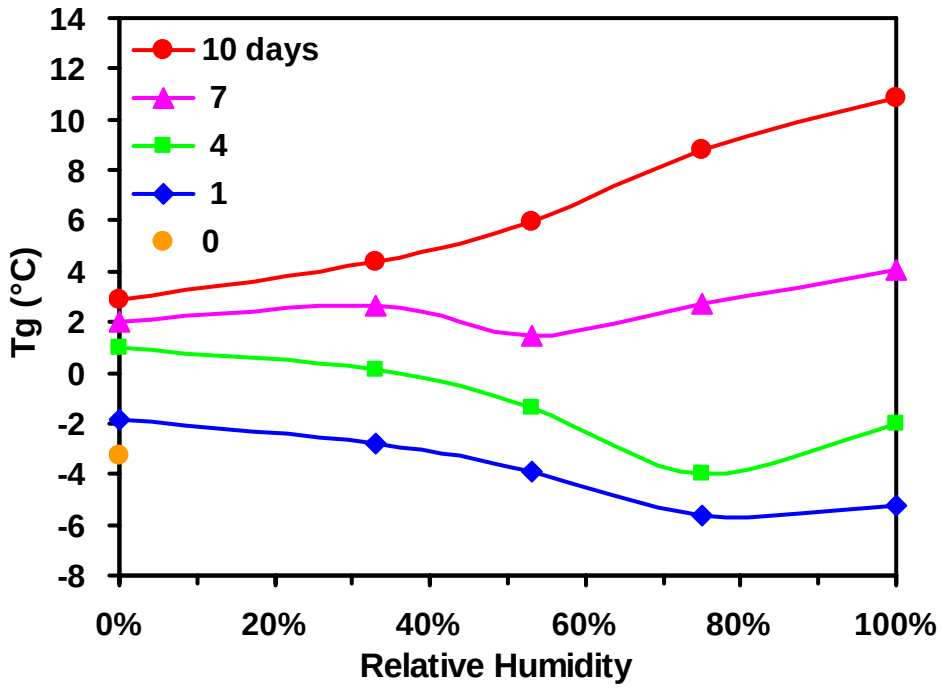

Figure 2.5 T_g of graphite/epoxy prepreg samples in chambers with various relative humidity over 10-day period.

where

α = reaction conversion,

$\lambda = \Delta C_{p\infty}/\Delta C_{p0}$, ratio of the isobaric heat capacities of the fully reacted and initial systems ($0 < \lambda < 1$),

T_{g0} = glass transition temperature of the initial system at $\alpha = 0$,

$T_{g\infty}$ = glass transition temperature of the completed reacted system at $\alpha = 1$.

Because water molecules act not only as a promoter of epoxy-amine reactions, but also as a plasticizer, the plasticization effect on the T_g of epoxy prepregs should be considered. A linear relationship has been successfully applied to calculate the T_g of polymer/plasticizer systems [34-36], especially at low concentration of plasticizers.

$$T_g = T_g' - k \cdot w \tag{2.13}$$

where

T_g' = glass transition temperature for the pure polymer,

k = coefficient ($k > 0$),

w = weight fraction of diluent/plasticizer in the polymer system.

The model used to calculate T_g in this study is a combination of Equations (2.12) and (2.13).

$$T_g = T_{g0} + \frac{\lambda \cdot \alpha}{1-(1-\lambda)\alpha}(T_{g\infty} - T_{g0}) - k \cdot w \tag{2.14}$$

All parameters used in the model are shown in Table 2.4. T_{g0} is determined through DSC by a fresh graphite/epoxy prepreg sample, and the value of $T_{g\infty}$ is from the product information sheet of IM7/8552 prepregs. The conversion α is calculated using the kinetic Equation (2.11). It is found that when $\lambda = 0.3$ and $k = 200$ K, the calculated T_g values from Equation (2.14) have a good agreement with the experimental results. The model prediction and experiment data at various RH are shown in Figure 2.6.

2.3.5 Tack Property

The tack property of graphite/epoxy prepregs was characterized by peeling tests. The peel forces of all samples are shown in Figure 2.7. For the 0 and 33% RH prepreg samples, the peel forces reached the maximum value on the 7th day, but the change was very small. For the samples from 53 and 75% RH chambers, the peel forces continued increasing during the 10-day period. This can be attributed to the effects of absorbed water molecules, which acted as both a curing promoter of the epoxy matrix and a plasticizer to soften the materials. The plasticization may enhance the mobility of polymer molecules, and thus improve the adhesion between sample parts. However, if too much moisture accumulates on the sample surface, the adhesion between sample parts will decrease. This explains why the 100% RH samples have lower peel forces than other samples.

T_{g0} (K)	$T_{g\infty}$ (K)	λ	k (K)
270.3	473.2	0.30	200

Table 2.4 Parameters in the T_g model of graphite/epoxy prepregs.

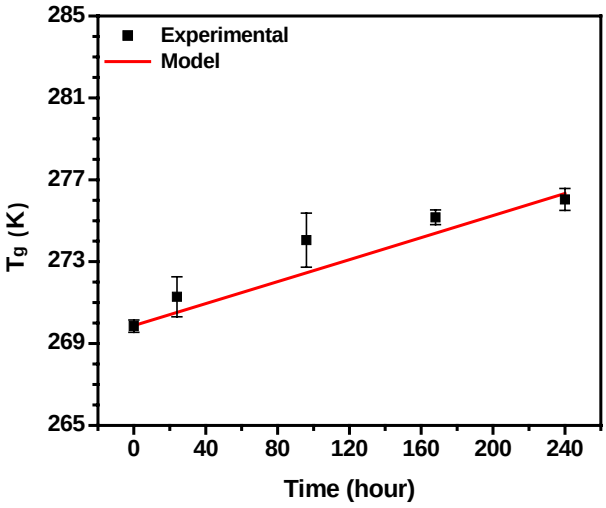

(a)

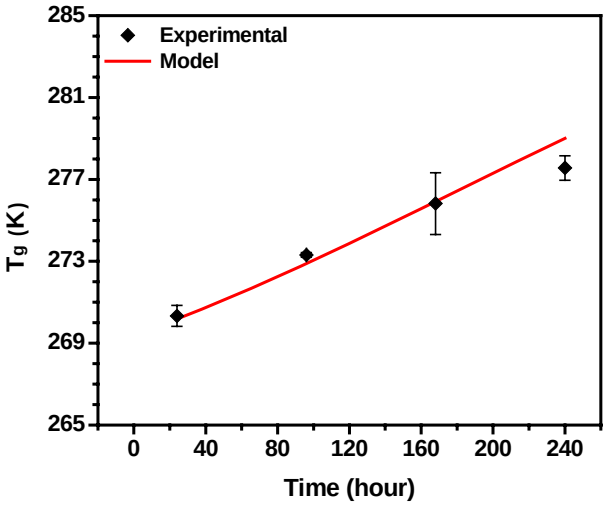

(b)

(Continued)

Figure 2.6 Experimental and calculated T_g of graphite/epoxy prepreg samples in chambers with various relative humidity: (a) 0%; (b) 33%; (c) 53%; (d) 75%; and (e) 100% RH.

Figure 2.6 continued

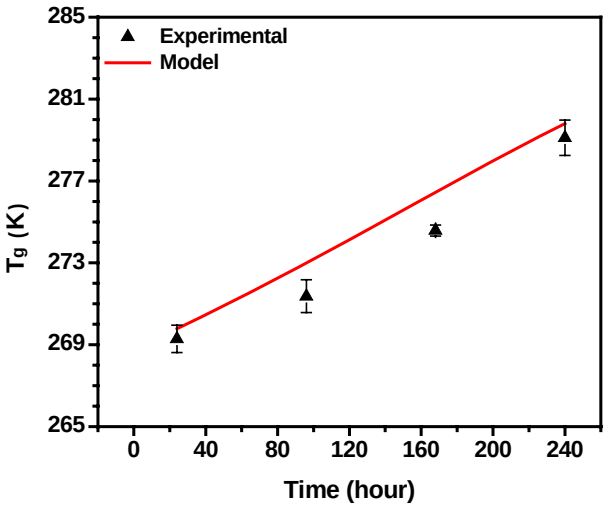

(c)

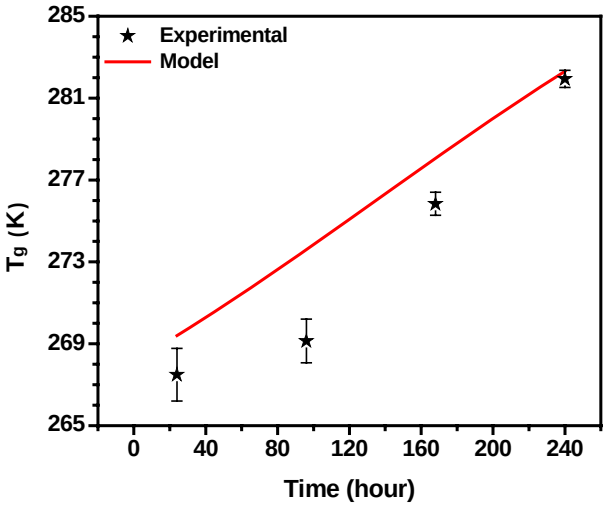

(d)

(Continued)

Figure 2.6 continued

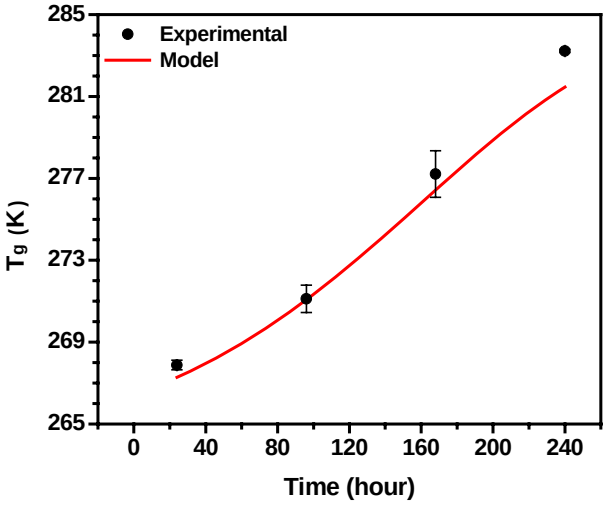

(e)

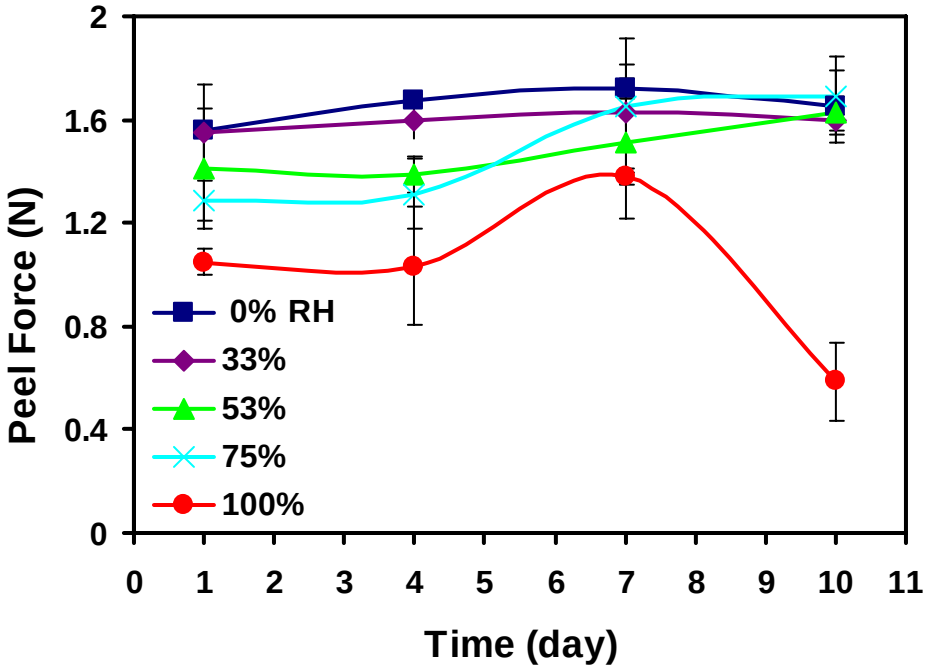

Figure 2.7 Peel forces of prepreg samples in chambers with various relative humidity over 10-day period.

2.3.6 Relationship between Glass Transition Temperature and Peel Force

A graph with peel force vs. T_g is shown in Figure 2.8. The peel forces correlate well with the glass transitions of the prepreg samples. The possible mechanism is explained as follows:

(1) The peel force is mainly determined by the number of entanglement of polymer chains at the interface of prepregs and the resistance of disentanglement.

(2) At the beginning, the T_g of the sample is far below the room temperature. The epoxy matrix is in the rubbery state and the entanglement of polymer chains at the prepreg interface is relatively easy. The rise of T_g indicates the increase of the reaction conversion and the growth of the polymer chains. This may lead to the increase of the disentanglement resistance, and thus the peel force increases gradually.

(3) When the T_g closes to the room temperature, polymer molecules lose their mobility greatly, resulting in much less entanglement at the interface between the prepregs. Therefore, the epoxy prepregs become less tacky and the peel forces begin to decline.

The trendline in Figure 2.8 is determined by curve fitting based on the experimental data. The expression of the trendline is shown in Equation (2.15). From this equation, the peel force would reach a peak value when the T_g is around 279.9 K (6.7 °C). After that, the peel force would decrease with the increase of T_g.

$$\text{Peel Force (N)} = -0.00269 \cdot T_g^{\,2} + 1.5058 \cdot T_g - 208.68 \qquad (2.15)$$

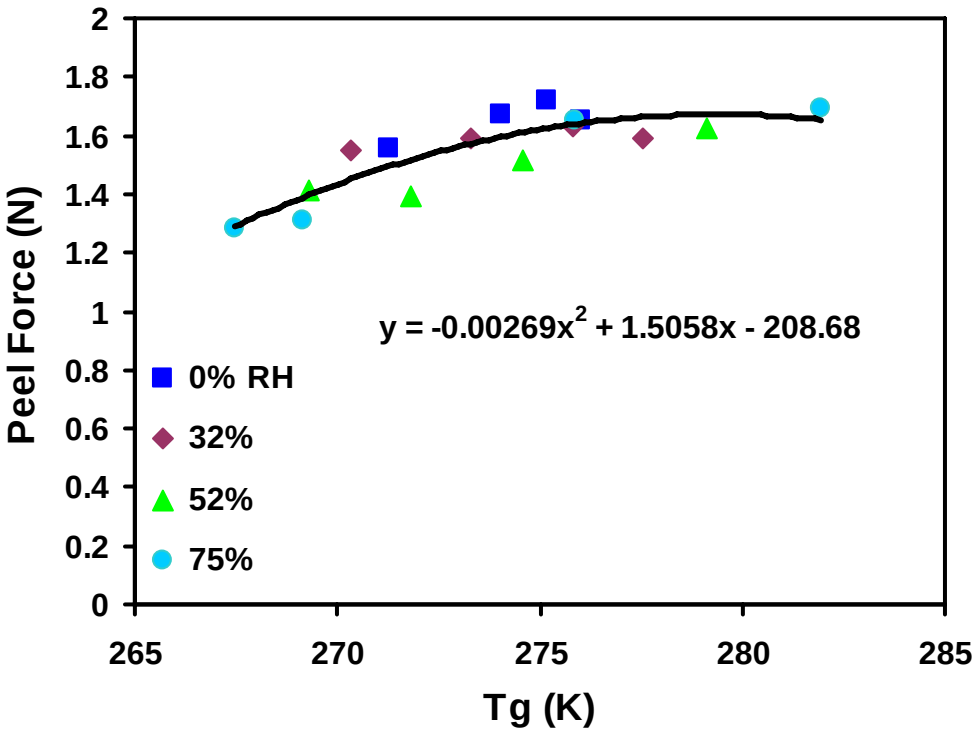

Figure 2.8 Relationship between T_g and peel force of graphite/epoxy prepreg samples.

2.4 Conclusions

The effects of humidity on the curing kinetics, T_g, and tack property of IM7/8552 graphite/epoxy prepregs were studied. It was found that a higher RH resulted in more moisture absorbed by the prepreg samples. The water in the graphite/epoxy prepregs acted as a plasticizer and a curing accelerator. A phenomenological kinetic model was proposed to describe the epoxy-amine reaction in the prepreg samples with the presence of moisture. The T_g of the epoxy matrix was predicted by a modified DiBenedetto equation, and the results had a good fit with the experimental data. The peel forces were applied to characterize the tack property of the prepreg samples. They correlated well with the T_g of the prepreg samples.

References

1. P. K. Mallick, *Fiber-Reinforced Composites*, Marcel Dekker: New York/Basel (1988).

2. S. Sourour, M. R. Kamal, *Thermochim. Acta*, **14**, 41 (1976).

3. T. R. Cuadrado, J. F. Macgregor, A. E. Hamielec, *J. Appl. Polym. Sci.*, **40**, 867 (1990).

4. J. M. Kenny, A. Trivisano, *Polym. Eng. Sci.*, **31**, 1426 (1991).

5. M. R. Vanlandingham, R. F. Eduljee, J. W. Gillespie, *J. Appl. Polym. Sci.*, **71**, 699 (1999).

6. V. L. Zvetkov, *Polymer*, **43**, 1069 (2002).

7. W. J. Mikols, J. C. Seferis, A. Apicella, L. Nicolais, *Polym. Compos.*, **3**, 118 (1982).

8. J. Zhou, J. P. Lucas, *Polymer*, **40**, 5505 (1999).

9. M. G. Lu, M. J. Shim, S. W. Kim, *J. Appl. Polym. Sci.*, **81**, 2253 (2001).

10. M. L. Costa, S. F. M. Almeida, J. M. Paiva, M. C. Rezende, *Mater. Res.*, **8**, 335 (2005).

11. Z. N. Sanjana, W. H. Schaefer, J. R. Ray, *Polym. Eng. Sci.*, **21**, 474 (1981).

12. J. Johnston, *Adhes. Age*, **26**, 34 (1983).

13. C. Creton, L. Leibler, *J. Polym. Sci. Part B: Polym. Phys.*, **34**, 545 (1996).

14. C. Gay, *Integr. Comp. Biol.*, **42**, 1123 (2002).

15. Y. Woo, *Inelastic Analysis of the Loop Tack Test for Pressure Sensitive Adhesives*, Doctorial Dissertation, Virginia Polytechnic Institute and State University (2002).

16. L. Greenspan, *J. Res. Nat. Bur. Stand.*, **81A**, 89 (1977).

17. http://www.omega.com/temperature/Z/pdf/z103.pdf, (retrieved on March 2006).

18. A. C. Loos, G. S. Springer, *J. Compos. Mater.*, **13**, 131 (1979).

19. J. B. Enns, J. K. Gillham, *J. Appl. Polym. Sci.*, **28**, 2831 (1983).

20. H. Lee, K. Neville, *Handbook of Epoxy Resins*, McGraw-Hill: New York/San Francisco/Toronto/London/Sydney (1967).

21. L. J. Lee, *Makromol. Chem., Macromol. Symp.*, **68**, 169 (1993).

22. J. M. Barton, *Adv. Polym. Sci.*, **72**, 111, (1985).

23. C. C. Riccardi, R. J. J. Williams, *J. Appl. Polym. Sci.*, **32**, 3445 (1986).

24. M. R. Kamal, S. Sourour, *Polym. Eng. Sci.*, **13**, 59 (1973).

25. A. Moroni, J. Mijovic, E. M. Pearce, C. C. Foun, *J. Appl. Polym. Sci.*, **32**, 3761 (1986).

26. C. Dispenza, J. T. Carter, P. T. McGrail, G. Spadaro, *Polym. Int.*, **48**, 1229 (1999).

27. D. M. Bates, D. G. Watts, *Nonlinear Regression and Its Applications*, Wiley: New York (1988).

28. J. J. Sahlin, N. A. Peppas, *Ind. Eng. Chem. Res.*, **30**, 211 (1991).

29. L. E. Nielsen, *J. Macromol. Sci. Revs. Macromol. Chem.*, **C3**, 69 (1969).

30. A. T. DiBenedetto, *J. Polym. Sci. Part B: Polym. Phys.*, **25**, 1949 (1987).

31. J. P. Pascault, R. J. J. Williams, *J. Polym. Sci. Part B: Polym. Phys.*, **28**, 85 (1990).

32. J. P. Pascault, R. J. J. Williams, *Polym. Bull.*, **24**, 115 (1990).

33. R. A. Venditti, J. K. Gillham, *J. Appl. Polym. Sci.*, **64**, 3 (1997).

34. J. D. Ferry, *Viscoelastic Properties of Polymers*, 3rd edition, Wiley: New York, 487 (1980).

35. K. A. Mauritz, R. F. Storey, S. E. George, *Macromolecules*, **23**, 441 (1990).

36. K. G. Wagner, M. Maus, A. Kornherr, G. Zifferer, *Chem. Phys. Lett.*, **406**, 90 (2005).

CHAPTER 3

STUDY OF ULTRASONIC CONSOLIDATION AND MARCEL FORMATION OF GLASS FIBER/EPOXY PREPREGS

3.1 Introduction

Advanced thermoset composites are widely used in the aerospace industry. By far, the most important process in terms of current aerospace production is hand lay-up of prepregs and autoclave or compression cure. It is estimated that at least half of all advanced composite aerospace structures are made by hand lay-up [1]. This process continues to be used because it is extremely flexible, capable of making a wide variety of shapes. Furthermore, hand lay-up dose not require the large capital investment compared with the automated processes. The first step in fabricating of advanced composites involves laying out prepreg tapes, which are sheets of unidirectional fibers coated with a partially cured thermoset resin. Layers of prepreg tapes with different fiber orientations are sequentially laid down on a mold in order to define the final shape of the component. Once the correct number of layers of prepreg is applied, the mold and composites structure are vacuum bagged. The vacuum removes entrapped gasses and promotes

good consolidation because of the forces generated by atmospheric pressure. The bagged component is then placed in an autoclave or a heated mold in order to cure the thermoset [1].

The applications of advanced composites are mainly structural and thus the quality of the composites is critical. However, the quality inconsistence of composite parts is one of the drawbacks of the hand lay-up process. For instance, voids created during manufacturing can lead to poor performance and crack propagation, eventually component failure [2-4]. Another example is the fiber marcelling (buckling) in thick and complex composite parts, which results in significant reduction of mechanical properties and fatigue life in applications [5-7]. These defects form at different steps in the manufacturing process. Most air is trapped between prepregs during hand lay-up. Although the vacuum-bagging procedure is usually applied to remove entrapped gas bubbles before curing the composites, it cannot fully eliminate voids. In addition, the fiber marcelling often occurs in the curing step. The mechanism of marcel formation is not well understood, especially its dependence on process variables [8]. Therefore, it is necessary to conduct a thorough study to reduce or eliminate the voids in the composites and establish the relationship between the process variables and the marcel formation.

High-powered ultrasonics has been used very successfully to process plastics for many decades. It has been proposed that this technology can be applied to reduce void content and increase component integrity during prepreg consolidation. By designing an ultrasonic tool with a round face, it may be possible to follow the laying down process of the prepreg tapes with an ultrasonic horn. The ultrasonic energy may force entrapped

gasses out of the interface between the prepreg plies. The mechanical vibrations of the ultrasonic energy may also coalesce entrapped gas bubbles and increase their mobility, and the gas bubbles may be pushed out by the "plowing" of the ultrasonic tool. Futhermore, the ultrasonic energy may also promote better wetting between the partially cured thermoset resin and fibers. The ultrasonic energy is very effective in welding plastics together by applying high cyclical stresses to the parts to induce hysteretic heating at the bond line. This heating may promote localized reduction of the viscosity of the uncured thermoset resin and allow for better wetting between plies. However, if the temperature increases too much, it may promote premature curing or scorching in the composite, leading to reduced mechanical properties.

After vacuum and/or ultrasonic consolidation, the prepreg parts need be cured in a closed mold with high pressure and elevated temperature. It was found that fiber marcels might form during this process, resulting in poor performance of the cured product.

Therefore, the overall goals of this research are to

- determine whether ultrasonic energy can be used to consolidate or debulk composite lay-ups;
- study the effect of ultrasonic consolidation on mechanical properties of the composites;
- find out the critical material and process variables that affect marcel formation during compression molding;
- establish the threshold marcelling conditions for various epoxy resin systems.

3.2 Experimental

3.2.1 Materials

Two types of unidirectional glass fiber/epoxy resin prepregs were used in this study, i.e. E773/S2 or 8552/S2 epoxy prepregs. Each prepreg is 152 mm × 152 mm (6 inch × 6 inch) in size. For the rheological studies, neat E773 and 8552 epoxy resins were used.

3.2.2 Measurement of Sample Thickness

The thickness of the stack of prepregs was measured using a Mitutoyo digital micrometer. In general, the average of nine measurements was recorded for each sample.

3.2.3 Measurement of Surface Temperature

The surface temperature (Φ) of the top ply was measured using a ThermaCAM® IR camera/thermal detector.

3.2.4 Ultrasonic Consolidation

The ultrasonic equipment used was a Dukane 40 KHz ultrasonic welding machine. Figure 3.1 shows a photograph of the experimental setup and key operation parameters.

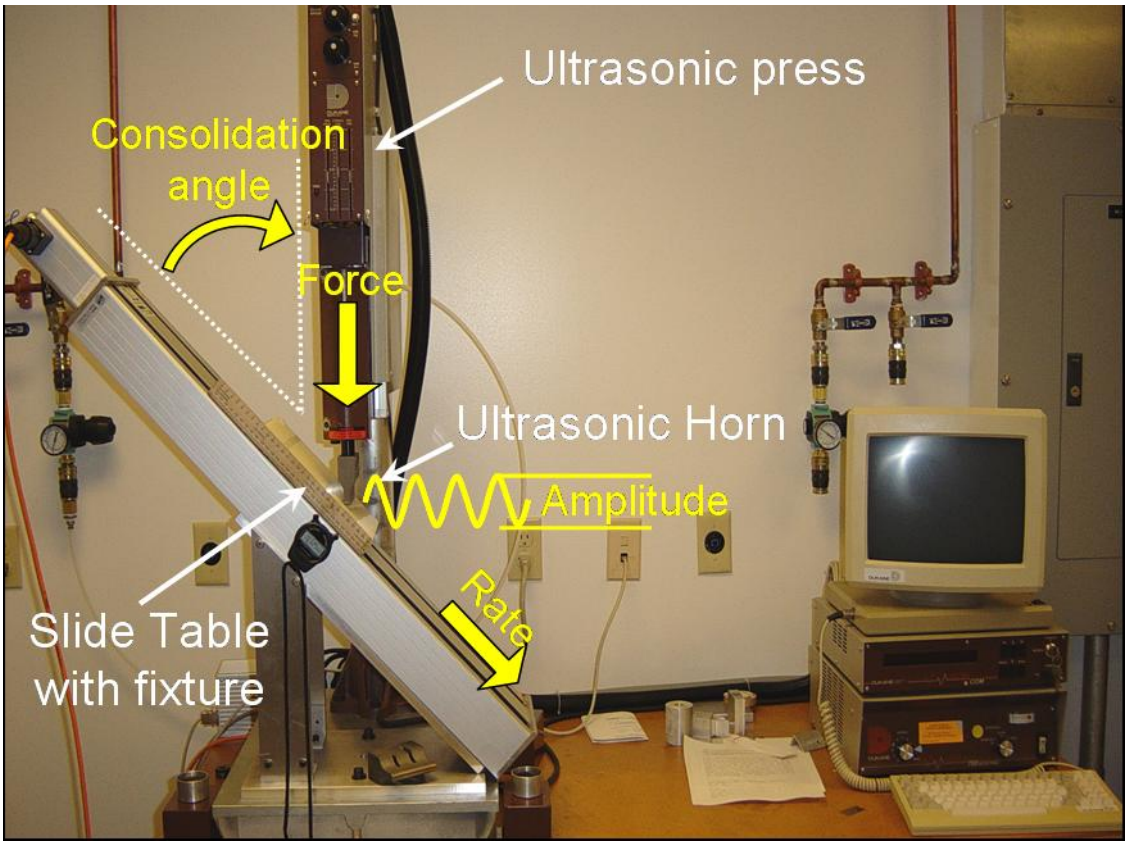

Figure 3.1 Photograph of ultrasonic consolidation set-up.

Each prepreg was individually placed into a square mold in a 0°/90° orientation. The number of plies placed in the mold (N) between ultrasonic treatments was varied at two levels. The final number of plies was held constant at 28. Other parameters that were evaluated included travel speed (R, 2 levels), contact force (F, 2 levels), amplitude of ultrasonic wave (A, 2 levels), and mold to horn angle (θ, 2 levels). A box design non-central point, design of experiment was constructed with these five parameters as shown in Table 3.1. All the parameters were normalized to dimensionless numbers by dividing the lower parameter settings by the higher parameter settings. The dependent parameters were also normalized to corresponding values of untreated samples.

3.2.5 Measurement of Shear Viscosity and Normal Stress

Rheological data were obtained using a Rheometrics Mechanical Spectrometer (RMS) 800. The normal stress or normal stress difference and shear viscosity of epoxy resins were measured with the cone and plate setup (50 mm diameter, 0.04 radian cone angle). These tests were carried out with the frequency from 0.01 to 100 rad/s at 25 °C.

3.2.6 Measurement of Temperature Profiles during Compression Molding

The mold cavity for marcel formation study is shown in Figure 3.2(a). Nine thermocouples were placed in the prepreg lay-up sample to obtain the temperature profiles during compression molding. The location of the thermocouples is shown in Figure 3.2 (b).

	Input									
Treatment No	Angle (^{o})		Amplitude (μm)		Rate (inch/min)		Force (lbs)		Interval	
1	-	0	-	15	-	1	-	8	-	7
2	-	0	-	15	-	1	+	25	+	4
3	-	0	-	15	+	0.5	-	8	+	4
4	-	0	-	15	+	0.5	+	25	-	7
5	-	0	+	30	-	1	-	8	+	4
6	-	0	+	30	-	1	+	25	-	7
7	-	0	+	30	+	0.5	-	8	-	7
8	-	0	+	30	+	0.5	+	25	+	4
9	+	45	-	15	-	1	-	8	+	4
10	+	45	-	15	-	1	+	25	-	7
11	+	45	-	15	+	0.5	-	8	-	7
12	+	45	-	15	+	0.5	+	25	+	4
13	+	45	+	30	-	1	-	8	-	7
14	+	45	+	30	-	1	+	25	+	4
15	+	45	+	30	+	0.5	-	8	+	4
16	+	45	+	30	+	0.5	+	25	-	7
17	-	0	-	15	-	1	-	8	-	7
18	+	45	+	30	+	0.5	+	25	-	7

Table 3.1 Design of experiments for ultrasonic consolidation.

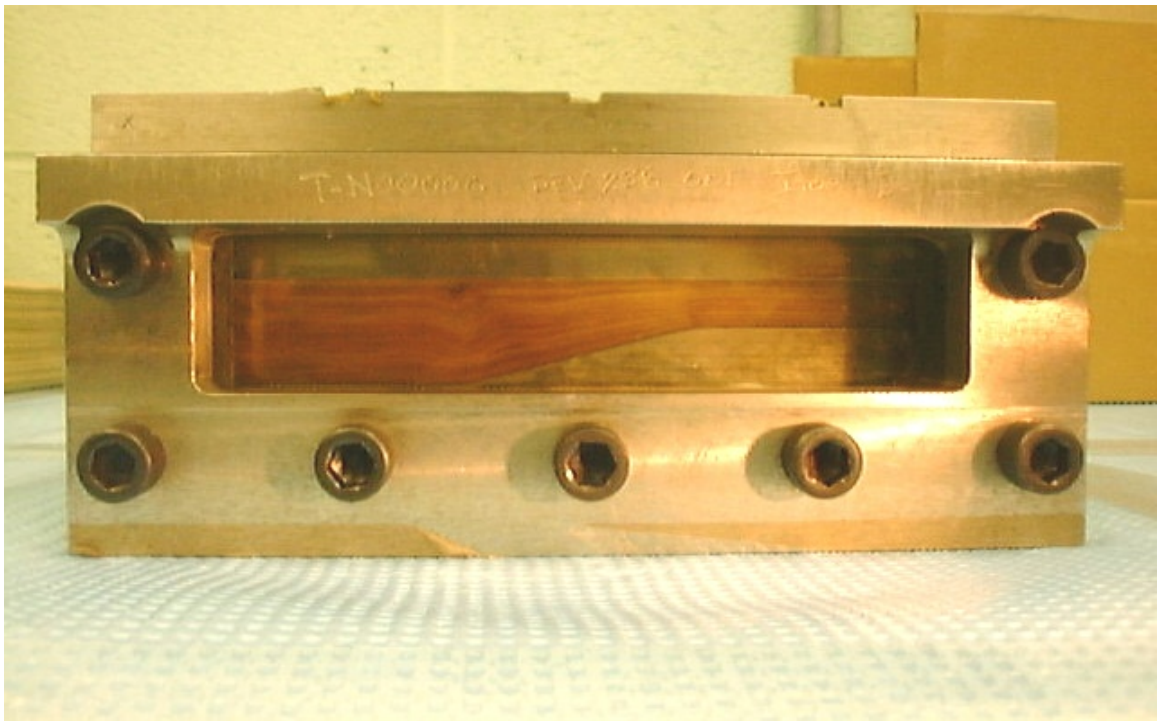

(a)

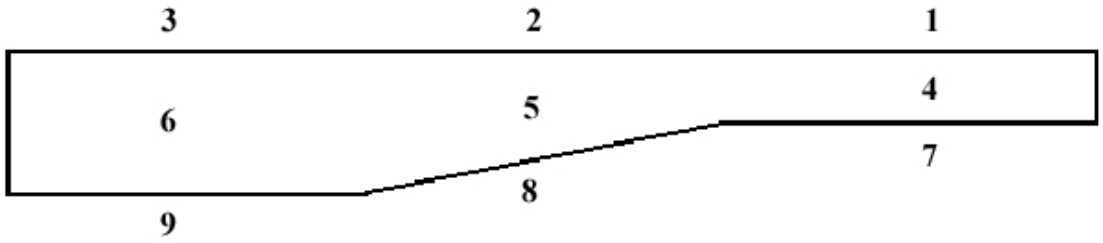

(b)

Figure 3.2 Study of marcel formation: (a) stainless steel mold and (b) distribution of thermocouples in prepreg lay-up samples.

3.2.7 Compression Molding

The experimental set-up of vacuum debulking and compression molding is shown in Figures 3.3 (a) and (b). An Instron 8500 press simulator was used to carry out the closed-cavity molding for two epoxy resins (E773 and 8552) provided by Bell Helicopter. Figures 3.4 (a) and (b) show the recommended cure cycles for these two resins. The molding process was recorded by a JVC digital camcorder through a glass window on the mold.

Each prepreg was individually placed into a tapered mold in a 0°/90° orientation. The parameters of experimental design included the number of total plies placed in the mold (TN, three levels), resin viscosity controlled by mold temperature (MT, three levels), pressure rate (PR, three levels), resin bleed path (B, three levels), and number of room-temperature vacuum debulking (NV, three levels). A fractional factorial design of experiment was constructed with these five parameters as shown in Table 3.2. The dependent parameter was the aspect ratio (height/width) of the largest marcel formed in the cured samples.

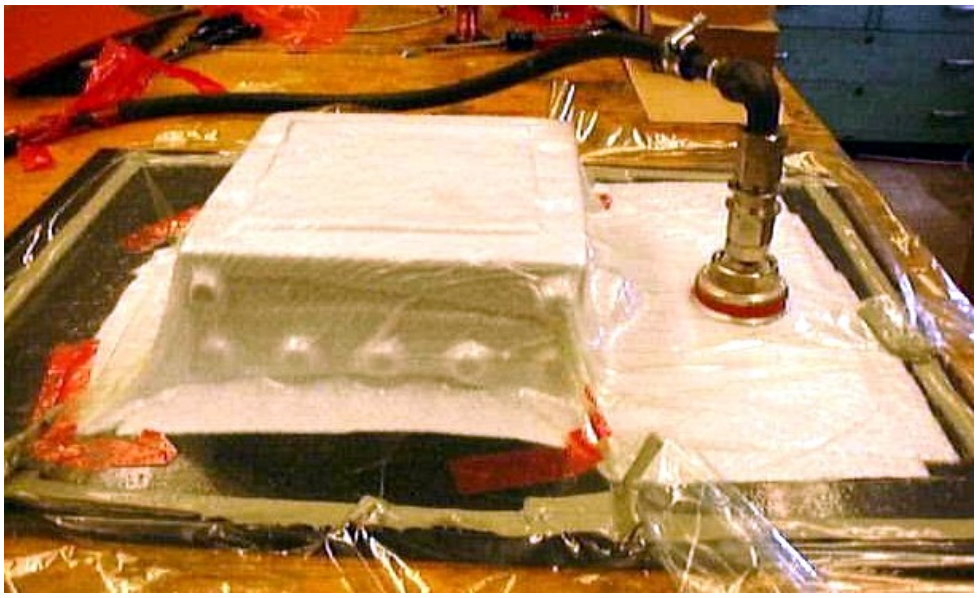

(a)

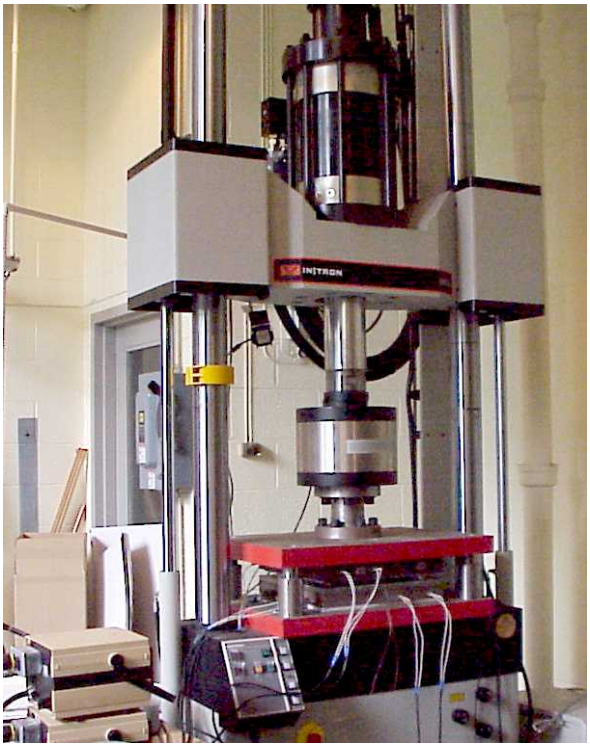

(b)

Figure 3.3 Experimental set-up of (a) vacuum debulking at room temperature and (b) Instron 8500 press simulator.

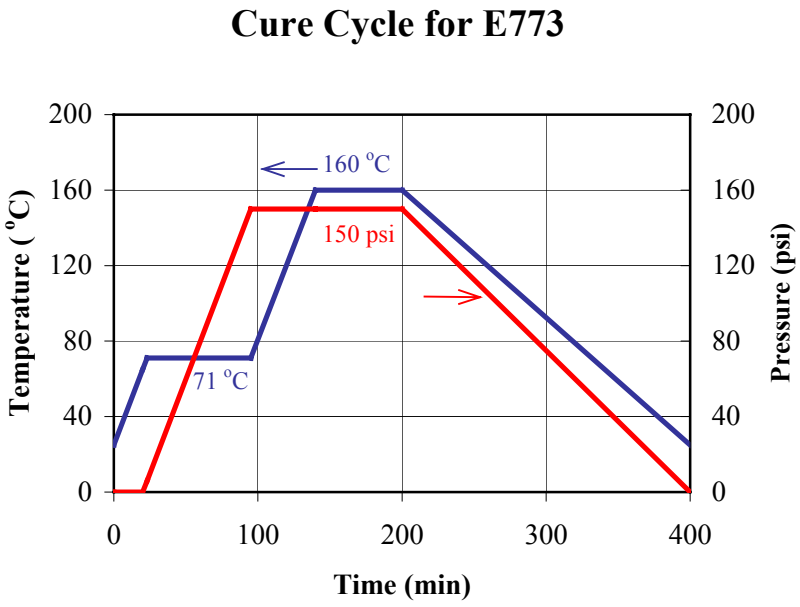

(a)

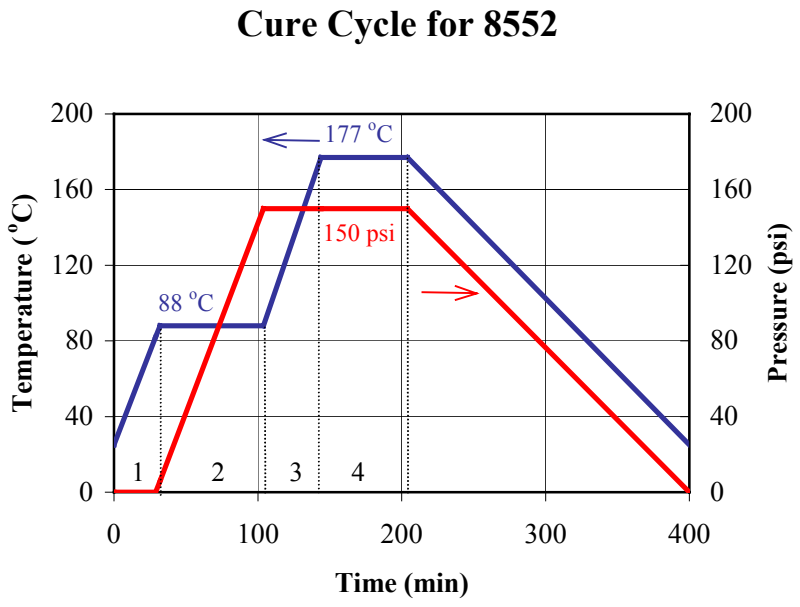

(b)

Figure 3.4 Typical closed-cavity-molding of (a) E773/S2 and (b) 8552/S2 tapered laminate.

DOE-Structure :									Line-of-Restriction										
1. Uncured Part Thick.					−							+					0	0	0
2. Viscosity		−				+				−				+			0	0	0
3. Pressure Rate	−		+		−		+		−		+		−		+		0	0	0
4. Resin Bleed Path	−	+	−	+	−	+	−	+	−	+	−	+	−	+	−	+	0	0	0
5. No. Vac. Debulk	+	−	−	+	−	+	+	−	−	+	+	−	+	−	−	+	0	0	0
Treatment No.	1	2	3	4	5	6	7	8	9	10	11	12	13	14	15	16	17	18	19
Unit-Structure :									Line-of-Restriction										
Factor Setting	1	2	3	4	5	6	7	8	9	10	11	12	13	14	15	16	17	18	19
Mold Setup	1	2	3	4	5	6	7	8	9	10	11	12	13	14	15	16	17	18	19
Part Layup	1	2	3	4	5	6	7	8	9	10	11	12	13	14	15	16	17	18	19
Run Order	**2**	**18**	**4**	**5**	**14**	**8**	**13**	**6**	**12**	**9**	**16**	**11**	**17**	**15**	**7**	**3**	**1**	**10**	**19**
Measurement :									Line-of-Restriction										
1. Max. Marcel Ratio	1	2	3	4	5	6	7	8	9	10	11	12	13	14	15	16	17	18	19
2. Marcel Develop. Condition	1	2	3	4	5	6	7	8	9	10	11	12	13	14	15	16	17	18	19
3. Laminate Thickness	1	2	3	4	5	6	7	8	9	10	11	12	13	14	15	16	17	18	19
4. Short-Beam-Shear	1	2	3	4	5	6	7	8	9	10	11	12	13	14	15	16	17	18	19

DOE Factor / Level	- Level	0 Level	+ Level
1. Uncured Part Thick.	93 plies	96 plies	99 plies
2. Viscosity	71°C / 180 min.*	56°C / 180 min.**	50°C / 180 min.***
3. Pressure Rate	1 psi/min.	4.5 psi/min.	8 psi/min.
4. Resin Bleed Path	Free	Partially Restricted	Restricted
5. No. of RT Vac. Debulk	None	1@/25"Hg/15min.	2@/25"Hg/15min.
	* 5 -10 Pa.s	** 30 - 35 Pa.s	*** 55 - 60 Pa.s

Table 3.2. Design of experiments for marcel formation study.

3.3 Results and Discussion

3.3.1 Ultrasonic Consolidation

3.3.1.1 *Sample Thickness*

Table 3.3 shows the results of the thickness of 28-ply prepreg samples after ultrasonic consolidation. Based on the statistic analysis, it can be found that the final thickness after ultrasonic treatment (but before final curing of the sample) is affected by rate, force, and amplitude (see Table 3.4). In more detail, the final thickness is inversely proportional to amplitude and force and directly proportional to speed. Higher amplitudes probably promote more heating and more squeeze flow during treatment, resulting in better consolidation. This is supported in the section detailing the temperature measurements. The higher forces promote better consolidation simply due to higher compressional forces [9]. A higher travel rate reduces the exposure time of the sample and thus reduces the heating, which in turn reduces the squeeze flow. Other parameters that were studied, horn angle and interval number, did not significantly affect the final sample thickness. According to the analysis results, cross terms and higher order terms of the independent variables also did not significantly affect the final thickness. Thus, the relationship between the dimensionless thickness and processing variables is defined in Equation 3.1.

$$T = 1.004 + 0.066 \cdot R - 0.047 \cdot F - 0.045 \cdot A \tag{3.1}$$

This equation indicates that a lower travel rate, higher consolidation force, and higher ultrasonic amplitude may lead to smaller thickness of uncured samples, meaning less voids in the composites.

	Input					Output
Treatment No	Angle (^{o})	Amplitude (μm)	Rate (inch/min)	Force (lbs)	Interval	Thickness (mm)
1	-	-	-	-	-	7.167
2	-	-	-	+	+	6.930
3	-	-	+	-	+	6.984
4	-	-	+	+	-	6.774
5	-	+	-	-	+	7.043
6	-	+	-	+	-	6.881
7	-	+	+	-	-	6.908
8	-	+	+	+	+	6.685
9	+	-	-	-	+	7.192
10	+	-	-	+	-	7.131
11	+	-	+	-	-	7.066
12	+	-	+	+	+	6.655
13	+	+	-	-	-	7.024
14	+	+	-	+	+	6.829
15	+	+	+	-	+	6.781
16	+	+	+	+	-	6.642
17	-	-	-	-	-	7.353
18	+	+	+	+	-	6.579

Table 3.3 Thickness of 28-ply prepreg samples after ultrasonic consolidation.

Effect	Coefficient	Std Error	t-ratio	Probability>|t|
Constant	1.004	0.007	152.075	<0.001
R	0.066	0.005	12.465	<0.001
F	-0.047	0.004	-12.036	<0.001
A	-0.045	0.005	-8.467	<0.001

Table 3.4 Statistical analysis of sample thickness (r^2=0.971).

3.3.1.2 *Surface Temperaturet*

The surface temperature is another important factor investigated for ultrasonic consolidation. If the temperature is too high during ultrasonic consolidation, some area of the prepreg sample may be pre-cured or even scorched. This will affect the property of the final product. Thus, the highest temperature during ultrasonic treatment needs to be controlled. The measured surface temperatures of 28-ply prepreg samples during ultrasonic consolidation are shown in Table 3.5. Using the same statistical approach as detailed in the previous section, Table 3.6 shows the relationship of temperature with the significant independent parameters. Again, the insignificant independent parameters were removed from the model. The relationship between the surface temperature and the independent parameters is detailed in Equation 3.2.

$$\Phi = 37.26 + 2.094 \cdot A - 0.920 \cdot N + 1.681 \cdot A \cdot F - 1.532 \cdot A \cdot R \qquad (3.2)$$

It can be seen that surface temperature is greatly dependent on amplitude [10]. For a given amplitude, the temperature is directly proportional to force and inversely proportional to rate. Increasing the force probably increases the mechanical coupling between the horn and the sample, increasing the overall efficiency of energy transfer. This explains why the cross product ($A \cdot F$) is proportionally related to temperature. In contrast, increasing the rate decreases the exposure time, reducing the heating time. In addition, it is seen that increasing the number of plies laid down between treatments (N) decreases the temperature. This is probably due to the increase in compliance of the system and reduction of the hysteresis heating. For example, Figure 3.5 shows the highest surface temperature as a function of the number of prepreg plies in an experiment. The surface temperature is the

highest for the thin sample and gradually decreases with the application of additional prepreg plies.

A typical thermal image of ultrasonic treatment is shown in Figure 3.6. An optical image is included in order to add clarity of the orientation and experiment setup. It can be seen that the temperature drops off relatively quickly once the horn passes a particular point. This suggests that the heating is localized at the top surface (horn/top layer interface), meaning that the heat generation is not a bulk effect and the controlled ultrasonic treatment may not affect the thermal history of the epoxy resin significantly.

	Input					Output
Treatment No	Angle (^{o})	Amplitude (μm)	Rate (inch/min)	Force (lbs)	Interval	Temperature (^{o}C)
1	-	-	-	-	-	83.4
2	-	-	-	+	+	89.2
3	-	-	+	-	+	87.5
4	-	-	+	+	-	96.9
5	-	+	-	-	+	103.1
6	-	+	-	+	-	108.1
7	-	+	+	-	-	103.6
8	-	+	+	+	+	151.9
9	+	-	-	-	+	87.5
10	+	-	-	+	-	86.2
11	+	-	+	-	-	91.2
12	+	-	+	+	+	98.7
13	+	+	-	-	-	102.7
14	+	+	-	+	+	138.3
15	+	+	+	-	+	122.3
16	+	+	+	+	-	134.5
17	-	-	-	-	-	81.3
18	+	+	+	+	-	140.9

Table 3.5 Highest surface temperatures of 28-ply prepreg samples during ultrasonic consolidation.

Effect	Coefficient	Std Error	t-ratio	Probability>|t|
CNST	37.26	0.000	8.759	<0.001
A	2.094	0.720	5.862	<0.001
N	-0.920	0.182	-2.289	<0.001
F·A	1.681	0.516	5.223	<0.001
R·A	-1.532	0.367	-3.500	<0.001

Table 3.6 Statistical analysis of surface temperature (r^2=0.918).

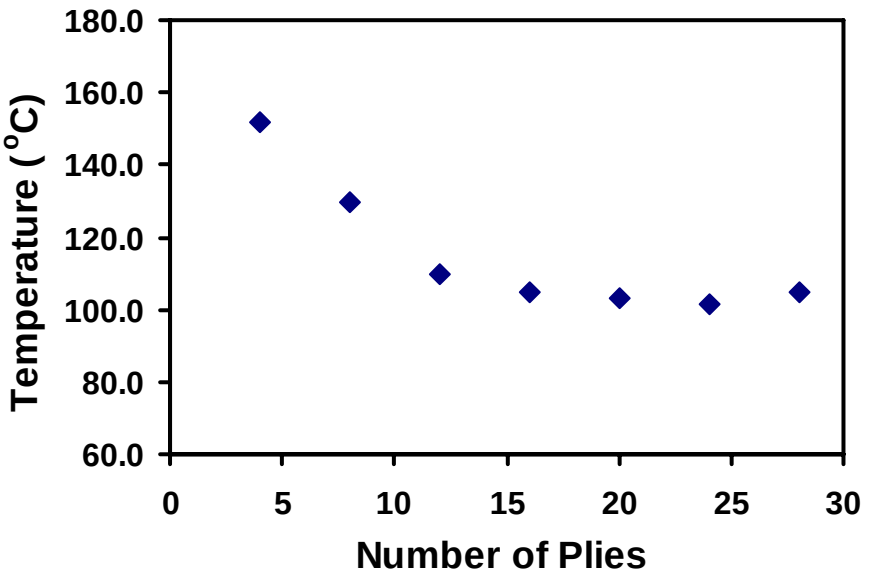

Figure 3.5 Highest surface temperature as a function of number of lay-up prepregs.

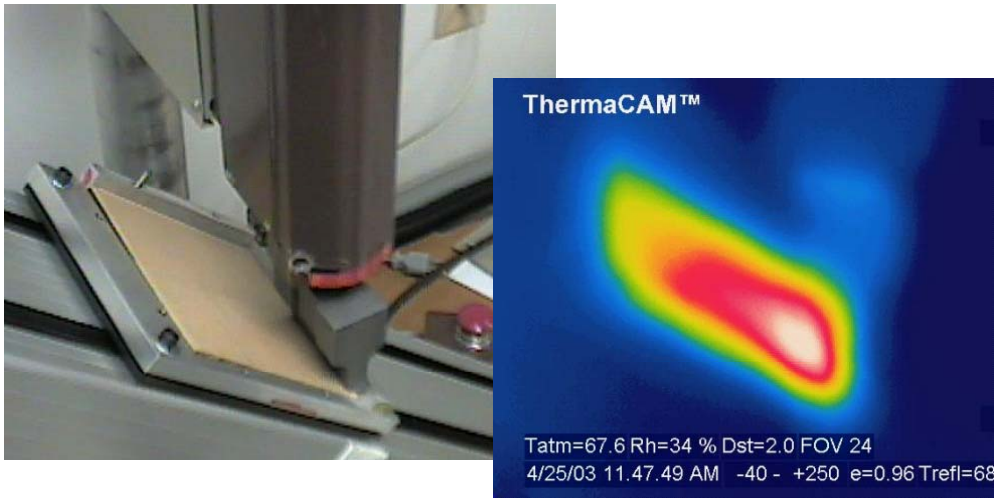

Figure 3.6 Typical temperature image from IR camera with optical image.

3.3.2 Marcel Formation

According to the recommended cure cycles, two experiments were carried out for E773 and 8552 epoxy/glass fiber prepregs, respectively. There is no marcel formation in the cure cycle for resin E773, but for resin 8552, the marcel formation is easily observed through the glass window. When the pressure reached about 80 psi, the fibers began to buckle. The marcel was completely formed at 100 psi in the second step of the cure cycle. Photo of the cross-section of molded 8552 composites is shown in Figures 3.7.

3.3.2.1 *Shear Viscosity*

In order to find out the difference between two epoxy resins (E773 and 8552), the rheological properties were compared as shown in Figures 3.8 (a) and (b). It can be found that the viscosity of 8552 at 82 °C is similar to that of E773 at 50 °C, but the normal stress of 8552 is about 3 times higher than that of E773 at the same conditions. This may lead to different behaviors of the samples during the compression molding process.

3.3.2.2 *Temperature Profile*

Nine thermocouples were embedded between the prepreg plies in the mold. The measured temperature profiles of two epoxy resins are shown in Figures 3.9 (a) and (b). From these figures, it is obvious that the whole prepreg part cannot be heated uniformly during the molding process. Temperatures near the bottom of the composite increased the fastest, followed with the temperatures near the top. The last part to be heated was in the middle of the composite. The temperatures of thermocouples 5 and 6 (T5 and T6)

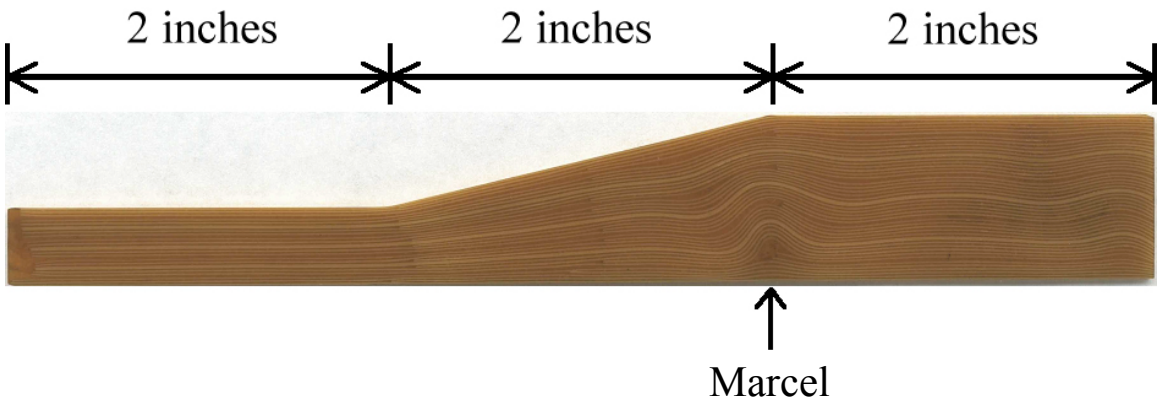

Figure 3.7 Fiber marcelling in the cured epoxy composite.

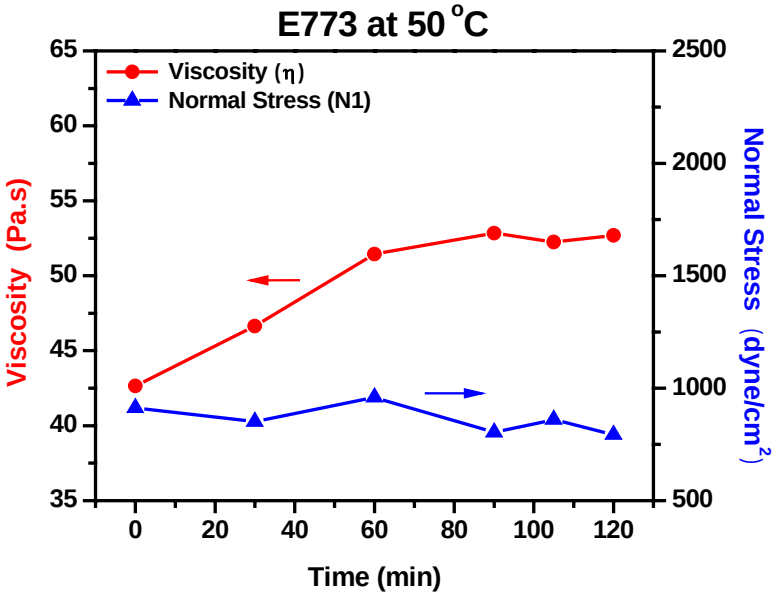

(a)

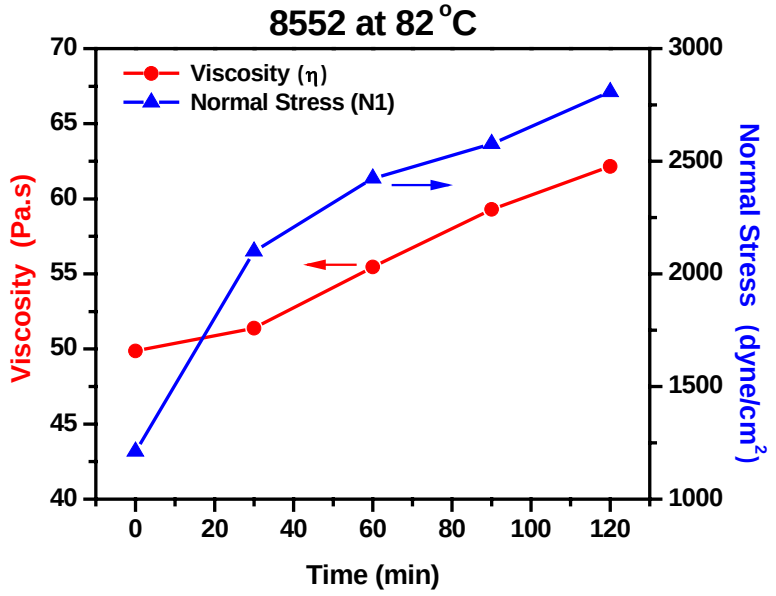

(b)

Figure 3.8 Shear viscosity of epoxy resin at processing temperature: (a) E773 at 50 °C and (b) 8552 at 82 °C.

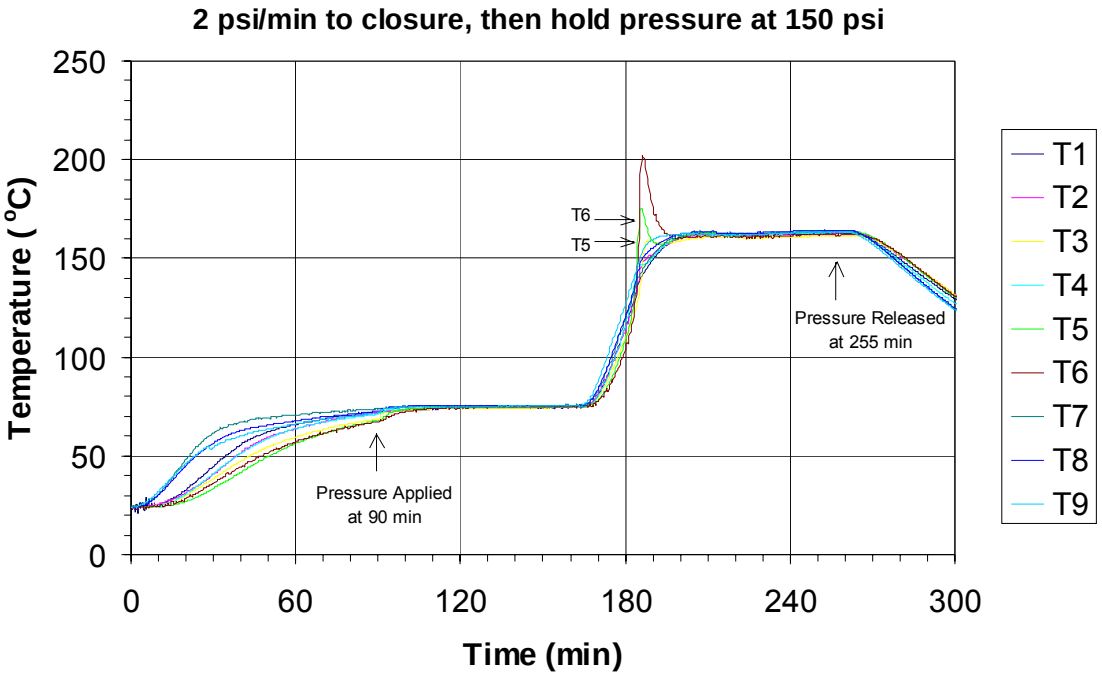

(a)

(Continued)

Figure 3.9 Temperature profiles of the parts during compression molding: (a) E773 and (b) 8552 composites.

Figure 3.9 continued

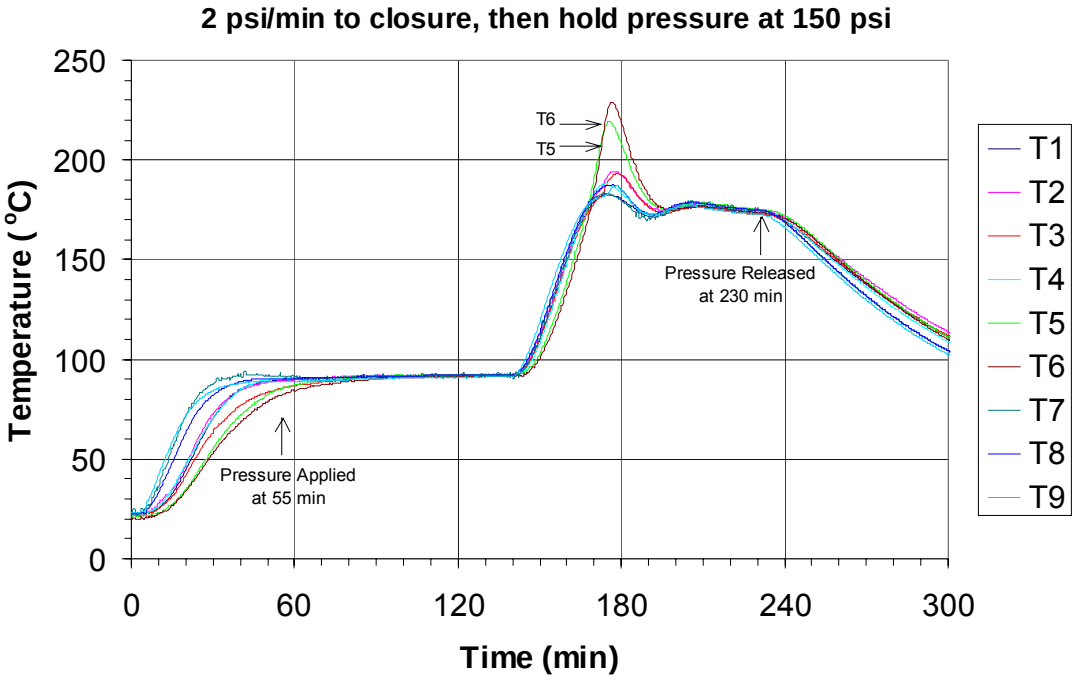

(b)

increased much slower than others when heating started in the second step of the cure cycle. This may result in a non-uniform distribution of rheological properties, such as viscosity and normal force, and the non-uniform build-up of stresses in the samples during heating and compressing. The non-uniform stress distribution is probably the main reason for marcel formation [8].

In addition, when the reaction exotherm started, T5 and T6 could reach much higher temperatures than at other locations, because the generated heat can not be transferred away fast enough in the middle of the prepreg plies.

3.3.2.3 *Aspect Ratio of Marcel*

To reduce or eliminate the marcel during compression molding, the process parameters need to be optimized. Nineteen experiments were designed to evaluate the five important parameters, including number of total plies placed in the molds, mold temperature, pressure rate, resin bleed path, and number of room-temperature vacuum debulking. Photos of several typical experiments are shown in Figures 3.10, 3.11, and 3.12. It can be seen that with various processing parameters, the marcels in the composite samples are different in occurrence time and size. It is possible to minimize the marcel formation through choosing appropriate processing parameters. Table 3.7 shows the input and output data of all nineteen experiments.

Based on the statistic analysis, it was found that the aspect ratio of marcels is affected by the mold temperature (resin viscosity) and pressure rate, and other parameters

are not important in these cases. Table 3.8 details the relationships of temperature with the significant independent parameters and their cross product term. The relationship between the largest aspect ratio of the marcel in the cured composite samples and the independent parameters is shown in the following equation:

$$\text{Aspect Ratio} = 4.6322 + (-0.0736)\cdot MT + 0.1960\cdot PR + (-0.0110)\cdot MT\cdot PR \qquad (3.3)$$

It can be seen that a higher mold temperature and a lower pressure rate lead to smaller marcel. This is reasonable because a high mold temperature results in low viscosity and normal stress, causing smaller stress to build up in the samples. Moreover, the surface of lay-up prepregs is usually not even. The lower compression rate also leads to smaller stresses generated in the sample.

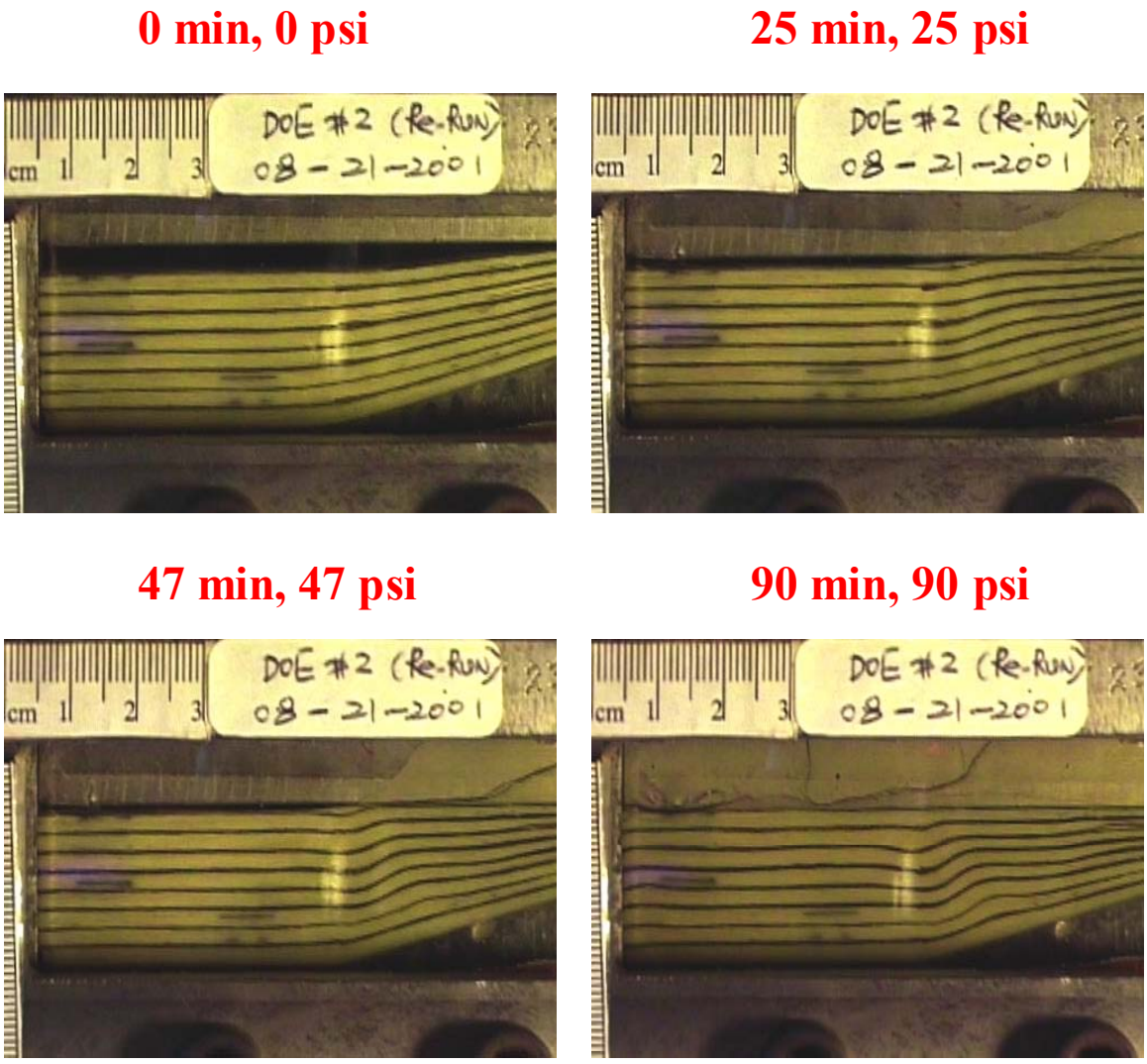

Figure 3.10 Pictures of the epoxy sample during compression molding: DOE #2.

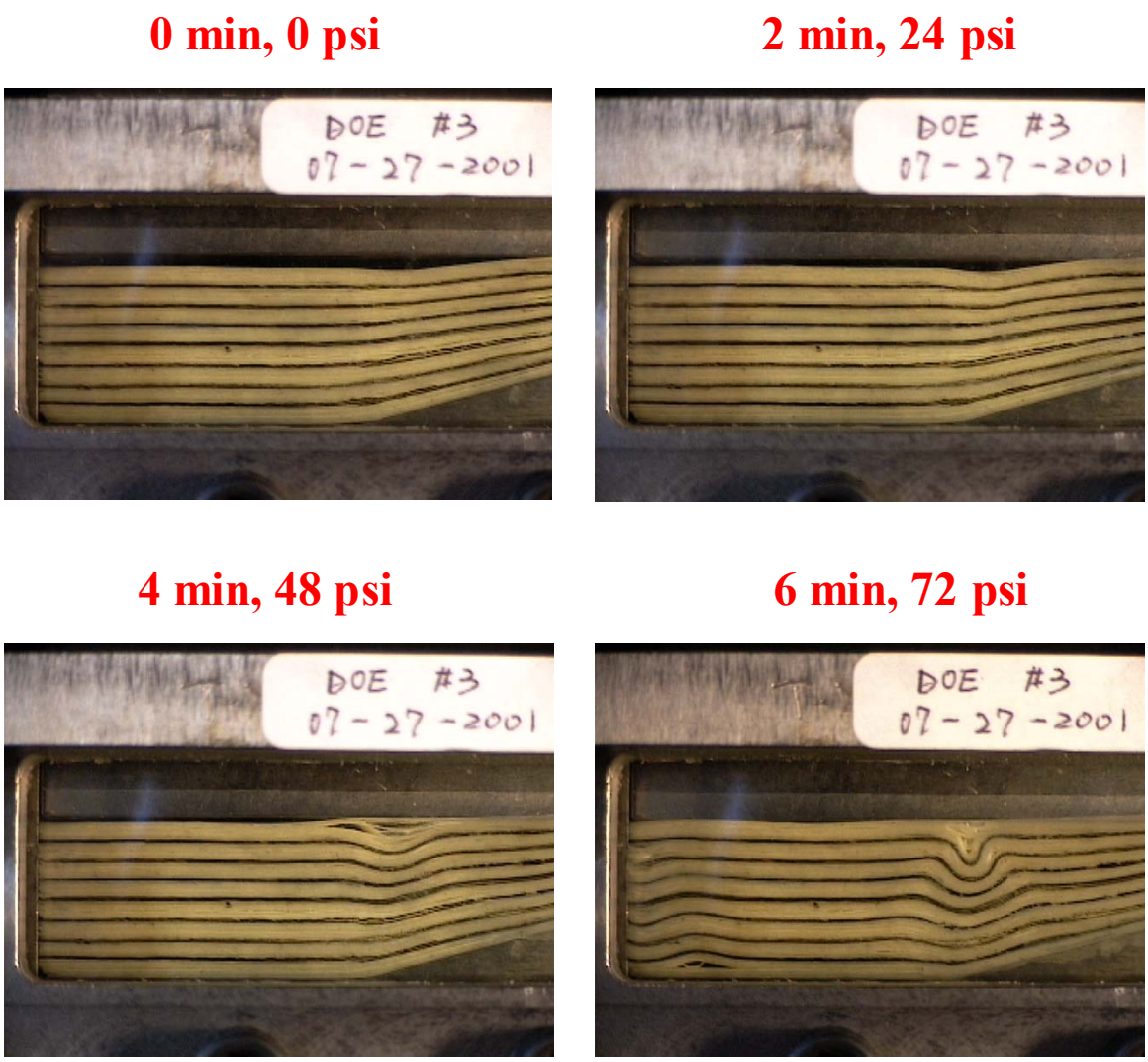

Figure 3.11 Pictures of the epoxy sample during compression molding: DOE #3.

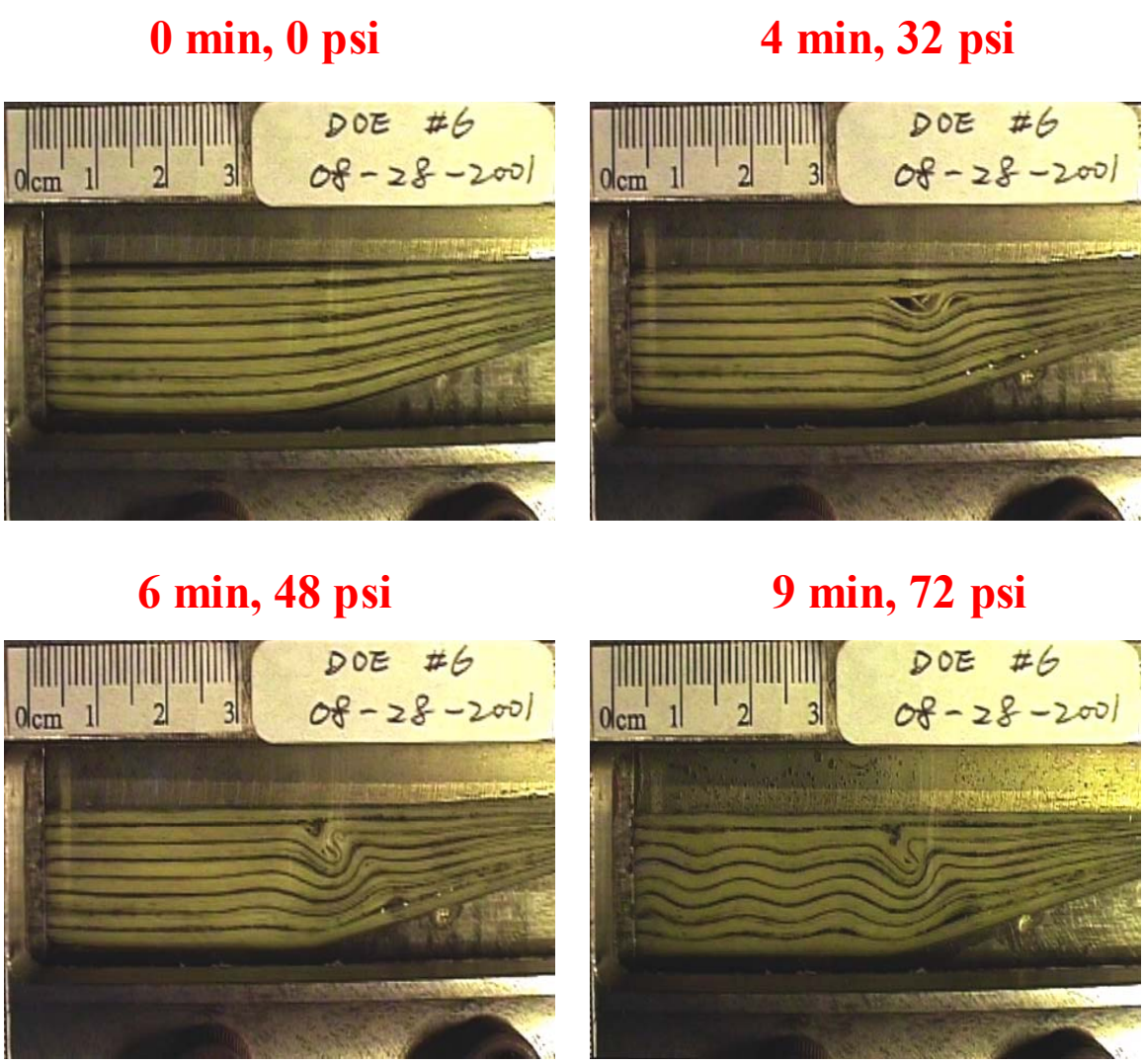

Figure 3.12 Pictures of the epoxy sample during compression molding: DOE #6.

	Input					Output
Run Order	Part Thick (ply)	T@PTarget (F)	Prate-Targe (psi/min)	Bleed Hole (inch)	# Debulk	Marcel Asp. Ratio
1	0	0	0	0	0	0.95
2	-	-	-	-	+	0.06
3	+	+	+	+	+	**13.90**
4	-	-	+	-	-	0.43
5	-	-	+	+	+	0.77
6	-	+	+	+	-	2.36
7	+	+	+	-	-	3.40
8	-	+	-	+	+	1.10
9	+	-	-	+	+	0.07
10	0	0	0	0	0	0.92
11	+	-	+	+	-	0.78
12	+	-	-	-	-	**0.00**
13	-	+	+	-	+	**3.60**
14	-	+	-	-	-	0.85
15	+	+	-	+	-	0.58
16	+	-	+	-	+	0.45
17	+	+	-	-	+	0.84
18	-	-	-	+	-	**0.00**
19	0	0	0	0	0	1.45

Table 3.7 Aspect ratio of marcel generated in compression molding experiments.

Effect	Coefficient	Std Error	t-ratio	Probability>|t|
CNST	4.6322	0.591	7.840	<0.001
MT	-0.0736	0.010	-7.712	<0.001
PR	0.1960	0.029	6.476	<0.001
MT·PR	-0.0110	0.003	-3.950	0.001

Table 3.8 Statistical analysis of marcel aspect ratio (r^2=0.982).

3.4 Conclusions

The primary results of this study include:

- ultrasonic treatment of advanced composites reduces the thickness of final parts before curing;
- amplitude has a significant effect on the peak temperature during ultrasonic treatment of composites;
- the compliance of the advanced composite affects the final peak temperature during ultrasonic treatment;
- the difference of rheological properties between E773 and 8552 resin is the main reason for different behavior of fiber marcelling during compression molding process;
- mold temperature (resin viscosity) and pressure rate have a significant effect on the aspect ratio of the marcel appearing in the compression molding process.

References

1. T. G. Gutowski, *Advanced Composites Manufacturing*, John Wiley & Sons: New York (1997).

2. S. R. Ghiorse, *SAMPE Quarterly*, **24**, 54 (1993).

3. S. F. M. Almeida, Z. D. Nougueira Neto, *Compos. Struct.*, **28**, 139 (1994).

4. M. L. Costa, S. F. M. Almeida, M. C. Rezende, *Compos. Sci. Technol.*, **61**, 2101 (2001).

5. M. R. Piggott, *Compos. Sci. Technol.*, **53**, 201 (1995).

6. H. M. Hsiao, I. M. Daniel, *Compos. Sci. Technol.*, **56**, 581 (1996).

7. M. R. Garnich, G. Karami, *J. Compos. Mater.*, **39**, 1225 (2005).

8. Y.-F. Chen, *American Helicopter Society 58th Annual Forum Proc.*, **56**, 391 (2002).

9. D. Grewell, *Proceedings of 1996 Annual Technical Conference – Society of Plastics Engineers*, **54**, (1996).

10. A. Benatar, T. G. Gutowski, *Polym. Eng. Sci.*, **29**, 1705 (1989).

CHAPTER 4

NANOCLAY AND LONG FIBER REINFORCED COMPOSITES BASED ON EPOXY AND PHENOLIC RESINS

4.1 Introduction

Among various thermoset polymers, epoxy resins provide superior overall performance, such as good mechanical properties, chemical resistance, and low shrinkage. They are high-performance materials for use in coating, adhesive, civil engineering, structural, electronic, and composite applications [1].

Phenolic resins were the first thermoset resin to be synthesized commercially in 1907. These resins not only are low-cost and easy to produce, but also exhibit excellent fire performance, good dimensional stability, excellent thermal insulation properties, and good chemical and corrosion resistance. These features enable phenolics to be used in myriad applications, such as household appliances, business equipment, wiring devices, and electrical systems [2].

Fiber reinforced plastics (FRPs) are the most widely used composites. In general, fibers are the principal load-carrying members, while the surrounding matrix keeps the

fibers in the desired location and orientation, acting as a load transfer medium and protecting fibers from environmental damage due to exposure to elevated temperature and humidity. Fiber-reinforced composites have low specific gravity, high internal damping, and high strength-to-weight ratio and modulus-to-weight ratio. There have been numerous applications based on FRPs [3, 4].

Nanocomposites are a type of composite in which the scale of the dispersed phase is less than 100 nm at least in one dimension. Due to the nanoscale dispersion and the high aspect ratios of the inorganic clays, polymer-layered silicate nanocomposites (PLSNs) exhibit light weight, dimensional stability, heat resistance, high stiffness, barrier properties, and improved toughness and strength with far less reinforcement loading than conventional composite counterparts [5-11]. The synthesis and characterization of PLSNs has become one of the frontiers in materials science.

In general, PLSNs can be divided into two categories: intercalated and exfoliated composites [5-8]. In an intercalated nanocomposite, a few polymer chains are inserted into the silicate galleries with fixed interlayer spacing. In contrast, an exfoliated nanocomposite is formed when the silicate nanolayers are delaminated and well dispersed in the continuous polymer matrix. The exfoliated state may maximize interfacial contact between the organic and inorganic phases, and as a result, nanocomposites with optimum performance properties can be achieved.

Although FRPs have good mechanical properties, cohesive failure of the polymer matrix may occur under tension, compression, or impact. If water or other small molecules diffuse into the interface between the matrix and fibers, interfacial strength

may drop substantially and adhesive failure may occur in the interfacial region. On the other hand, however, the loading of clay often cannot reach a very high level (<10 wt%) due to the dispersion difficulty. Thus, mechanical properties of PLSNs are relatively low compared with those of highly loaded FRPs (>50 wt%).

In this study, we try to combine the advantages of both FRPs and PLSNs to synthesize high-performance thermoset polymer composites based on epoxy and phenolic resins.

4.2 Experimental

4.2.1 Preparation of Epoxy Samples

The epoxide resin used for the formation of the neat epoxy polymer, the epoxy-clay nanocomposites, and the epoxy-clay-carbon fiber composites is a diglycidyl ether of bisphenol A (DGEBA), EPON 828 with an epoxy equivalent weight of ~187, provided by Resolution Performance Products. The curing agent is a polyoxypropylene diamine, Jeffamine D230 with a molecular weight of ~230 provided by Huntsman Chemicals. The clay used is an industrially purified and organically treated montmorillonite, Cloisite® 10A, provided by Southern Clay. The carbon fiber is a 25.4 mm (1 inch) chopped fiber, Zoltek XP3304815R-X19, obtained from Ashland Chemical Company.

The neat epoxy polymer was formed by mixing the epoxy monomer (EPON 828) with the curing agent (Jeffamine D230). The mixture was degassed at 50 °C for 30 min, cured in a silicone rubber mold at 65 °C for 1 h and 120 °C for 1 h, and then post-cured at 180 °C for additional 2 h.

The preparation of epoxy-clay nanocomposites was similar to the formation of the pure epoxy resin. In one method (a), EPON 828 and the clay were mixed under stirring for 30 min and sonicated for another 30 min at room temperature. The curing agent D230 was then added into the mixture and degassed at 50 °C for 30 min. In the second method (b), the clay was initially mixed with D230. The mixture was sonicated for 30 min at room temperature, and then EPON 828 was added.

The epoxy-clay-carbon fiber prepregs were prepared by the hand lay-up method. The prepregs were compression molded under a pressure of 3.45×10^6 Pa at 120 °C for 1 h and post-cured at 180 °C for additional 2 h. The content of carbon fiber was 25 wt.%.

4.2.2 Preparation of Phenolic Samples

Both phenol and formaldehyde solution are obtained from Fisher Scientific. The curing agent is hexamethylenetetramine (HMTA) from ICN Biomedicals Incorporated. The clay used is an industrially purified montmorillonite, Cloisite® Na^+ clay from Southern Clay. A type of 1.27 cm (half inch) chopped PAN-based carbon fiber, Zoltek XP3304815R-X19, is provided from Ashland Chemical Company.

Phenolic-clay nanocomposites were prepared by in-situ condensation. In a typical reaction, phenol (1.0 mol), 37% formaldehyde solution (0.85 mol), and the desire amount of Na^+-clay were added into a 500-ml three-neck flask equipped with a mechanical stirrer, a thermometer, and a reflux condenser. A small amount of hydrochloride acid (~0.005 mol) was added as the catalyst. The mixtures were heated at 95 °C with stirring for 3 h and then dehydrated under reduced pressure at 120 °C for another 3 h to obtain phenolic-clay composites. Cured phenolic-clay composites were obtained by mixing the uncured mixtures (1.8 g) with HMTA (0.2 g), cured at 120 °C for 2 h, and post-cured at 180 °C and 200 °C for additional 2 h respectively.

To prepare phenolic-clay-carbon fiber composites, phenolic-clay mixtures were dissolved in ethyl alcohol (weight ratio = 1 : 1) with a desired amount of HMTA. The

resin solution is mixed with carbon fiber. Then the mixture was dried at room temperature for 24 h, and compression molded under a pressure of 3.45×10^6 Pa at 120 °C for 2 h and post-cured at 180 °C and 200 °C for additional 2 h respectively.

4.2.3 Structure Analysis

X-ray diffraction (XRD) patterns were obtained on a Scintag XDS-2000 X-ray diffractometer equipped with CuKα X-ray radiation at 45 kV and 20 mA. All samples were scanned from 1° to 10° at a scanning rate of 1°/min.

Scanning Electron Microscopy (SEM) photos of fractured samples were obtained on a Hitachi S-4300 microscopy at 10 kV and 10 mA.

4.2.4 Measurement of Mechanical and Thermal Properties

Thermal mechanical analysis (TMA) was performed on a TA 2940 thermal mechanical analyzer to measure glass transition temperature (T_g) and coefficients of linear thermal expansion. The heating rate was 5 °C/min. For each sample, three specimens were tested.

Tensile tests were carried out with an Instron 8511 Testing Machine under a strain rate of 5 mm/min at either 25 or 80 °C. All test specimens were made according to ASTM D638-01. Five specimens were tested for each sample.

Flexural properties were tested with an Instron 8511 Testing Machine according to ASTM D790-03. The support span of 3-point bending tests was 50.8 mm. Five specimens were tested for each composite sample.

4.2.5 Test of Water Absorption

Water absorption tests were carried out according to ASTM D570-98. The dimensions of the specimens were 76.2 mm long, 25.4 mm wide, and 3.2 mm thick. Two specimens were tested for each sample.

The water content of each sample was calculated by the following equation,

$$\text{Water Content } \% = \frac{M_t - M_0}{M_0} \times 100\% \tag{4.1}$$

where M_0 and M_t are the initial sample weight and the sample weight on the t-th days, respectively.

4.3 Results and Discussion

4.3.1 Epoxy Composites

Clay dispersion in the composites was verified using XRD. The typical XRD patterns of the clay 10A and composites are shown in Figure 4.1. The XRD pattern of the clay 10A powder exhibits a strong silicate diffraction peak at $2\theta = 4.81°$ corresponding to a basal spacing of 1.8 nm. For the composite obtained by method (a), the diffraction peak shifts to 3.07° corresponding to a spacing of 2.9 nm. This means an intercalated structure of clays in the composites. The diffraction peak of the clay disappears completely in the composite prepared by method (b), implying that an exfoliated epoxy-clay nanocomposite was obtained. This is probably because the size of diamine molecules is smaller and more flexible than epoxy molecules. Also the diamine is more hydrophilic than the epoxide. It is much easier for diamine monomers to insert into the gallery of clay. In method (b), D230 was mixed with clay first, which provided more time for the diamine molecules to diffuse into the gallery of clay. The polymerization occurring between the amine group and the epoxy group in the clay galleries led to the propagation of polymer chains, causing the spacing of the clay layers to increase gradually. Finally, the clay was delaminated by polymer molecules. This is demonstrated by the change of the diffraction peak in the composite during the curing of a resin-clay mixture prepared by method (b) as shown in Figure 4.2.

A typical TMA curve of epoxy-clay nanocomposite is shown in Figure 4.3, in which T_g and thermal expansion coefficients can be determined. Table 4.1 shows the TMA results of neat epoxy resin and epoxy-clay nanocomposites. It can be seen that

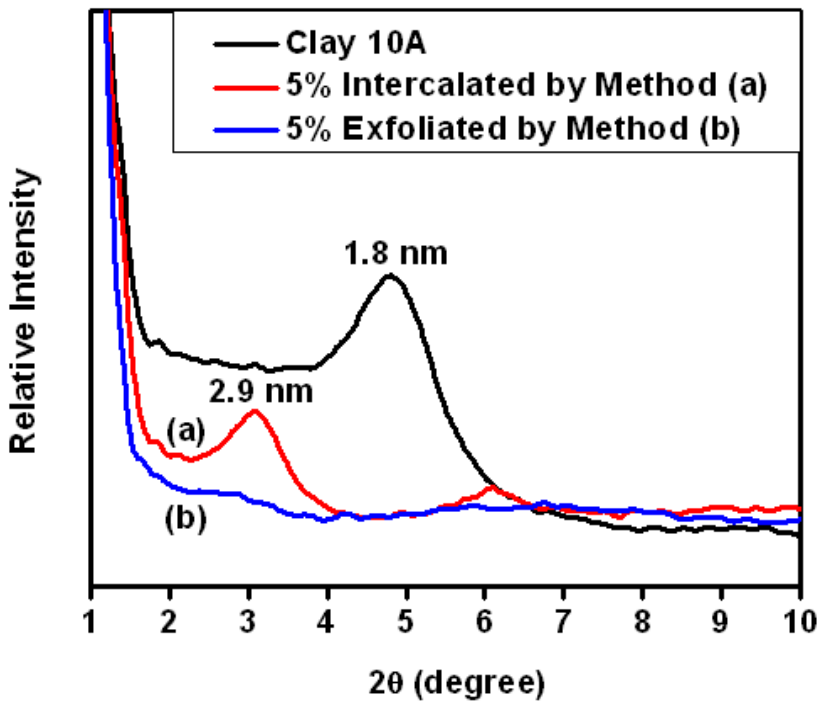

Figure 4.1 XRD patterns of Clay 10A: (a) intercalated 5% and (b) exfoliated 5% epoxy nanocomposite.

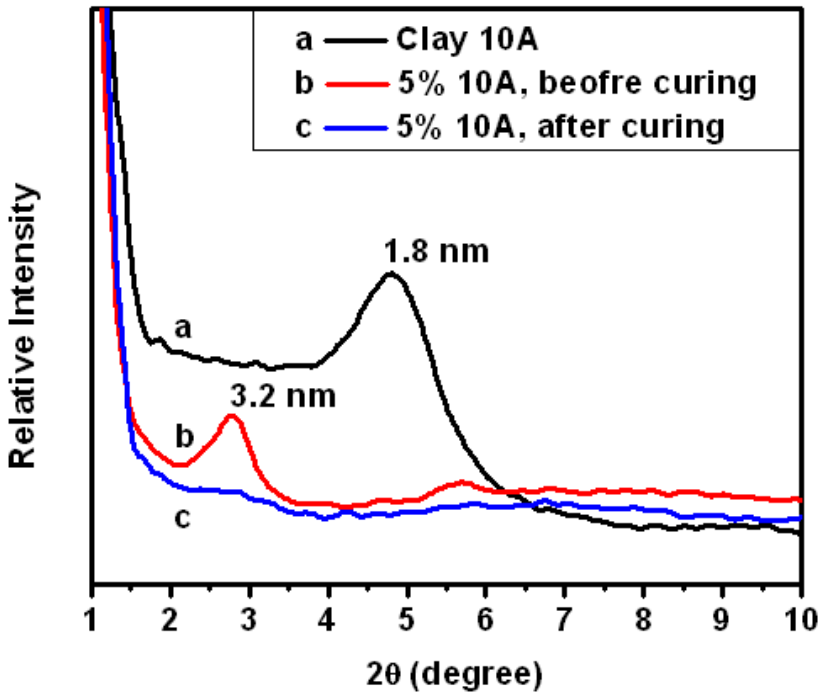

Figure 4.2 XRD patterns of (a) Clay 10A, (b) 5% epoxy nanocomposite at gel point prepared by method (b), and (c) 5% epoxy nanocomposite after post-curing.

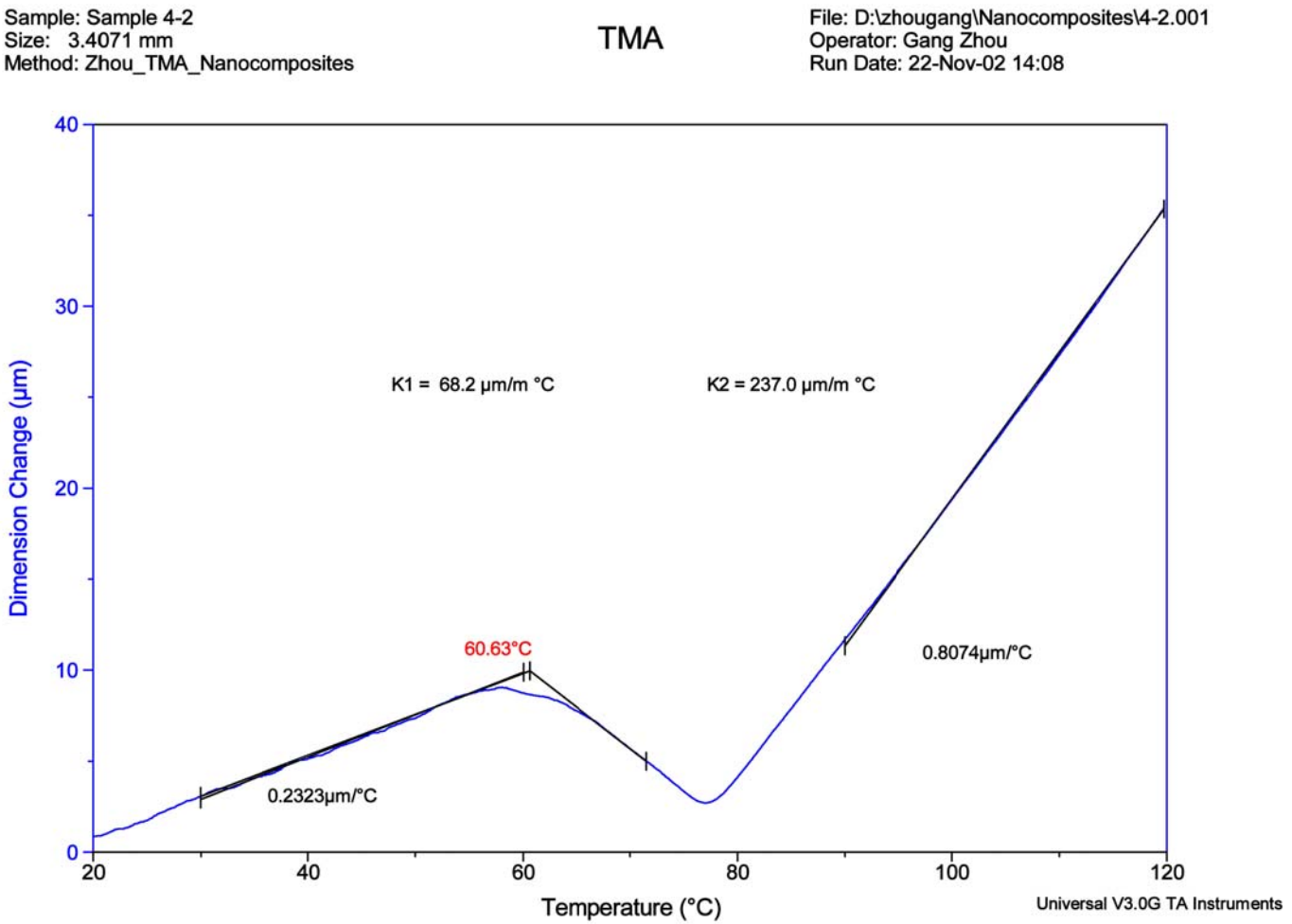

Figure 4.3 A typical TMA curve of epoxy-clay nanocomposites.

Samples	Neat Epoxy Resin	3% Clay Nanocomposite	5% Clay Nanocomposite
α_1 (μm/m·°C) [a]	70.6	65.9	49.6
α_2 (μm/m·°C) [b]	258.9	242.6	232.9

[a] α_1 is the mean coefficient of linear thermal expansion in the temperature range of 30~60 °C (below T_g).

[b] α_2 is the mean coefficient of linear thermal expansion in the temperature range of 90~120 °C (above T_g).

Table 4.1 The coefficient of linear thermal expansion of epoxy prepared by Method (b).

when the clay loading increases, the coefficients of linear thermal expansion of nanocomposites decline. The reason is that the dispersed clay layers can interact with the surrounding polymer molecules, restrict the movement of polymer chains, and help to hold the structure of the composites. These results indicate that the addition of the nanoclay can improve the thermal stability of epoxy resins.

The tensile strength and modulus of two kinds of epoxy-clay nanocomposites were measured to assess the reinforcement effect of the clay in both a glassy and a rubbery matrix. As shown in Figure 4.4, the modulus of the intercalative nanocomposite (5% clay loading) increased 17%, but the strength declined 24% at the glassy state (25 °C) compared with the pure epoxy. However, in the rubbery state (80 °C), both modulus and strength increased substantially, especially for exfoliated nanocomposites (see Figures 4.5 and 4.6). With 5% clay loading, the tensile modulus and strength of the exfoliated nanocomposites improved 80% and 64% respectively. The reason is that the mobility of polymer chain can be restricted by the presence of the clay layers in the polymer matrix at the rubbery state. In exfoliated nanocomposites, the crystal structure of clay is destroyed and the clay layers are uniformly dispersed in the matrix, so that the interaction between the polymer and the clay is much stronger than that in intercalated nanocomposites. In addition, platelet alignment under strain may also contribute to improved performance of clays in a rubbery matrix as compared with a glassy matrix. The induced alignment of the clay layers can block the propagation of fracture in the polymer matrix [12]. Similar results were also observed for the intercalated epoxy/clay nanocomposites reinforced by 25 wt% carbon fiber, as shown in Figure 4.7. Because the

reinforcement in these composites is mainly from carbon fibers, the improvement caused by nanoclays is not as great as that in the composites without carbon fibers.

The barrier property of nanoclay is evaluated through the water absorption tests. From Figures 4.8 and 4.9, it can be seen that the amount of water absorbed by the composites and the rate of water absorption decreased with an increase of clay content in the composites. After 168 hours (7 days), the water absorbed by the composite with 5% clay is about 15 percent lower than that in the composite without clay. Due to the presence of clay in the polymer matrix, the diffusion path of water molecules would increase, so the rate of water absorption becomes smaller. This lowers the permeability of water or other small molecules in and out of the composites, improving the water resistance of composites and extending the longevity of long fiber-reinforced composites.

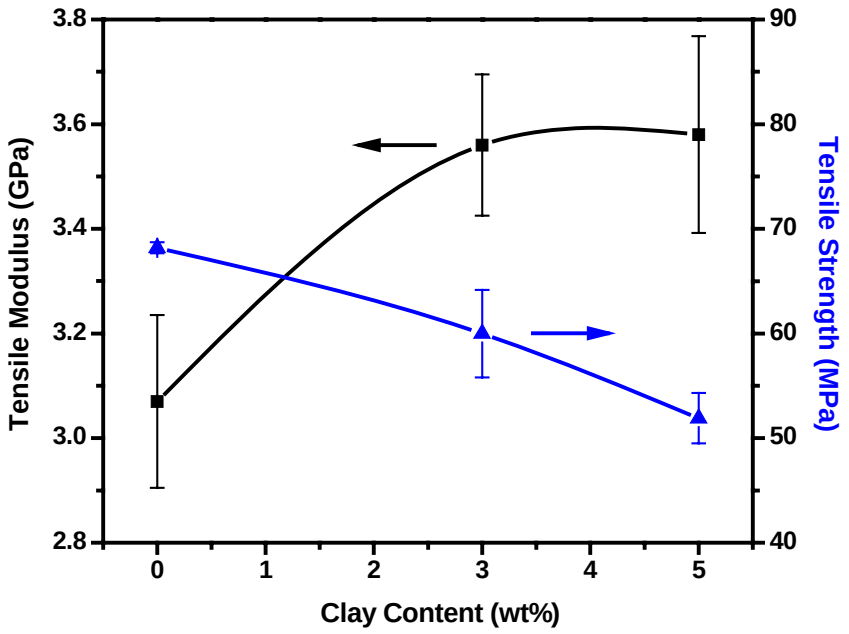

Figure 4.4 Dependence of tensile modulus (■) and strength (▲) of intercalated epoxy-clay nanocomposites on clay loading at ambient temperature (25 °C).

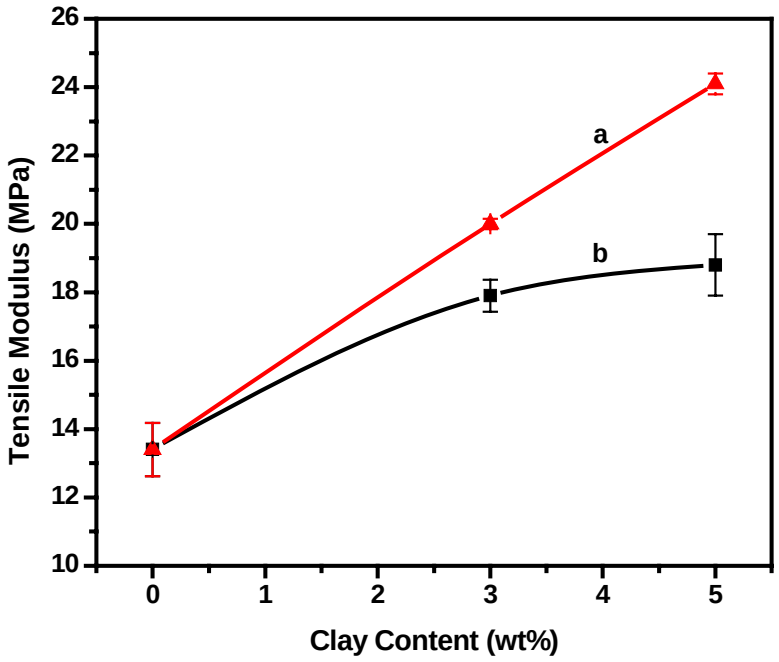

Figure 4.5 Dependence of tensile modulus of epoxy-clay nanocomposites on clay loading at 80 °C: (a) exfoliated and (b) intercalated epoxy nanocomposites.

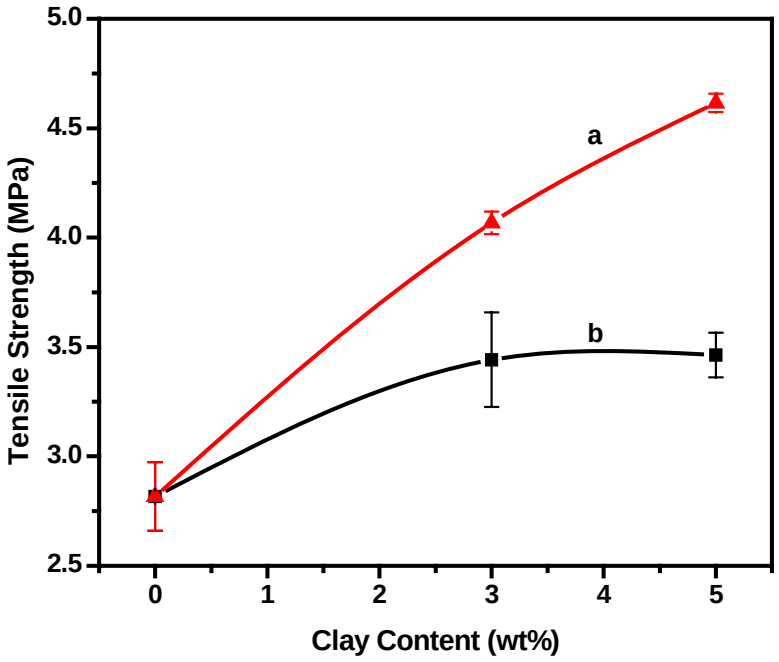

Figure 4.6 Dependence of tensile strength of epoxy-clay nanocomposites on clay loading at 80 °C: (a) exfoliated and (b) intercalated epoxy nanocomposites.

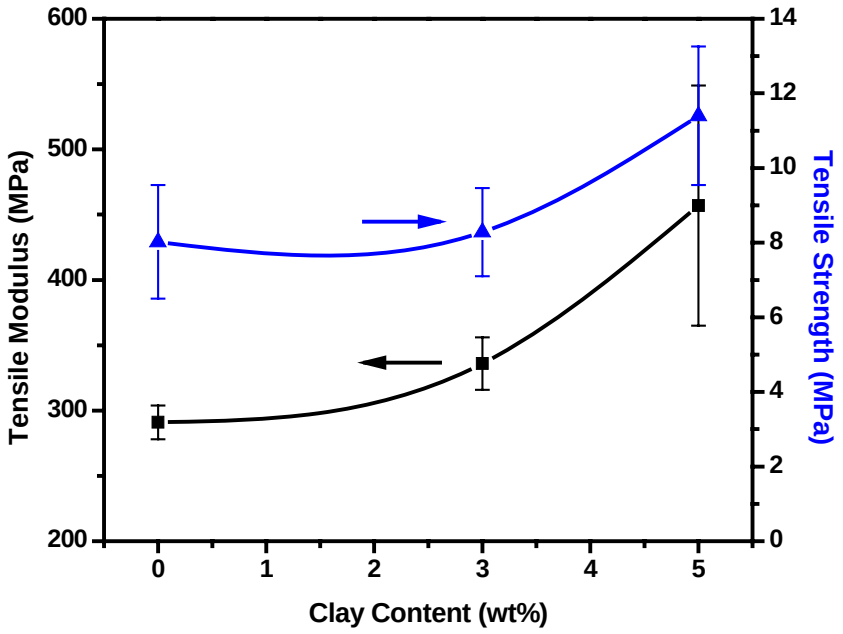

Figure 4.7 Dependence of tensile modulus (■) and strength (▲) of epoxy-clay-carbon fiber composites on clay loading at 80 °C (25 wt.% carbon fibers).

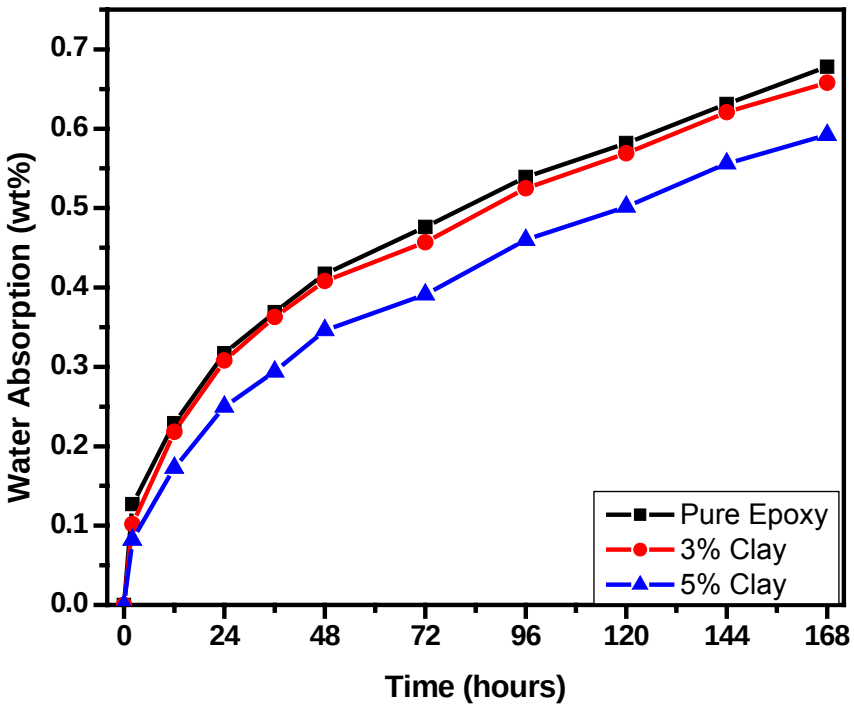

Figure 4.8 Water content of pure epoxy resin (■),epoxy-3% clay nanocomposite (●), and epoxy-5% clay nanocomposite (▲) when immersed in deionized water at room temperature.

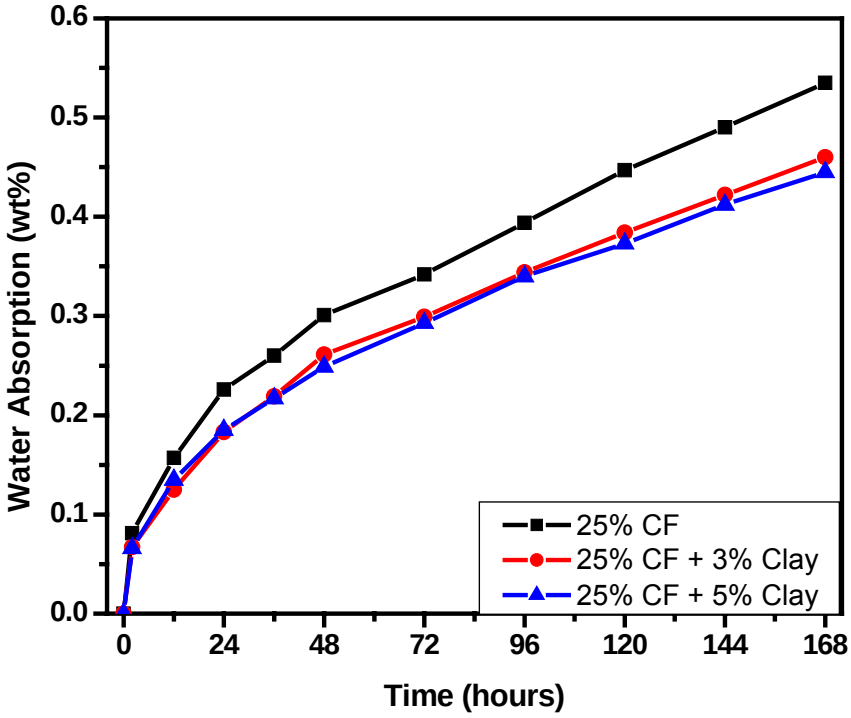

Figure 4.9 Water content of epoxy-25wt% carbon fiber composite (■),epoxy-3wt% clay-25wt% carbon fiber composite (●), and epoxy-5wt% clay-25wt% carbon fiber composite (▲) when immersed in deionized water at room temperature.

4.3.2 Phenolic Composites

Clay dispersion in the composites was verified using XRD. The typical XRD patterns of the clay and composites are shown in Figure 4.10. The XRD pattern of the Na^+-clay powder exhibits a strong silicate (001) diffraction peak at $2\theta = 7.15°$ corresponding to a basal spacing of 1.1 nm. For both uncured and cured phenolic composites, the (001) diffraction peak of clay disappears completely, implying that the phenolic-clay exfoliated nanocomposites can be readily prepared during the sample preparation stage and retained in the curing processes. It is known that pristine Na^+-clay mainly contains hydrated sodium ions to counterbalance the layer charge, making nanoclay hydrophilic [13]. Therefore, nanoclay particles can easily exfoliate in water. Since the polycondensation of phenol and formaldehyde is carried out in the aqueous system and a large number of sodium ions exist in the galleries of Na^+-clay, hydrophilic phenol and formaldehyde molecules can readily intercalate into the galleries by polar-polar and charge interactions [14]. Moreover, the protons (H^+) in the reaction system can easily exchange the sodium ions of Na^+-clay and insert into the galleries of clay [15]. These protons can catalyze the condensation reaction of phenols and formaldehydes. The growth of polymer chains can expand the silicate galleries, and finally the nanoclay can exfoliate completely. Therefore, in the polymerization condition of phenolic resins, Na^+-clay can delaminate entirely with the formation of high molecular weight phenolics. Even with dehydration and curing, the exfoliated state of clay remains in the cross-linking structure of phenolic nanocomposites.

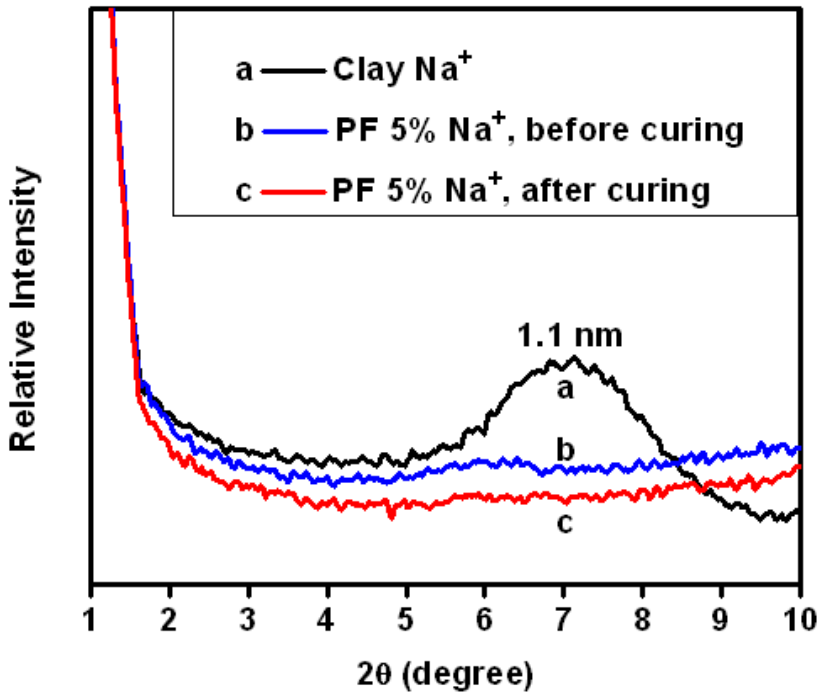

Figure 4.10 XRD patterns of (a) Cloisite Na^+, 5% phenolic nanocomposites (b) before curing and (c) after curing.

The flexural properties of phenolic composites are shown in Figures 4.11 and 4.12. It can be seen that the incorporation of long carbon fibers and nanoclay can improve the flexural properties of phenolic resins. For example, when adding 25 wt.% carbon fibers into phenolic resins, both flexural strength and modulus increase more than 2 times. The additional 5 wt.% nanoclay can contribute another 17% and 10% improvement in the flexural strength and modulus, respectively. In the phenolic-carbon fiber-nanoclay composites, the carbon fibers with high strength and modulus provide the main enhancement of the mechanical properties, and the exfoliated nanoclays may reinforce the resin-rich area in the composites, preventing crack generation and crack propagation in the polymer matrix between the carbon fibers. The synergic effects of long fiber and nanoparticles lead to the largest improvement of the flexural properties of phenolic composites.

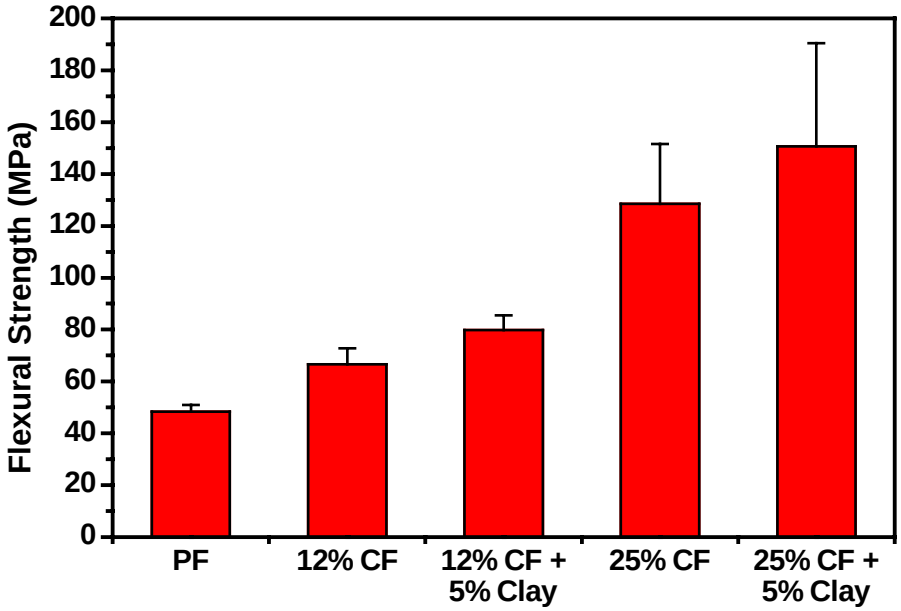

Figure 4.11 Flexure strength of phenolic-carbon fiber-Na^+ clay composites at ambient temperature (25 °C).

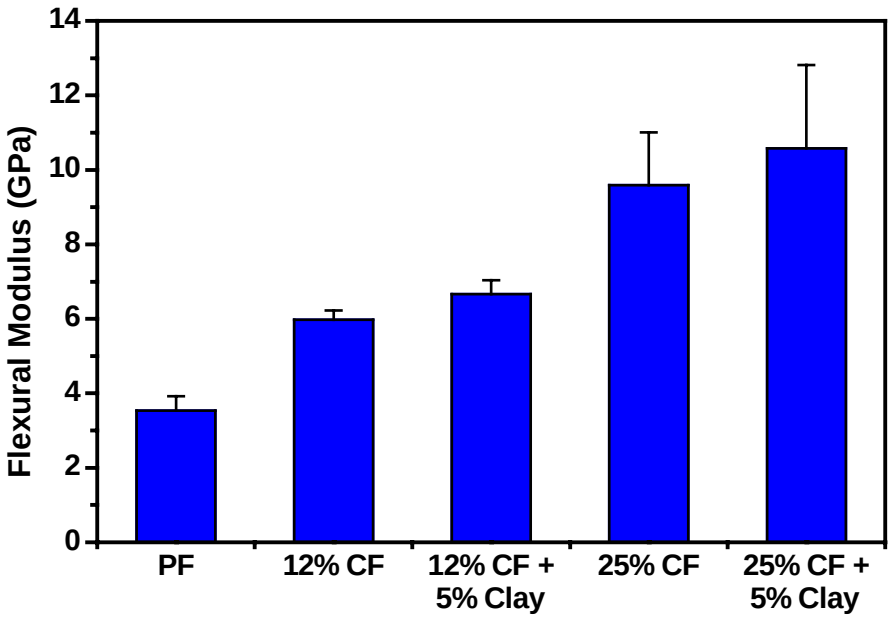

Figure 4.12 Flexure modulus of phenolic-carbon fiber-Na^+ clay composites at ambient temperature (25 °C).

4.3.3 Comparison of Epoxy and Phenolic Composites

From above results, it can be found that organically modified clays need to be used in the epoxy system to obtain the exfoliated structure. While for the phenolic system, raw clays without any organic surfactant can delaminate easily during in-situ polymerization. This is because that epoxy resin is more hydrophobic and phenolic resin is more hydrophilic. In addition, the synthesis of phenolic resin takes place in the aqueous solution, in which Na^+-clay particles can be readily exfoliated by water molecules.

From the results shown in Figure 4.13, it can be seen that the introduction of nanoclay shifts the T_g of phenolic resins to a higher temperature considerably. This, however, is not the case for epoxy systems. The T_g of phenolic resins rises from 207 °C of the pure phenolic resin to 247 °C of the phenolic-5% clay nanocomposite. On the other hand, the T_g of the epoxy nanocomposites only increases less than 10 °C with the same clay loading. This difference may be explained by the interactions between the polymer matrix and nanoclays. In general, the nanoclays in the epoxy system may cause an increase of T_g because of the molecular interactions at the epoxy-clay interface, resulting in restricted motions of polymer segments near the organic-inorganic interface [7, 16]. It has been also found that the presence of nanoclays may decrease the crosslink of epoxy resins [17, 18]. The void of the crosslink would lead to long soft segments in the polymer chains, resulting in a decline of T_g. The T_g of epoxy-clay nanocomposites is determined by the competition of these two factors. For phenolic resin, the dramatic increase of the T_g is due to the strong interfacial interaction between the silicate nanolayers and phenolic matrix, which reduces the molecular mobility of the matrix molecules. In addition, the

structure of phenolic resin is much different from that of epoxy resin. Every phenol ring can be a crosslinking site because it is a tri-functional molecule. Therefore, a large number of crosslinks exist in phenolic resin, resulting in a rigid structure. Even the presence of nanoclays may affect some crosslinks in the phenolic resin, there are still a lot of crosslinks left in the system, consequently the T_g may not be affected significantly by the slight decrease of crosslinks.

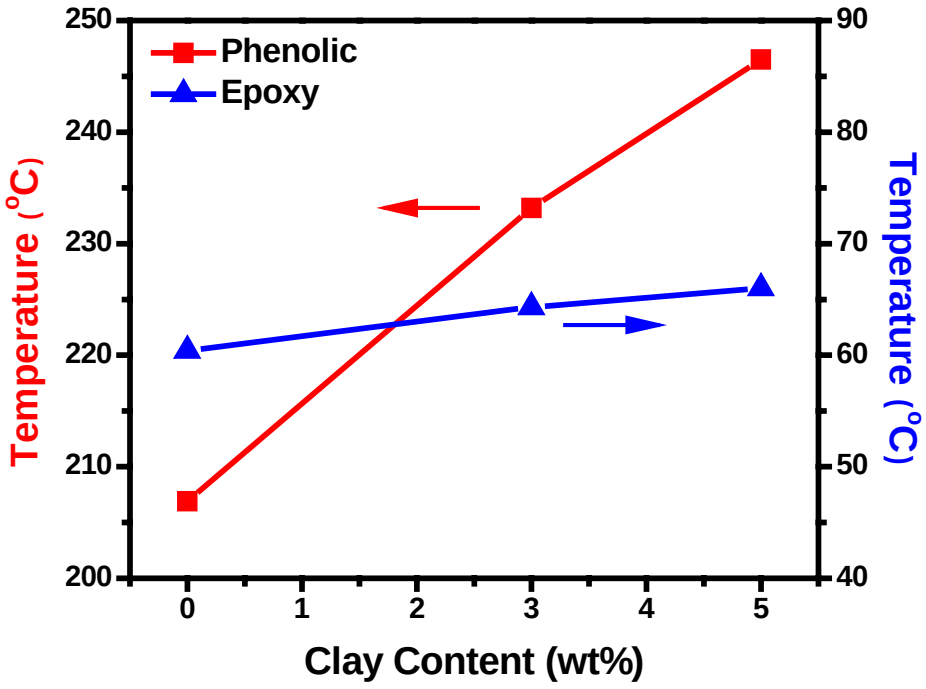

Figure 4.13 Dependence of glass transition temperature of Epoxy and phenolic nanocomposites on clay loading.

4.4 Conclusions

A series of epoxy-clay and epoxy-clay-carbon fiber composites were prepared. Adding nanoclay into the epoxy resin can substantially improve the tensile strength and modulus of materials above the glass transition temperature. It also enhances the thermal stability and lowers the water permeability compared with the neat epoxy resin. The dispersion state of nanoclay in the polymer matrix is affected by the mixing sequence. Both intercalated and exfoliated nanocomposites can be obtained.

Phenolic-raw clay nanocomposites and phenolic-carbon fiber-raw clay hybrid composites were also prepared. Exfoliated nanocomposites were obtained by in-situ polymerization. Adding nanoclay into the phenolic matrix can enhance the flexural properties and T_g substantially.

References

1. H. Lee, K. Neville, *Handbook of Epoxy Resins*, McGraw-Hill: New York/San Francisco/Toronto/London/Sydney (1967).

2. A. Gardziella, L. A. Pilato, A. Knop, *Phenolic Resins: Chemistry, Applications, Standardization, Safety, and Ecology*, Springer-Verlag (1999).

3. J. F. Monk, *Thermosetting Plastics 2nd Edition*, Addison Wesley Longman: Great Britain (1997).

4. P. K. Mallick, *Fiber-Reinforced Composites*, Marcel Dekker: New York/Basel (1988).

5. X. Wang, Z. Qi, F. Wang, *Eng. Plast. Appl.*, **27**, 1 (1998).

6. Z. Wang, T. Lan, T. J. Pinnavaia, *Chem. Mater.*, **8**, 2200 (1996).

7. P. B. Messersmith, E. P. Giannelis, *Chem. Mater.*, **6**, 1719 (1994).

8. R. Krishnamoorti, R. A. Vaia, E. P. Giannelis, *Chem. Mater.*, **8**, 1728 (1996).

9. R. A. Vaia, K. D. Jandt, E. J. Kramer, E. P. Giannelis, *Chem. Mater.*, **8**, 2628 (1996).

10. Z. Wang, T. J. Pinnavaia, *Chem. Mater.*, **10**, 1820 (1998).

11. K. Yano, A. Usuki, A. Okada, T. Kurauchi, O. Kamigaito, *J. Polym. Sci. Part A: Polym. Chem.*, **31**, 2493 (1993).

12. T. J. Pinnavaia, T. Lan, Z. Wang, H. Shi, P. D. Kaviratna, *ACS Sym. Ser.*, **622**, 250 (1996).

13. T. J. Pinnavaia, *Science*, **220**, 365 (1983).

14. H. Wang, T. Zhao, L. Zhi, Y. Yan, Y. Yu, *Macromol. Rapid Commun.*, **23**, 44 (2002).

15. B. K. G. Theng, *The Chemistry of Clay-Organic Reactions*, John Wiley & Sons: New York (1974).

16. J. M. Brown, D. Curliss, R. A. Vaia, *Chem. Mater.*, **12**, 3376 (1998).

17. O. Becker, R. Varley, G. Simon, *Polymer*, **43**, 4365 (2002).

18. W.-B. Xu, S.-P. Bao, P.-S. He, *J. Appl. Polym. Sci.*, **84**, 842 (2001).

CHAPTER 5

PREPARATION, STRUCTURE, AND PROPERTIES OF NANOPARTICLE AND LONG FIBER REINFORCED UNSATURATED POLYESTER COMPOSITES

5.1 Introduction

Fiber reinforced plastics (FRPs) are the most widely used composites. In general, fibers are the principal load-carrying members, while the surrounding matrix keeps the fibers in the desired location and orientation, acting as a load transfer medium and protecting fibers from environmental damage when exposed to elevated temperature and humidity. Fiber-reinforced composites have low specific gravity, good internal damping, a high strength-to-weight ratio and a high modulus-to-weight ratio [1-3].

Although fiber-reinforced plastics have good in-plane mechanical properties that are determined by the long fibers, the properties in the transverse and the thickness directions defined by the characteristics of the matrix resin are much weaker. Under tension, compression, shear, or impact, failure of the polymer matrix may take place [4]. Nanoparticles, on the other hand, may directly reinforce the polymer matrix. Polymer-nanoparticle composites have been extensively studied since the 1990s [5-11].

Because of the nanoscale dispersion and the high aspect ratios of the nanoparticles, polymer nanocomposites exhibit light weight, dimensional stability, heat and flame resistance, barrier properties, and improved toughness and strength with far less reinforcement loading than conventional composite counterparts [12, 13]. However, the loading of nanoparticles in polymer nanocomposites often cannot reach a high level (<10 wt.%) due to the dispersion difficulty. Thus, mechanical properties of polymer nanocomposites are relatively low compared with those of highly loaded FRPs (>50 wt.%).

It would be desirable to combine the advantages of both FRP and polymer nanocomposites to produce a superior composite — long fibers and nanoparticles reinforced polymer composites. Continuous fibers can provide good mechanical properties to the composites, while nanoparticles may strengthen the matrix between the long fibers in order to reduce the matrix failure in the composites and extend the longevity of the composites.

To succeed in producing these new composites, two questions need to be answered: How to well disperse nanoparticles into FRPs? And can the resin processability be maintained with the presence of nanoparticles? Pre-mixing nanoparticles into polymer resins is a common approach to make nanoparticles reinforced polymer-long fiber composites [14-17]. However, well-dispersed nanoparticles may greatly increase the resin viscosity and cause difficulties during composite processing [18, 19]. To solve these problems, a new method is proposed to pre-bind nanoparticles onto the long fibers instead of mixing them with the polymer resin. In this work, these two

approaches were investigated using the Seeman composite resin infusion molding process (SCRIMP).

SCRIMP is a promising vacuum assisted resin transfer molding (VARTM) technique, for manufacturing large composite parts. It is more cost effective than prepreg/autoclave process and more environmentally friendly than hand lay-up and spray-up processes. Although its origin can be traced back to early 1950s [20], SCRIMP and similar processes were developed primarily in the 1980s and 1990s [21-24]. As SCRIMP is used to produce very large parts, the mold filling time becomes extremely crucial for controlling the molding cycle and consequently the economics of the process. In this context, several related issues of the process, such as resin flow [25-27] and preform compaction [28, 29], have been investigated in the past. All these studies focused on systems consisting of only two main components, namely the long fiber reinforcement (glass or carbon fibers) and a resin matrix. Our study deals with a third component, nanofibers. We compare the nanoparticle dispersion and the properties of SCRIMP molded composites. In addition, the mold filling time of this novel three-component system is measured and a simplified model to estimate the effect of nanoparticle loading on the mold filling time is developed.

5.2 Experimental

5.2.1 Materials

An unsaturated polyester (UP) resin, Aropol Q6585, provided by Ashland Chemical was used in this study, which contains 35 wt.% styrene and 65 wt.% unsaturated polyester prepolymer. The prepolymer is a step-growth polymerization product of 1:1 maleic anhydride and propylene glycol, with about 10.13 internal vinylene groups per molecule and an average molecular weight of 1560 g $mole^{-1}$. Styrene from Aldrich was used as the crosslinking monomer. All tested samples were formulated with extra styrene to provide a ratio of styrene C=C double bond to unsaturated polyester C=C double bond equal to 2. A single component initiator, methyl ethyl ketone peroxide (MEKP, Hi-point® 90, Witco), was used in this study, which contains 38% peroxide. Cobalt octoate (CoOct, a mineral spirit solution containing 6 wt.% active cobalt, Pfaltz & Bauer) was employed as the promoter to decompose the initiator at low temperatures. The amount of MEKP and CoOct added into the UP resin was 1.5 wt.% and 0.5 wt.% respectively. The inhibitor, 300 ppm benzoquinone (BQ, Aldrich), was used to control the curing process.

The carbon nanofiber (CNF) used in this study was Pyrograf®-III (PR19-LHT-OX), which is an oxidized vapor grown carbon nanofiber from Applied Sciences Inc. The length of CNFs is about 30-100 μm and the diameter is 100-200 nm. A stitched unidirectional glass fiber (GF) mat, QM6408 from Brunswick Technologies, was used as the long fiber reinforcement.

All materials were used as received without further purification in order to mimic industrial applications.

5.2.2 Preparation of UP-CNF Nanocomposites

For comparison, UP-CNF nanocomposites were prepared. A desired amount of CNFs was added into the UP/styrene solution, and the mixture was sonicated for 2 h. The promoter CoOct, inhibitor BQ, and initiator MEKP were added into the system after ultrasonication. The mixture was degassed in a vacuum chamber for 10 min, and then cured in a silicone rubber mold at room temperature (~25 °C) for 12 h, and post-cured at 150 °C for additional 2 h.

5.2.3 Preparation of UP-CNF-GF Nanocomposites

In the pre-mixing approach, the resin mixture was prepared the same way as in UP-CNF nanocomposites, and the GF mats were used without further treatment. While in the pre-binding approach, the neat UP resin was used instead. The GF mats were treated using the following procedure: CNFs were pre-mixed with Q6585 prepolymer (binder) at a weight ratio of 1:1. Then, 10 g mixture was dissolved in 490 g acetone to prepare a 1 wt.% CNF solution. The solution was sonicated for 2 h, and then was sprayed onto both sides of the GF mats. The GF mats were placed in a fume hood for solvent evaporation until the weight of the fiber mats did not decrease with time. The amount of CNFs on the fiber mat was determined by the weight difference of the fiber mat before and after spraying.

SCRIMP was used to impregnate the GF preforms. Flow visualization was done using a JVC digital video camcorder. The schematic of the system setup is shown in Figure 5.1. Three layers of GF mats with pre-bound CNFs were sealed in a vacuum bag. Each layer was 240 mm in length and 160 mm in width. The inlet was inserted into a resin tank and the outlet was connected to a vacuum pump. Before mold filling, vacuum was applied to force the bag to press tightly against the fiber stack. The neat UP resin or UP-CNF mixture was degassed in a vacuum chamber for 10 min, and then was introduced into the fiber preforms. After the mold was fully filled, the inlet and outlet pipes were clamped to maintain the vacuum pressure in the system. The samples were cured at room temperature (~25 °C) for 12 h, and post-cured at 150 °C for an additional 2 h. The GF content in the composites was controlled at 48-51 wt.%.

5.2.4 Rheological Charaterization

Shear viscosities of UP resins with various CNF contents were measured on a TA Instruments advanced rheometric expansion system (ARES). The steady-state shear experiments were conducted with 25 mm parallel plates through the strain-controlled method.

5.2.5 Measurement of Mechanical and Thermal Properties

Flexural properties were tested with an Instron 5848 Testing Machine according to ASTM D790-03. The support span of 3-point bending tests was 25.4 mm. Five specimens were tested for each composite sample.

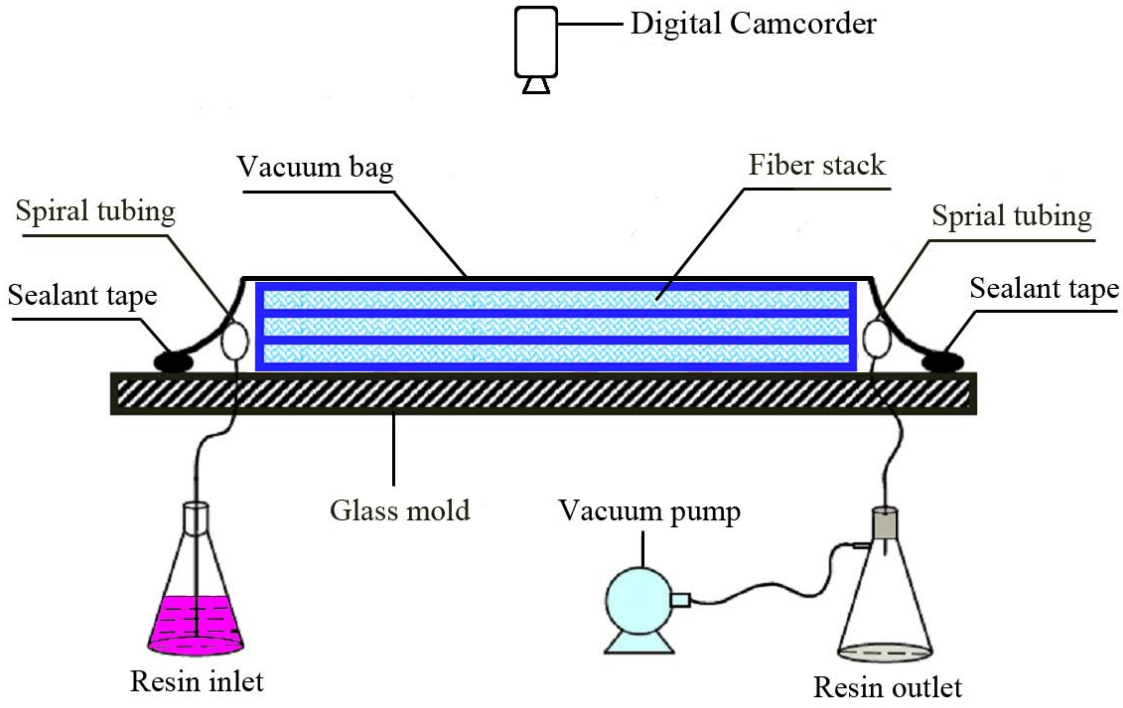

Figure 5.1 Schematic of experimental set-up for VARTM.

Thermal mechanical analysis (TMA) was performed on a TA 2940 thermal mechanical analyzer to measure the glass transition temperature and thermal expansion coefficients. The heating rate was 5 °C/min. For each sample, three specimens were tested.

5.2.6 Morphological Charaterization

Scanning electron microscopy (SEM) was carried out on a Hitachi S-4300 scanning electron microscope. The GF mat sample with pre-bound CNFs was coated with a thin layer of gold. The fracture surfaces of UP-CNF nanocomposites were also characterized by SEM.

5.3 Mold Filling Analysis

Flow in SCRIMP can be modeled as viscous flow through porous media. The thermosetting fluids used in the composite manufacturing are considered as Newtonian fluids, i.e., their viscosity is independent of the fluid velocity of the flow. In general, Darcy's law holds for the flow through porous media:

$$Q = \frac{k \cdot \mathrm{A} \cdot \Delta P}{\mu \cdot \Delta L} \tag{5.1}$$

where Q is the volumetric flow rate (m^3/s), μ is the fluid viscosity (Pa·s), A is the cross sectional area of the composite sample (m^2), $\Delta P/\Delta L$ is the pressure drop per unit length (Pa/m), and k is the permeability of the porous medium (m^2). As the thickness of the GF reinforcement is small in our experiments, the flow can be considered as one-dimensional. For a one-dimensional flow, Equation (5.2) can be used to calculate the permeability of the GF fiber mat [30].

$$t = \frac{\mu \cdot \varphi}{2k \cdot \Delta P} s^2 \tag{5.2}$$

where s is the distance from the inlet to the flow front (obtained from observing the flow), t is the corresponding time, and φ is the porosity of the reinforcement medium, which is given by Equation (5.3):

$$\varphi = 1 - \frac{n \cdot \xi}{d \cdot \rho_f} \tag{5.3}$$

where n is the number of reinforcement layers inside the mold (3 in this study), ξ is the surface density of the unidirectional GF mat (0.27 kg/m^2), d is the thickness of the mold

cavity, and ρ_f is the density of the GF (for E-glass, ρ_f = 2560 kg/m^3). The porosity value turns out to be 0.71 for the stack of three GF mats without CNFs. The porosity value changed as CNFs were sprayed onto the GF mats because nanoparticles occupy some pore space in the GF mats. This in turn affects the permeability and the mold filling time.

Based on Equation (5.2), the permeability can be calculated by plotting t vs. s^2. The slopes of the curves are inversely proportional to the permeability of the GF mats. For calculating the changed porosity of the GF mats after spraying the CNFs, the following equation is used:

$$\varphi = \frac{V_p}{V_t} \tag{5.4}$$

where V_p is the pore volume and V_t is the total volume of the cured composite. V_p is given by

$$V_p = V_t - (V_f + V_{cnf}) \tag{5.5}$$

where V_f is the volume occupied by the GF reinforcement and V_{cnf} is the volume occupied by the CNFs.

From the weight increase after spraying CNFs on the GF mats to achieve a particular value of CNF loading, the porosity can be calculated using Equations (5.4) and (5.5). In order to predict the filling time, the permeability of the system must also be determined. Permeability modeling for Newtonian flow through various porous media and fiber bed has been studied by several researchers [31, 32]. The simplest model is to consider the porous media as a bundle of capillaries. Then the permeability can be

calculated by the following equation:

$$k = \frac{\varphi^3}{\tau^2 \cdot \mathrm{A}_\mathrm{v}^2} \tag{5.6}$$

where τ is tortuosity and A_v is surface area per unit volume. Another model is the capillary network model, in which a large number of capillaries are arranged in the form of a regular network. The well-known Kozeny-Carman equation is based on this approach as shown in Equation (5.7).

$$k = \frac{\varphi^3}{C \cdot \mathrm{A}_\mathrm{v}^2 \cdot (1-\varphi)^2} \tag{5.7}$$

where C is a constant. Once the values of porosity and permeability are obtained, they can be inserted back into Equation (5.2) to predicting the mold filling time.

5.4 Results and Discussion

5.4.1 Mold Filling

Figure 5.2 shows the plot of flow front length vs. filling time for samples with various CNF loading. It can be seen that there is a significant effect of nanoparticles on the mold filling time. While a 0% CNF loading has a filling time of 45 s, the filling time of 3.5% and 5% CNF samples is much longer. This can be attributed to the fact that CNFs filled in the pore space within the long fiber mats and reduced the pore volume within the sample. In turn, the mold filling time increased as the resin had to flow through smaller gaps.

The plot of filling time vs. square of the flow length is shown Figure 5.3, which is used to determine the permeability of the reinforcement. It can be seen that as the CNF loading increases, the slope of the curve increases. Based on Equation (5.2), the permeability k and the porosity φ are the variables for the slope change if the resin viscosity μ and the pressure difference ΔP remain unchanged in the three experiments. Based on the rheological tests, the viscosity (μ) of the UP resin is about 0.035 Pa·s at 25 °C. The vacuum pressure (ΔP) is about 98205 Pa (29 inch mercury). The porosity φ can be calculated by Equations (5.4) and (5.5), and then the values of permeability are determined through Equation (5.2). According to Equation (5.6), the values of $\tau \cdot A_v$ can be calculated. As shown in Table 5.1, the porosity decreases slightly with the increase of the CNF loading in the samples, but the permeability reduces significantly. This is because the product of the tortuosity (τ) and the surface area per unit volume (A_v) dramatically increase when adding CNFs into the sample.

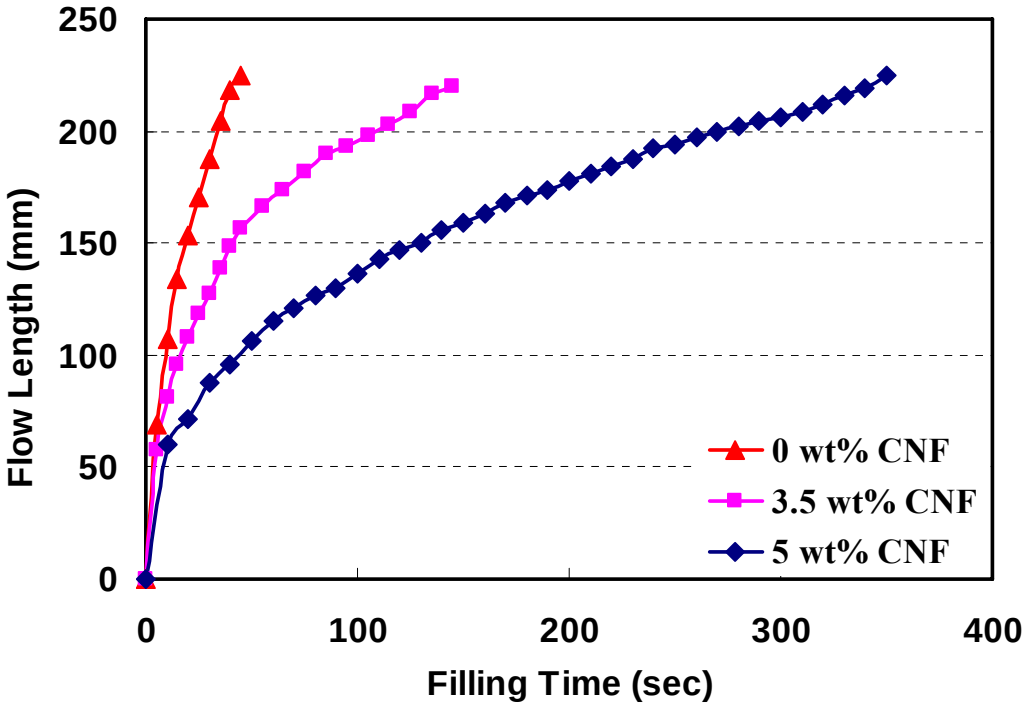

Figure 5.2 Comparison of mold filling profile with various CNF contents.

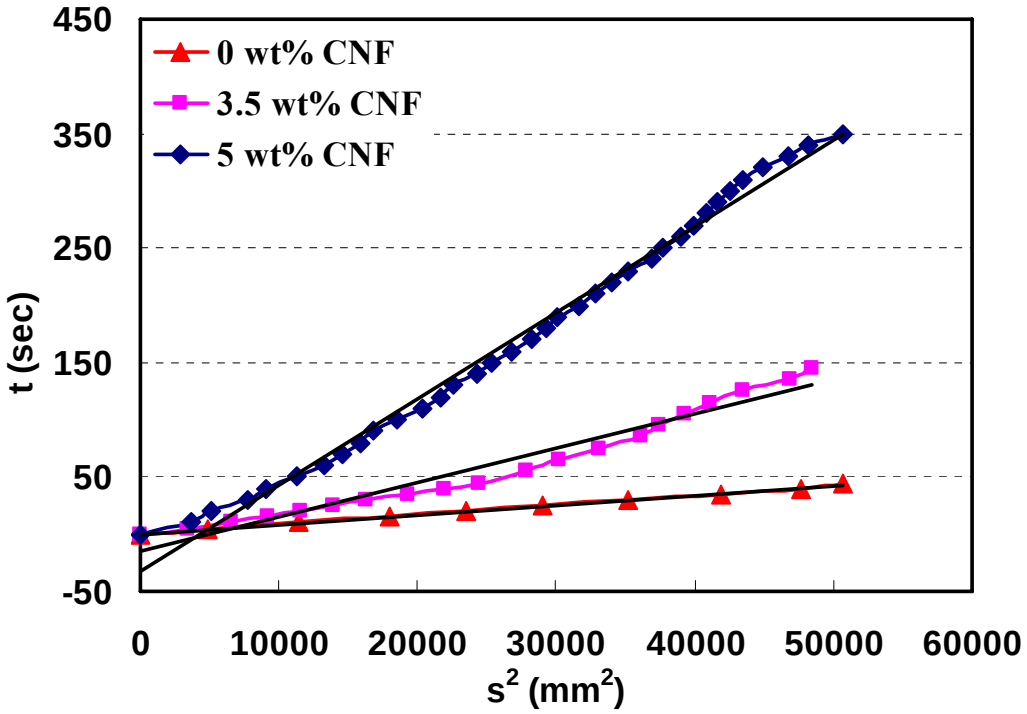

Figure 5.3 Filling time vs. (flow length)^2 plots for permeability calculation.

CNF content (wt.%)	0	3.5	5
Porosity	0.710	0.671	0.659
Permeability (m^2)	1.43×10^{-10}	4.65×10^{-11}	1.78×10^{-11}
$\tau\cdot A_v$ (m^{-1})	5.01×10^{4}	8.06×10^{4}	1.27×10^{5}

Table 5.1 Permeability and porosity values of reinforcement with various CNF loadings.

Figures 5.4(a) and 5.4(b) show 1% and 5% CNF on the GF mat, respectively. It can be seen that the CNFs may form network structure at higher CNF loading, leading to the increase of the tortuosity of the fiber mat. With the increase in the CNF loading, the surface area per unit volume (A_v) of the fiber mats also rises. This may cause the permeability of the fiber mats decreased significantly (see Figure 5.5). In addition, it has been found that the uniform distribution of CNFs on the GF mats can be obtained using powerful ultrasonic device and spray gun.

Figure 5.6 compares the calculated and experimental flow front positions for the three experimental samples. It can be seen that for 0% CNF sample, there is a very good agreement between the calculated and experimental flow front data. This is because there are no CNF sprayed onto the GF mats to affect the flow properties. On the other hand, there is a slight difference between the experimental and calculated flow front for 3.5% and 5% CNF loading samples. The flow front in the experiment is slightly slower than the calculated data towards the end of the mold (latter stages of the mold filling). This can be attributed to the increase of resin viscosity when nanoparticles are dispersed in the polymer resin [29]. The hypothesis is that as the resin fills the mold, the binder (which is also UP resin here) slowly dissolves in the UP/styrene resin feed and the CNFs diffuse from the GF surface into the resin. This may increase the resin viscosity, and hence the advance of the flow front becomes slower.

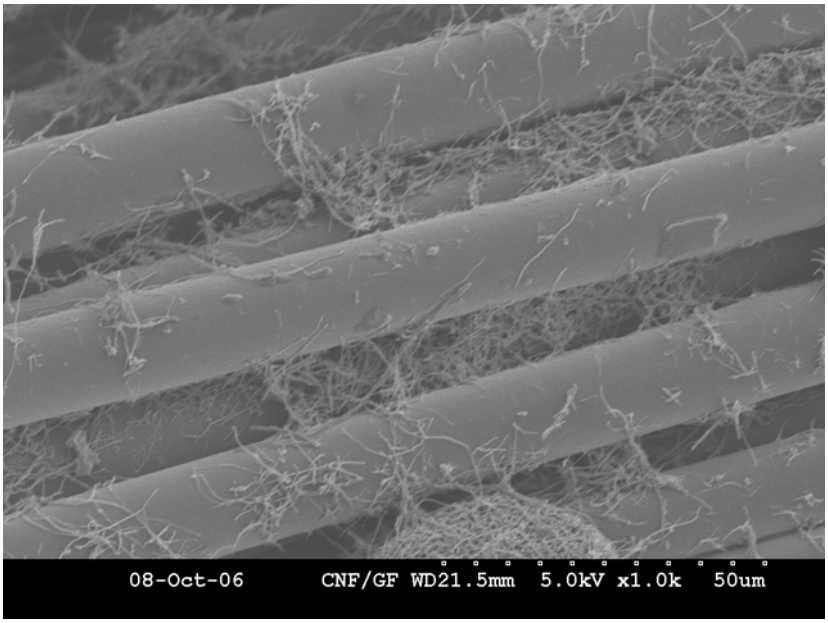

(a)

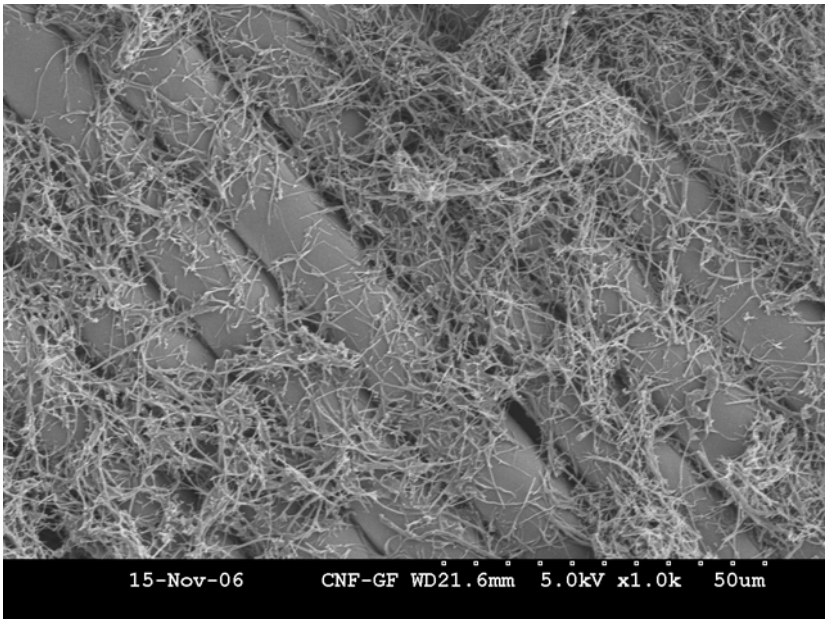

(b)

Figure 5.4 SEM pictures of (a) 1 wt.% and (b) 5 wt.% CNFs pre-binding on GF mats.

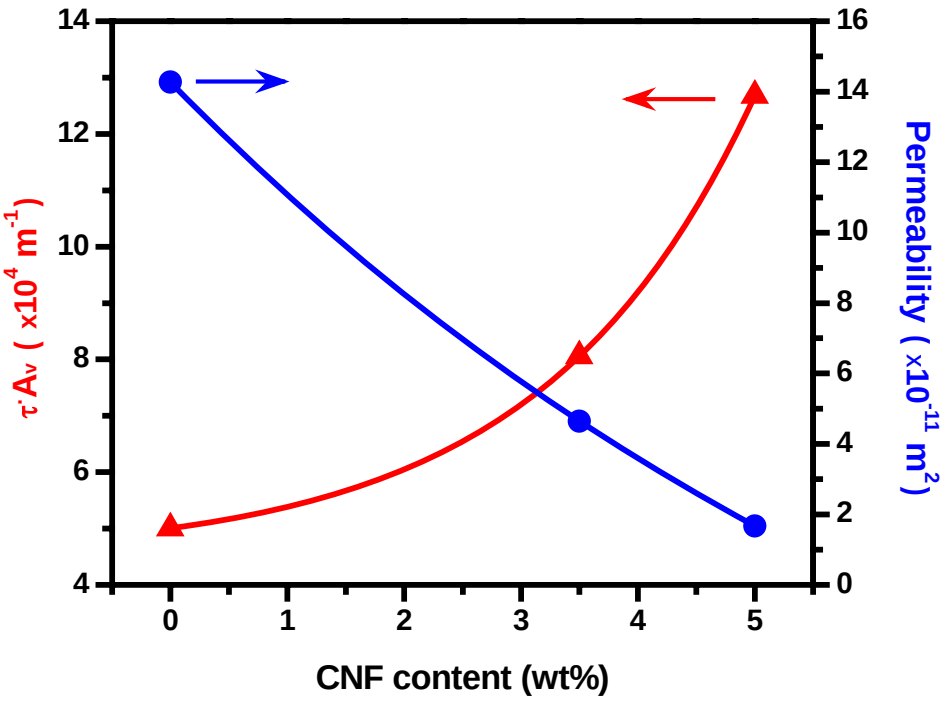

Figure 5.5 Permeability (●) and $\tau \cdot A_v$ (▲) for various CNF loadings.

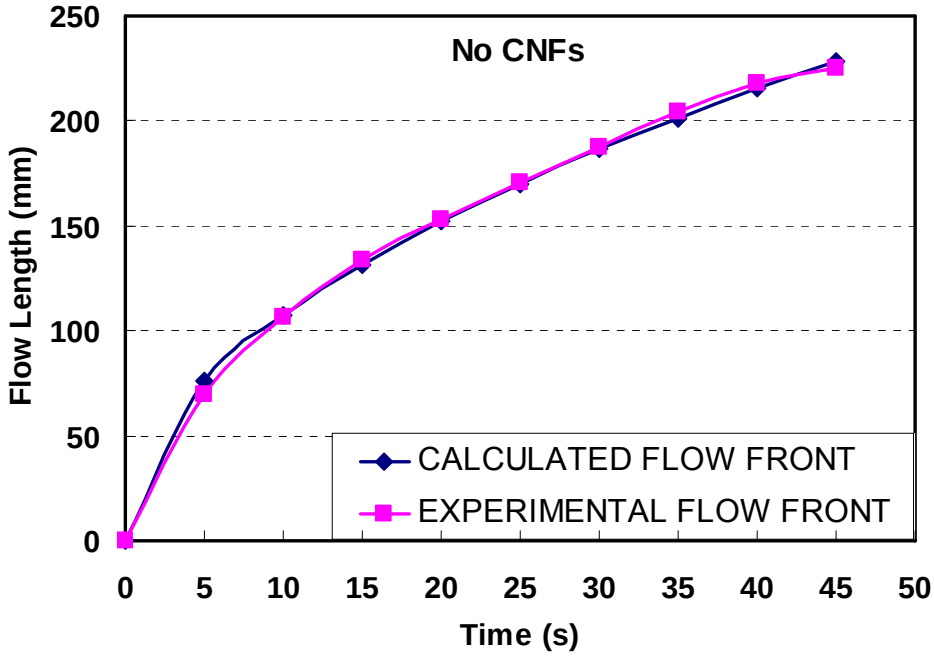

(a)

(Continued)

Figure 5.6 Experimental and calculated flow length for various CNF loadings: (a) 0 wt.%, (b) 3.5 wt.%, and (c) 5 wt.%.

Figure 5.6 continued

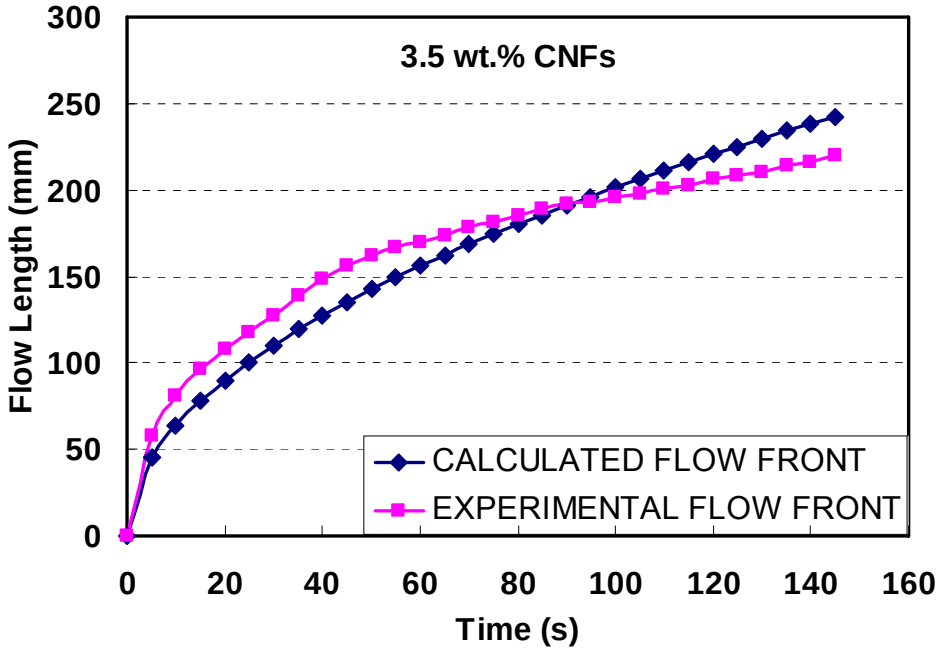

(b)

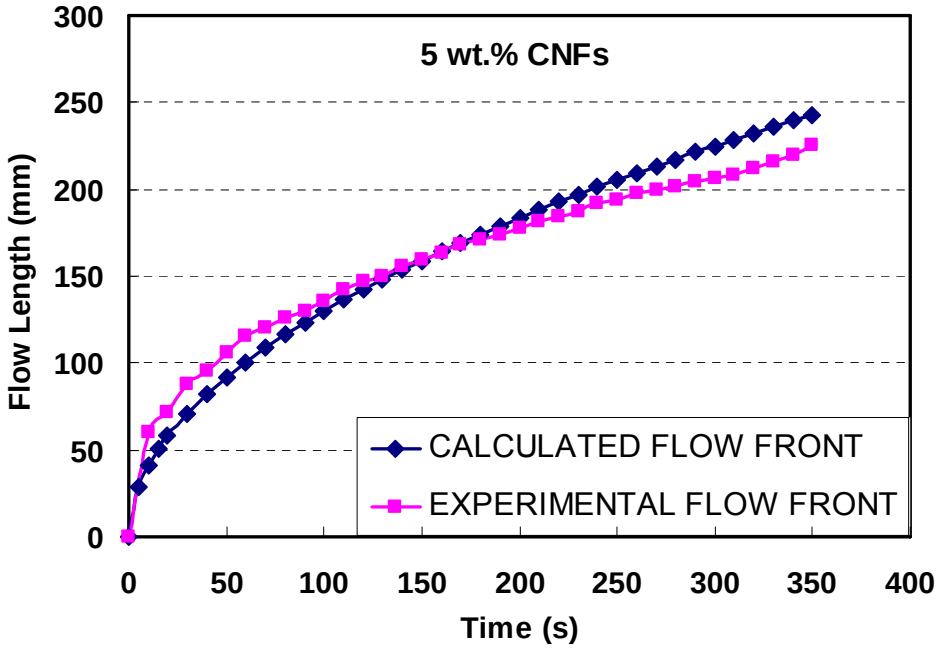

(c)

5.4.2 Mechanical and Thermal Properties

Figure 5.7 shows the flexural properties of UP-CNF nanocomposites. It is obvious that a small amount of CNFs can improve both flexural strength and modulus of the UP resin. For example, the flexural strength increased about 133% with the addition of 5 wt.% CNFs in the UP resin. This is attributed to the high aspect ratio of CNFs, which can make the UP resin much stronger. From the SEM pictures of the fracture surfaces shown in Figure 5.8, it can be seen that CNFs are well dispersed in the UP matrix. Because the UP resin used in this study is very brittle, the improvement of flexural modulus (about 21% with 5 wt.% CNFs) is not as great as that of flexural strength.

Thermal properties of UP-CNF nanocomposites were also improved. As shown in Table 5.2, the glass transition temperature (T_g) of the UP resin ascended and the thermal expansion coefficients declined with an increase of the CNF content in the composites. Well-dispersed CNFs have a large surface area and strong interactions with polymer molecules, which may restrict the movement of polymer chains and lead to higher transition temperatures and lower thermal expansion coefficients.

Form Figure 5.9, it can be seen that the shear viscosity of UP resin increases with the addition of CNFs. The unfilled UP/St mixture exhibited Newtonian behavior; that is the viscosity of the UP system was almost constant (~0.035 Pa·s at 25 °C) at various shear rates. When adding CNFs into the UP resin, all of the CNF filled UP/St mixtures showed non-Newtonian shear thinning behavior, and the shear viscosity of the UP/St mixture increased dramatically, especially in the low shear rate region.

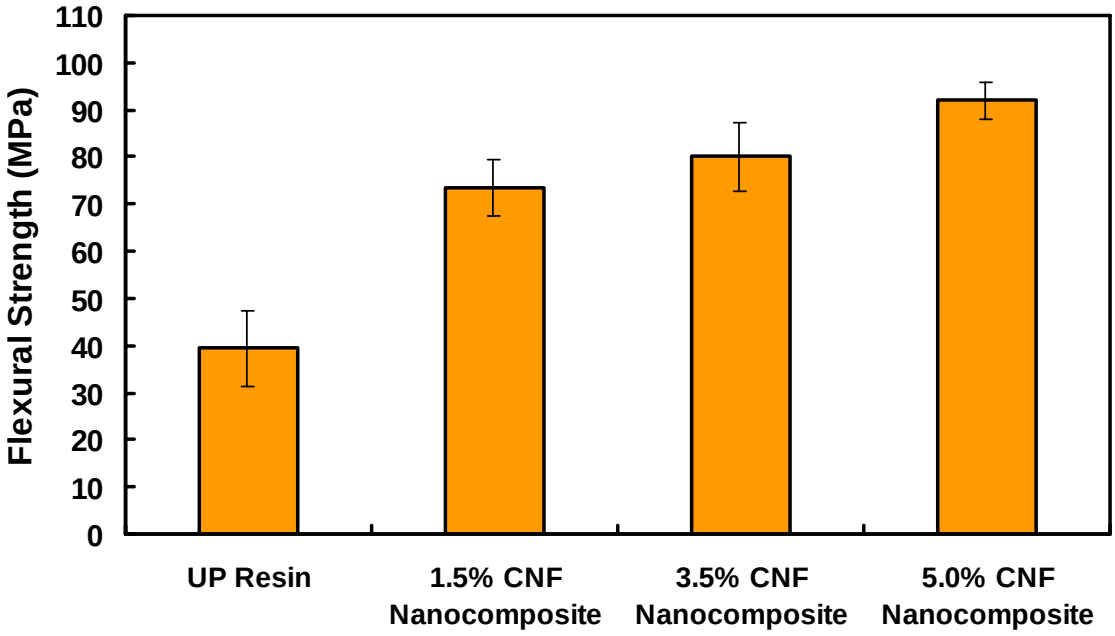

(a)

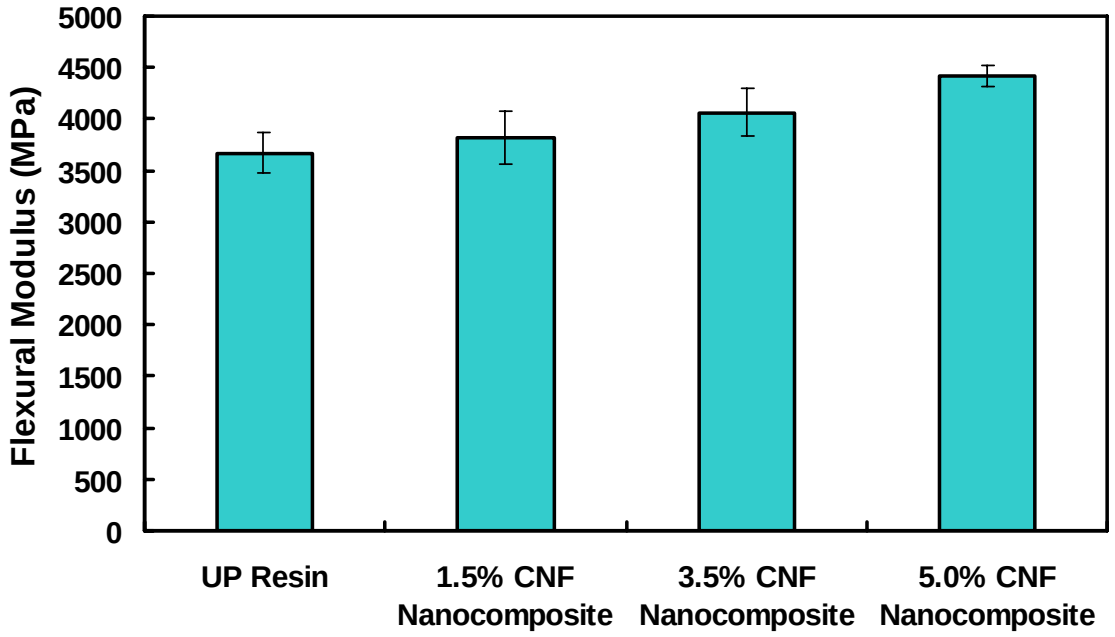

(b)

Figure 5.7 Flexural properties of UP-CNF nanocomposites: (a) flexural strength; (b) flexural modulus.

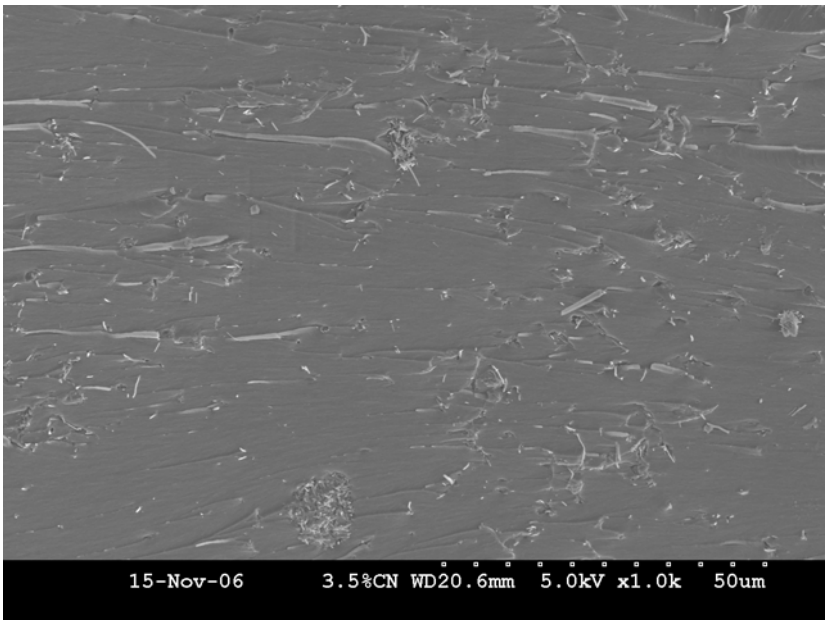

(a)

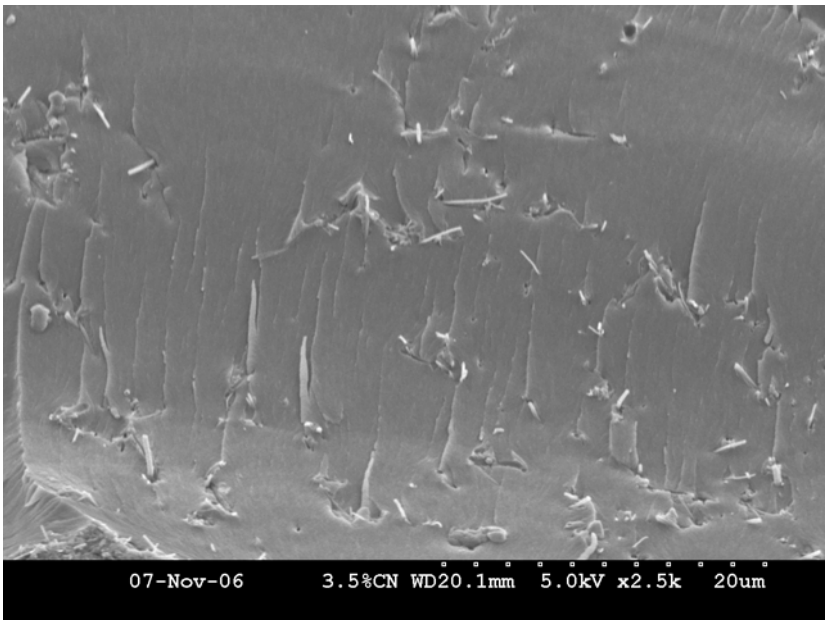

(b)

Figure 5.8 SEM pictures of 3.5 wt.% CNFs dispersed in UP resins: (a) 1,000 and (b) 2,500 magnification.

Sample	Tg (^{o}C)	α_1 (μm/m/^{o}C) (50-125 ^{o}C, below Tg)	α_2 (μm/m/^{o}C) (175-250 ^{o}C, above Tg)
UP Resin	140.0 ± 3.7	98.0 ± 0.8	153.8 ± 2.6
UP + 1.5 wt.% CNF	148.2 ± 0.7	93.9 ± 0.9	152.4 ± 1.0
UP + 3.5 wt.% CNF	151.6 ± 7.0	90.0 ± 1.1	150.3 ± 4.7

Table 5.2 Thermal Properties of UP-CNF Nanocomposites.

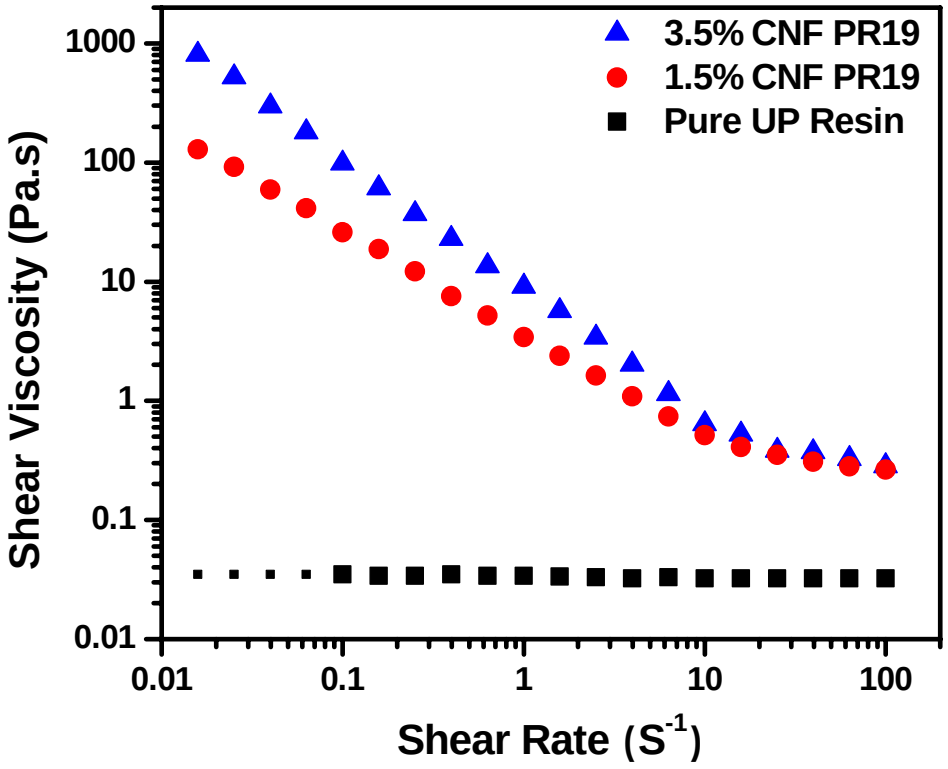

Figure 5.9 Shear viscosity of unreacted UP resins with various CNF contents at 25 °C.

During the preparation of the UP-CNF-GF composites, it was found that the long fiber mats might filter out CNFs, especially when the CNFs content is high (>1.5 wt.%). In Figure 5.10, the appearances of 3.5 wt.% CNF pre-mixing and pre-binding samples are shown respectively. For the CNF pre-mixing sample in Figure 5.10(a), it was found that CNFs concentrated near the resin inlet, and very few could reach the outlet because of the filter effect of the GF mats. The high content of CNFs also increased the resin viscosity and caused the slow flow during mold filling, which may result in more CNFs to be filtered out. On the other hand, our new approach can avoid such drawbacks. First, the pre-bound CNFs did not cause any viscosity increase of the UP resin. Second, when the UP resin flowed into the mold, the binder would dissolve and the pre-bound CNFs could release into the resin gradually. This does not require the CNFs to flow through the fiber mats from the inlet to the outlet, and thus prevents the CNFs from being filtered. Moreover, CNFs are hydrophobic particles because of their surface characteristics. After the binder dissolves, the pre-bound CNFs prefer to diffuse from the hydrophilic GF surface to the hydrophobic polymer resin. Therefore, the CNF pre-binding sample shown in Figure 5.10(b) indicates a uniform distribution of CNFs. The SEM picture of pre-bound CNFs on the GF mat is shown in Figure 5.4.

The flexural properties of UP-CNF-GF composites prepared by both methods are compared in Figure 5.11. All samples with GFs were tested in the transverse direction (90°) in order to reduce the effects of long fibers and emphasize the reinforcement of nanofibers. It can be seen that the improvements of the flexural properties of CNF pre-mixing samples are much lower than those of CNF pre-binding composites. For the

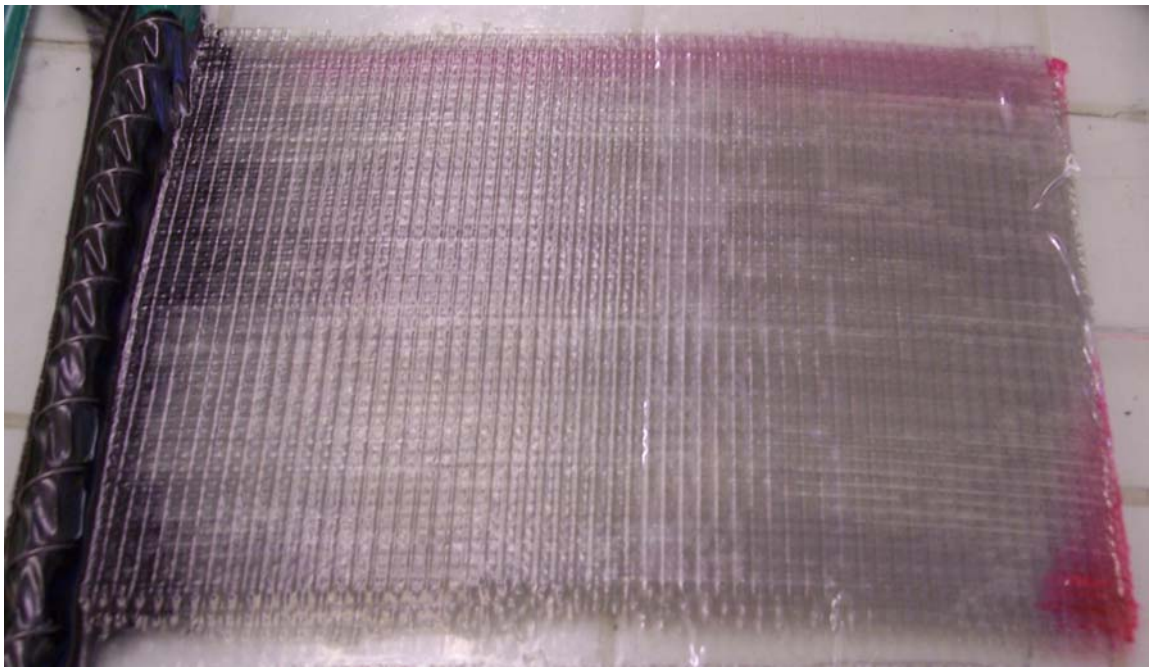

(a)

(Continued)

Figure 5.10 Pictures of UP-CNF-GF hybrid composites: (a) 3.5 wt.% CNF pre-mixing sample; (b) 3.5 wt.% CNF pre-binding sample. (Resins flow from left to right.)

Figure 5.10 continued

(b)

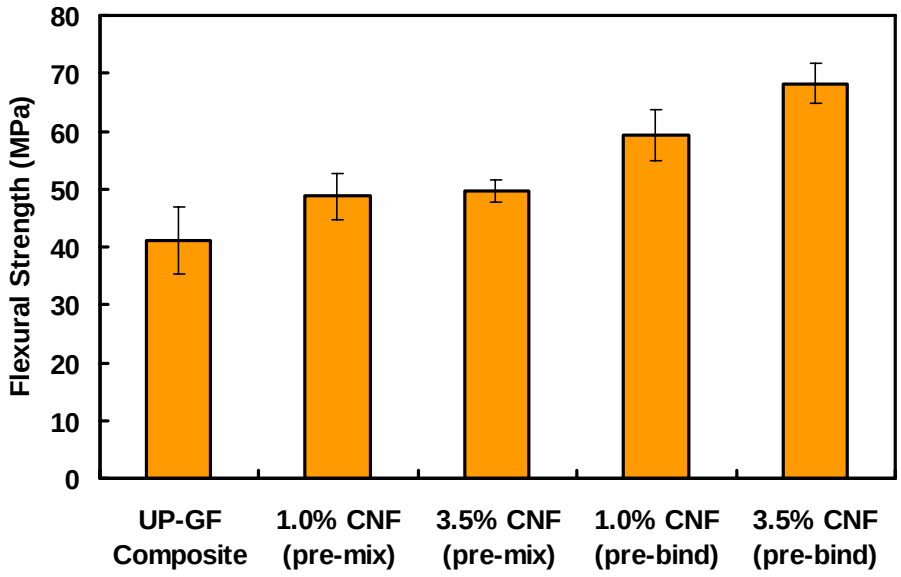

(a)

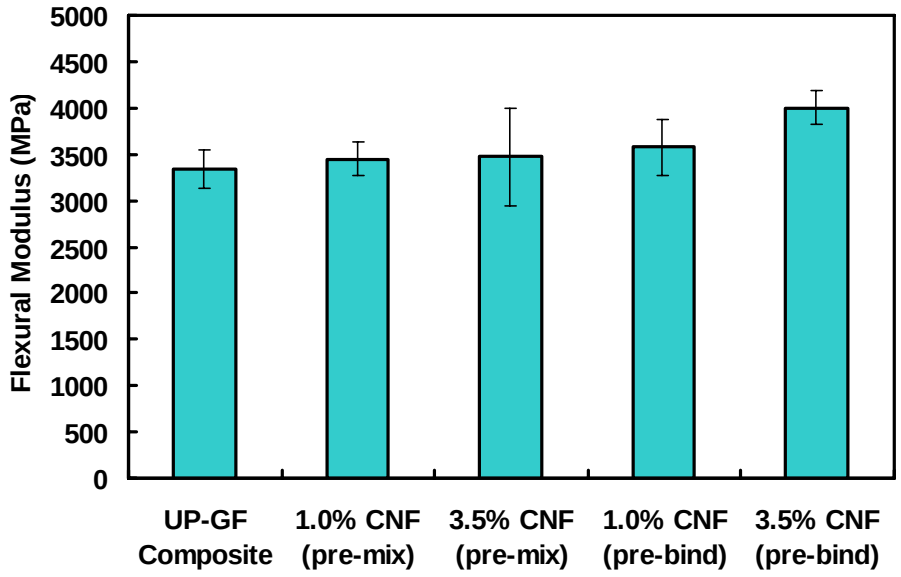

(b)

Figure 5.11 Flexural properties of UP-CNF-GF hybrid composites: (a) flexural strength; (b) flexural modulus. (All samples are tested in transverse direction.)

3.5 wt.% CNF samples, the flexural strength and modulus of the pre-binding samples are 66% and 20% higher than those of UP-GF composites respectively, but the improvements of the pre-mixing samples are only 20% and 4%. This is due to the filter effect of long fibers, resulting in very few nanoparticles in the composite samples. For the CNF pre-binding samples, the improvement of flexural properties results from the reinforcement of the UP matrix with nanoparticles. The CNFs with a high aspect ratio can prevent crack generation and propagation in the polymer matrix between long fibers.

5.5 Conclusions

CNF reinforced UP and UP-GF composites have been prepared. The addition of CNFs can improve both thermal and mechanical properties of the UP resin. Compared with the pre-mixing approach, our new pre-binding method can reduce the filter effect of long fibers on CNFs and produce composites with better distribution of nanoparticles, resulting in better mechanical properties.

Mold filling experiments for the hybrid long fiber and nanoparticle composites have been also conducted. The presence of CNFs on the GF mats may decrease the porosity and permeability, and thus increase the mold filling time. A simplified model to predict the filling time and the flow front length for 0, 3.5, and 5 wt.% CNFs was derived. The calculated values and experimental date agreed reasonably well.

References

1. R. P. Sheldon, *Composite Polymeric Materials*, Applied Science Publishers: London/New York (1982).

2. P. K. Mallick, *Fiber-Reinforced Composites*, Marcel Dekker: New York/Basel (1988).

3. D. Hull, *An Introduction to Composite Materials*, Cambridge University Press: London/New York/New Rochelle/Melbourne/ Sydney (1981).

4. R. L. McCullough, *Concepts of Fiber-Resin Composites*, Marcel Dekker: New York (1971).

5. K. Yano, A. Usuki, A. Okada, T. Kurauchi, O. Kamigaito, *J. Polym. Sci. Part A: Polym. Chem.*, **31**, 2493 (1993).

6. P. B. Messersmith, E. P. Giannelis, *Chem. Mater.*, **6**, 1719 (1994).

7. X. Wang, Z. Qi, F. Wang, *Eng. Plast. Appl.*, **27**, 1 (1998).

8. R. A. Vaia, K. D. Jandt, E. J. Kramer, E. P. Giannelis, *Chem. Mater.*, **8**, 2628 (1996).

9. K. Lozano, E. V. Barrera, *J. Appl. Polym. Sci.*, **79**, 125 (2001).

10. H. Ma, J. Zeng, M. L. Realff, S. Kumar, D. A. Schiraldi, *Polym. Mater. Sci. Eng.*, **86**, 411 (2002).

11. J. Sandler, A. H. Windle, P. Werner, V. Altstadt, M. V. Es, M. S. P. Shaffer, *J. Mater. Sci.*, **38**, 2135 (2003).

12. P. C. LeBaron, Z. Wang, T. J. Pinnavaia, *Appl. Clay Sci.*, **15**, 11 (1999).

13. J. Njuguna, K. Pielichowski, *Adv. Eng. Mater.*, **5**, 769 (2003).

14. B. P. Rice, C. Chen, L. Cloos, D. Curliss, *SAMPE Journal*, **37**, 7 (2001).

15. L. Aktas, Y. K. Hamidi, M. C. Altan, *Plast. Rubber Compos.*, **33**, 267 (2004).

16. F. H. Gojny, M. H.G. Wichmann, B. Fiedler, W. Bauhofer, K. Schulter, *Composites Part A*, **36**, 1525 (2005).

17. R. Sadeghiam, S. Gangireddy, B. Minaie, K.-T. Hsiao, *Composites Part A*, **37**, 1787 (2006).

18. L. Xu, *Integrated Analysis of Liquid Composite Molding (LCM) Process*, Doctorial Dissertation, The Ohio State University (2004).

19. J. Xu, S. Chatterjee, K. W. Koelling, Y. Wang, S. E. Bechtel, *Rheol. Acta*, **44**, 537 (2005).

20. K. D. Potter, *Composites Part A*, **30**, 619 (1996).

21. T. G. Gutowski, *Advanced Composites Manufacturing*, John Wiley & Sons: New York (1997).

22. W. H. Seemann, *U.S. Patent 4,902,215* (1990).

23. W. H. Seemann, *U.S. Patent 5,052,906* (1991).

24. W. H. Seemann, *U.S. Patent 5,316,462* (1994).

25. S. G. Advani, M. S. Sozer, *Process Molding in Composites Manufacturing*, Marcel Dekker: New York, (2003).

26. K. Han, S. Jiang, C. Zhang, B. Wang, *Composites Part A*, **31**, 79 (2000).

27. K. T. Hsiao, R. Mathur, S. G. Advani, J. W. Gillespie Jr, B. K. Fink, *J. Manuf. Sci. Eng.*, **122**, 463 (2000).

28. N. C. Correia, F. Robitaille, A. C. Long, C. D. Rudd, P. Simacek, S. G. Advani, *J. Fluid Eng.*, **126**, 201 (2004).

29. S. V. Lomov and I. Verpoest, *J. Reinf. Plast. Compos.*, **19**, 1329 (2000).

30. X. Sun, S. Li, L.J. Lee, *Polym. Compos.*, **19**, 807 (1998).

31. L. Skartsis, J. L. Kardos, B. Khomani, *Polym. Eng. Sci.*, **32**, 221 (1992).

32. L. J. Lee, *Makromol. Chem., Macromol. Symp.*, **68**, 169 (1993).

CHAPTER 6

CONCLUSIONS AND RECOMMENDATIONS

6.1 Conclusions

The effects of humidity on the curing kinetics, T_g, and tack property of IM7/8552 graphite/epoxy prepregs were studied. It was found that higher RH of the environment resulted in more moisture absorbed by the prepreg samples. Water in the graphite/epoxy prepregs acted as a plasticizer and a curing accelerator. A phenomenological kinetic model was proposed to describe the epoxy-amine reaction in the prepreg samples with the presence of moisture. The T_g of the epoxy matrix was predicted by a modified DiBenedetto equation, and the results had a good fit with the experimental data. The peel forces were applied to characterize the tack property of the prepreg samples. They correlated well with the T_g of the prepreg samples.

The mechanism of marcel formation (fiber buckling) during compression molding was also investigated. Based on the experimental data, a statistic model was built to estimate the marcel size in the epoxy composites. The model can be also used to determine the proper processing parameters, such as mold temperature and pressure rate, to eliminate the fiber waviness.

In this study, ultrasonic consolidation was compared with ordinary vacuum debulking at room temperature or high temperature during the preparation of epoxy composites. The results indicated that the ultrasonic consolidation is more efficient to lower the void content in the composites than the low-temperature vacuum debulking, and can achieve a similar or better results when compared to the high-temperature vacuum debulking. Therefore, the ultrasonication treatment becomes a promising approach for composite processing and may replace the common debulking process in production.

Epoxy, phenolic, and unsaturated polyester nanocomposites were prepared repectively. Mechanical, thermal, and/or barrier properties of these nanocomposites were compared to neat resins. It is found that the addition of nanoparticles, such as nanoclays or carbon nanofibers, into the polymer matrix can improve the strength and modulus, enhance the thermal stability, and lower the water absorption rate.

Furthermore, great efforts have been made to combine the advantages of both fiber-reinforced plastics and polymer nanocomposites to produce a superior composite: long fibers and nanoparticles reinforced polymer composites. According to the characteristics of different polymer resins (epoxy, phenolic, and unsaturated polyester resins) and long fibers (glass or carbon fibers), several processes were selected to prepare various hybrid composites, such as compression molding and vacuum assisted resin transfer molding. The processing conditions were determined to achieve good dispersion of nanoparticles in polymer. The mechanical and thermal properties of these long fiber-nanoparticle reinforced composites were also measured. The significant improvement of these properties can be attributed to the synergic effects of long fiber

and nanoparticles. These long fiber and nanoparticle reinforced polymer materials may have a numerous applications in future.

6.2 Recommendation

6.2.1 Epoxy prepreg Processing

Because design of experiments (DOE) was applied in the marcel formation study, the number of experiments was significant reduced. However, each experiment is still time-consuming and labor-intensive. From the prepreg lay-up to curing composites, it usually takes more than eight hours for each experiment. Therefore, the future study may focus on the computer simulation using the finite element model, which has been widely used in the analysis and simulation of composite processing [1, 2]. The computer experiments can be carried out quickly with different process variables, are easy to change from simple mold to complex shape, and are helpful for better understanding the mechanism of fiber buckling.

6.2.2 Polymer-Long Fiber-Nanoparticle Composites

In this study, epoxy-long fiber-nanoparticle composites were prepared through the sheet-molding compound (SMC) process. The 25-mm (1 inch) chopped carbon fibers were used as long fiber reinforcement. However, many epoxy composites are made with continuous glass or graphite fibers, especially in aerospace applications. Therefore, further study on epoxy-long fiber-nanoparticle composites may switch to continuous fibers through vacuum-assisted resin transfer molding (RTM) or high-pressure RTM processes. Making epoxy prepregs with continuous fibers is another way to prepare composites. In this method, nanoparticles may be dispersed into the epoxy resin first, and then the mixture is brushed or cast onto the long fiber mats and partially cured at room or

elevated temperature to form prepregs. Finally, the prepregs can be made into epoxy composites through compression molding.

Another interesting area is about the dispersion of nanoparticles into long fiber reinforced composites. In this study, a powerful ultrasonic device, Branson digital sonifier® S-450D, was used to disperse carbon nanofibers (CNFs) in the unsaturated polyester (UP) resin. Figure 6.1 shows the flexural properties of UP-CNF clear casting samples. It can be seen that the flexural strength of the sample sonicated by sonifier® S-450D (CNF-U) is much larger than that of the sample with ordinary ultrasonic bath (CNF). This means the use of the sonifier® S-450D may lead to better dispersion of CNFs in the UP resin. Therefore, the sonifier® is strongly recommended for the dispersion of nanoparticles. It is necessary to find a way to apply ultrasonic forces to disperse nanoparticles into long fiber reinforced polymers.

It is also reported that the surface modification of nanoparticles may improve the compatibility between the polymer matrix and nanoparticles to achieve good dispersion [3, 4], and better thermal and mechanical properties of composites. The preliminary results of surface treated and non-treated CNFs are also shown in Figure 6.1. The flexural strength and modulus of the UP sample with oxidized CNFs (CNF-OX) are both higher than those of the composite with non-oxidized CNFs (CNF). In the future study, the effects of surface modification of nanoparticles, such as nanoclay and CNF, should be studied.

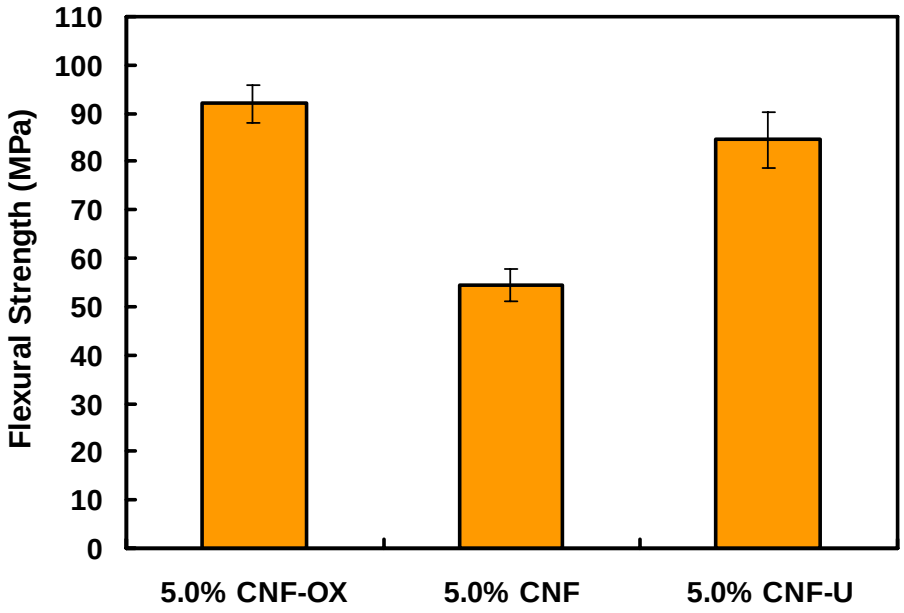

(a)

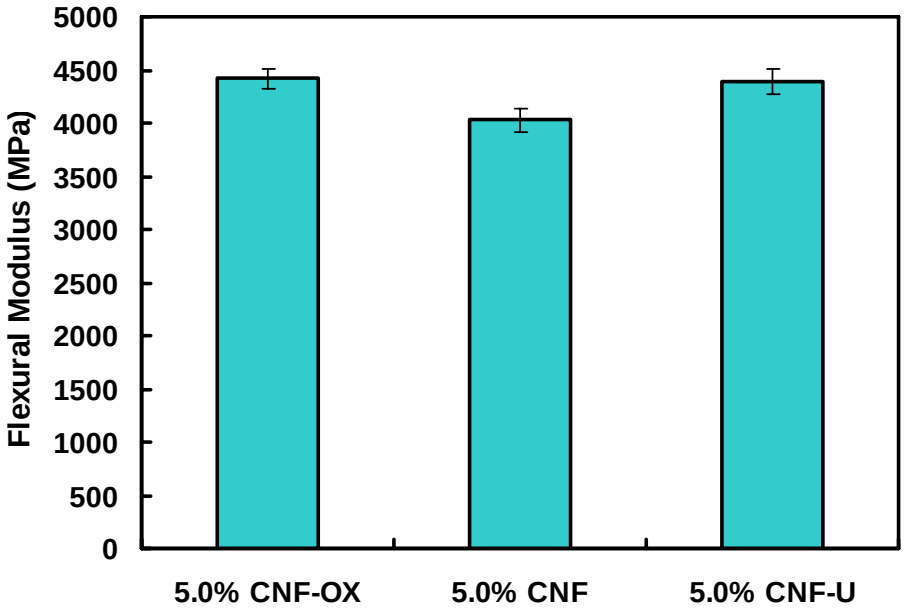

(b)

Figure 6.1 Flexural properties of UP-CNF nanocomposites: (a) flexural strength and (b) flexural modulus.

Nanoparticles not only improve the mechanical and thermal properties of polymers, but also may provide some functional features to polymeric materials. For example, thermal and electrical conductivity of polymer materials may be changed by adding CNFs. On the other hand, the addition of nanoclays may lower the thermal conductivity of polymer matrix. All of these effects can be further investigated.

In the mold filling study, it has been found that the CNFs may be filter out by the glass fiber mat because of their high aspect ratio (30-100 μm in length and 100-200 nm in diameter). Therefore, the pre-binding method is preferred in using CNFs to reinforce polymer-long fiber composites. However, for smaller nanoparticles such as nanoclay, the pre-mixing method may be feasible. According to Darcy's law, the flow of fluids in porous media can be described in the following equation:

$$Q = \frac{k \cdot A \cdot \Delta P}{\mu \cdot \Delta L} \tag{6.1}$$

where Q is the volumetric flow rate (m^3/s), μ is the fluid viscosity (Pa·s), A is the cross sectional area of the composite sample (m^2), $\Delta P/\Delta L$ is the pressure drop per unit length (Pa/m), and k is the permeability of the porous medium (m^2). In pre-binding method, the permeability will decrease with the increase of nanoparticle loading, and other parameters remain unchanged. In pre-mixing method, the permeability will be constant, but the viscosity of the resin may increase significantly with the addition of nanoparticles (see Figure 6.2). It seems that the flow rate declines and the mold filling time is extended in both approaches. However, it is not clear which method is better than another. Thus, it is still very interesting to compare these two methods.

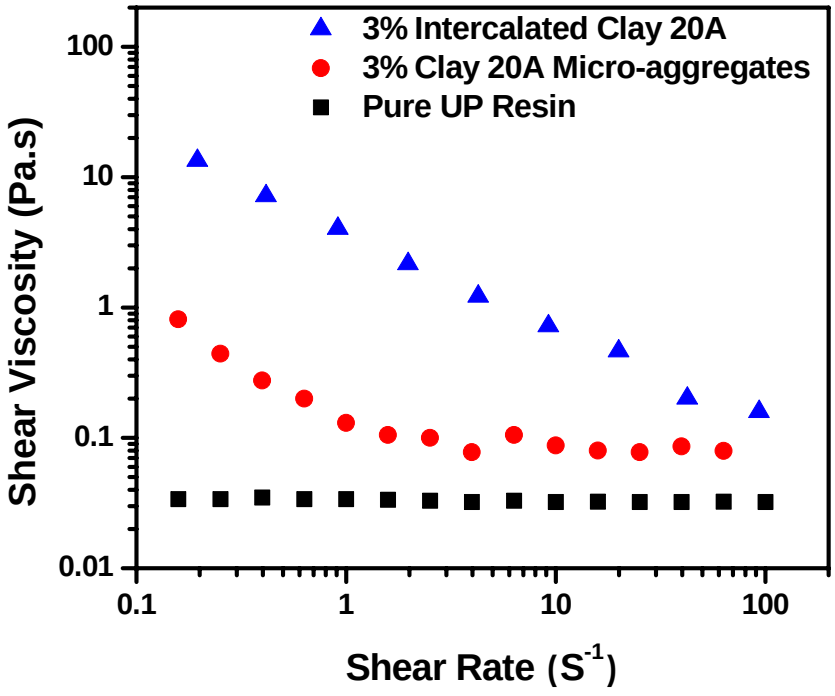

Figure 6.2 Shear viscosity of unreacted UP resins with various nanoclay contents at 25 °C.

References

1. T. G. Gutowski, *Advanced Composites Manufacturing*, John Wiley & Sons: New York (1997).

2. Y.-J. Juang, *Polymer Processing and Rheological Analysis Near the Glass Transition Temperature*, Doctorial Dissertation, The Ohio State University (2001).

3. E. T. Thostenson, C. Li, T.-W. Chou, *Compos. Sci. Technol.*, **65**, 491 (2005).

4. Z. Fan, K.-T. Hsiao, S. G. Advani, *Carbon*, **42**, 871 (2004).

BIBLIOGRAPHY

A. Allaoui, S. Bai, H.M. Cheng, J.B. Bai, *Compos. Sci. Technol.*, **62**, 1993 (2002).

A. B. Morgan, J. W. Gilman, T. Kashiwagi, C. L. Jackson, *Proc. Fire Retardant Chemicals Association*, Washington, DC, 25 (2000).

A. Benatar, T. G. Gutowski, *Polym. Eng. Sci.*, **29**, 1705 (1989)

A. C. Loos, G. S. Springer, *J. Compos. Mater.*, **13**, 131 (1979).

A. Gardziella, L. A. Pilato, A. Knop, *Phenolic Resins: Chemistry, Applications, Standardization, Safety, and Ecology*, Springer-Verlag (1999).

A. Gu, S.-W. Kuo, F.-C. Chang, *J. Appl. Polym. Sci.*, **79**, 1902 (2001).

A. Knop, W. Scheib, *Chemistry and Application of Phenolic Resins*, Springer-Verlag: Berlin/Heidelberg/New York (1979).

A. Moroni, J. Mijovic, E. M. Pearce, C. C. Foun, *J. Appl. Polym. Sci.*, **32**, 3761 (1986).

A. Nogales, G. Broza, Z. Roslaniec, K. Schulte, I. Sics, B. S. Hsiao, A. Sanz, M. C. García-Gutiérrez, D. R. Rueda, C. Domingo, T. A. Ezquerra, *Macromolecules*, **37**, 7669 (2004).

A. Oberlin, M. Endo, T. Koyama, *J. Cryst. Growth*, **32**, 335 (1976).

A. P. Shah, R. K. Gupta, *Proceedings of 2002 Annual Technical Conference – Society of Plastics Engineers*, **60**, 2270 (2002).

A. Perrella, *Reinforced Plastics*, **39**, 48 (1995).

A. S. Zerda, A. J. Lesser, *J. Polym. Sci. Part B: Polym.Phys.*, **39**, 1137 (2001).

A. Sorrentino, M. Tortora, V. Vittoria, *J. Polym. Sci. Part B: Polym.Phys.*, **44**, 265 (2006).

A. T. DiBenedetto, *J. Polym. Sci. Part B: Polym. Phys.*, **25**, 1949 (1987).

A. Thess, R. Lee, P. Nikolaev, H. Dai, P. Petit, J. Robert, C. Xu, Y. H. Lee, S. G. Kim, A. G. Rinzler, D. T. Colbert, G. E. Scuseria, D. Tomanek, J. E. Fischer, R. E. Smalley, *Science*, **273**, 483 (1996).

A. Usuki, M. Kawasumi, Y. Kojima, A. Okada, T. Kurauchi, O. Kamigaito, *J. Mater. Res.*, **8**, 1174 (1993).

A. Usuki, Y. Kojima, M. Kawasumi, A. Okada, Y. Fukushima, T. Kurauchi, O. Kamigaito, *J. Mater. Res.*, **8**, 1179 (1993).

A. Yasmin, J. Lou, I. M. Daniel, *Compos. Sci. Technol.*, **66**, 1182 (2006).

B. A. Davis, P. J. Gramman, T. A. Osswald, A. C. Rios, *Compression Molding*, Hanser Gardner Publications: Cincinnati (2003).

B. A. Higgins, W. J. Brittain, *Eur. Polym. J.*, **41**, 889 (2005).

B. C. Trivedi, B. M. Culbertson, *Maleic Anhydride*, Plenum Press: New York/London (1982).

B. K. G. Theng, *Formation and properties of clay-polymer complexes*, Elsevier: New York (1979).

B. K. G. Theng, *The Chemistry of Clay-Organic Reactions*, John Wiley & Sons: New York (1974).

B. O. Lee, W. J. Woo, M.-S. Kim, *Macromol. Mater. Eng.*, **286**, 114 (2001).

B. P. Rice, C. Chen, L. Cloos, D. Curliss, *SAMPE Journal*, **37**, 7 (2001).

B. Safadi, R. Andrews, E. A. Grulke, *J. Appl. Polym. Sci.*, **84**, 2660 (2002).

C. A. Harper, *Handbook of Plastics, Elastomers, and Composites,* 4th Edition, McGraw-Hill: New York/Chicago/San Francisco (2002).

C. A. Mitchell, J. L. Bahr, S. Arepalli, J. M. Tour, R. Krishnamoorti, *Macromolecules*, **35**, 8825 (2002).

C. Bower, R. Rosen, L. Jin, J. Han, O. Zhou, *Appl. Phys. Lett.*, **74**, 3317 (1999).

C. C. Riccardi, R. J. J. Williams, *J. Appl. Polym. Sci.*, **32**, 3445 (1986).

C. Chen, M. Khobaib, D. Curliss, *Prog. Org. Coat.*, **47**, 376 (2003).

C. Creton, L. Leibler, *J. Polym. Sci. Part B: Polym. Phys.*, **34**, 545 (1996).

C. Dispenza, J. T. Carter, P. T. McGrail, G. Spadaro, *Polym. Int.*, **48**, 1229 (1999).

C. Gay, *Integr. Comp. Biol.*, **42**, 1123 (2002).

C. Journet, W. K. Maser, P. Bernier, A. Loiseau, M. Lamy de la Chapelle, S. Lefrant, P. Deniard, R. Lee, J. E. Fischer, *Nature*, **388**, 756 (1997).

C. Lu, Y.-W. Mai, *Phys. Rev. Lett.*, **95**, 088303 (2005).

C. Park, Z. Ounaies, K. A. Watson, R. E. Crooks, J. Smith Jr., S. E. Lowther, J. W. Connell, E. J. Siochi, J. S. Harrison, T. L. St. Clair, *Chem. Phys. Lett.*, **364**, 303 (2002).

C. S. Triantafillidis, P. C. LeBaron, T. J. Pinnavaia, *Chem. Mater.*, **14**, 4088 (2002).

C. Velasco-Santos, A. L. Martinez-Hernandez, F. T. Fisher, R. Ruoff, V. M. Castano, *Chem. Mater.*, **15**, 4470 (2003).

C. Zeng, L. J. Lee, *Macromolecules*, **34**, 4098 (2001).

C. Zilg, R. Mülhaupt, J. Finter, *Macromol. Chem. Phys.*, **200**, 661 (1999).

C. Zilg, R. Thomann, J. Finter, R. Mülhaupt, *Macromol. Mater. Eng.*, **280/281**, 41 (2000).

C. Zilg, R. Thomann, R. Muelhaupt, J. Finter, *Adv. Mater.*, **11**, 49 (1999).

D. Grewell, *Proceedings of 1996 Annual Technical Conference – Society of Plastics Engineers*, **54**, (1996)

D. Hull, *An Introduction to Composite Materials*, Cambridge University Press: London/New York/New Rochelle/Melbourne/ Sydney (1981).

D. J. Greenland, *J. Colloid Sci.*, **18**, 647 (1963).

D. J. Suh, Y. T. Lim, O. O. Park, *Polymer*, **41**, 8857 (2000).

D. M. Bates, D. G. Watts, *Nonlinear Regression and Its Applications*, Wiley: New York (1988).

D. M. Lincoln, R. A. Vaia, Z. G. Wang, B. S. Hsiao, *Polymer*, **42**, 1621 (2001).

D. S. Bethune, C. H. Kiang, M. S. de Vries, G. Gorman, R. Savoy, J. Vazquez, R. Beyers, *Nature*, **363**, 605 (1993).

E. Hammel, X. Tang, M. Trampert, T. Schmitt, K. Mauthner, A. Eder, P. Potschke, *Carbon*, **42**, 1153 (2004).

E. Manias, W. J. Han, K. D. Jandt, E. J. Kramer, E. P. Giannelis, *Macromolecules*, **33**, 7955 (2000).

E. P. Giannelis, *Adv. Mater.*, **8**, 29 (1996).

E. Ruiz-Hitzky, P. Aranda, B. Casal, J. C. Galvan, *Adv. Mater.*, **7**, 180 (1995).

E. T. Thostenson, C. Li, T.-W. Chou, *Compos. Sci. Technol.*, **65**, 491 (2005).

E. W. Wong, P. E. Sheehan, C. M. Lieber, *Science*, **277**, 1971 (1997).

F. Gao, *Mater. Today*, **7**, 50 (2004).

F. H. Gojny, M. H.G. Wichmann, B. Fiedler, W. Bauhofer, K. Schulter, *Composites Part A*, **36**, 1525 (2005).

F. Hussain, M. Hojjati, M. Okamoto, R. E. Gorga, *J. Compos. Mater.*, **40**, 1511 (2006).

G. Jimenez, N. Ogata, H. Kawai, T. Ogihara, *J. Appl. Polym. Sci.*, **64**, 2211 (1997).

H. Dai, E. W. Wong, C. M. Lieber, *Science*, **272**, 523 (1996).

H. F. Mark, N. M. Bikales, C. G. Overberger, G. Menges, *Encyclopedia of Polymer Science and Engineering*, John Wiley & Sons: New York, **12** (1988).

H. Lee, K. Neville, *Handbook of Epoxy Resins*, McGraw-Hill: New York/San Francisco/Toronto/London/Sydney (1967).

H. M. Hsiao, I. M. Daniel, *Compos. Sci. Technol.*, **56**, 581 (1996).

H. Ma, J. Zeng, M. L. Realff, S. Kumar, D. A. Schiraldi, *Compos. Sci. Technol.*, **63**, 1617 (2003).

H. Ma, J. Zeng, M. L. Realff, S. Kumar, D. A. Schiraldi, *Polym. Mater. Sci. Eng.*, **86**, 411 (2002).

H. R. Dennis, D. L. Hunter, D. Chang, S. Kim, J. L. White, J. W. Cho, D. R. Paul, *Polymer*, **42**, 9513 (2001).

H. Wang, T. Zhao, L. Zhi, Y. Yan, Y. Yu, *Macromol. Rapid Commun.*, **23**, 44 (2002).

H. Y. Byun, M. H. Choi, I. J. Chung, *Chem. Mater.*, **1**3, 4221 (2001).

How ingredients influence unsaturated polyester properties, Amoco Chemicals Corporation/Bulletin IP-70 (1980).

http://www.omega.com/temperature/Z/pdf/z103.pdf, (retrieved on March 2006).

I. C. Finegan, G. G. Tibbetts, D. G. Glasgow, J.-M. Ting, M. L. Lake, *J. Mater. Sci.*, **38**, 3485 (2003).

I. Chun, D. H. Reneker, H. Fong, X. Fang, J. Deitzel, N. B. Tan, K. Kearns, *J. Adv. Mater.*, **31**, 36 (1999).

I. Mironi-Harpaz, M. Narkis, A. Siegmann, *Polym. Eng. Sci.*, **45**, 174 (2005).

I.-J. Chin, T. Thurn-Albrecht, H.-C. Kim, T. P. Russell, J. Wang, *Polymer*, **42**, 5947 (2001).

J. B. Enns, J. K. Gillham, *J. Appl. Polym. Sci.*, **28**, 2831 (1983).

J. Billingham, C. Breen, J. Yarwood, *Vibr. Spectosc.*, **14**, 19 (1997).

J. C. Kearns, R. L. Shambaugh, *J. Appl. Polym. Sci.*, **86**, 2079 (2002).

J. D. Ferry, *Viscoelastic Properties of Polymers*, 3rd edition, Wiley: New York, 487 (1980).

J. F. Monk, *Thermosetting Plastics 2nd Edition*, Addison Wesley Longman: Great Britain (1997).

J. Fröhlich, R. Thomann, O. Gryshchuk, J. Karger-Kocsis, R. Mülhaupt, *J. Appl. Polym. Sci.*, **92**, 3088 (2004).

J. H. Koo, C. U. Pittman, Jr., K. Liang, H. Cho, L. A. Pilato, Z. P. Luo, G. Pruett, P. Winzek, *Proc. SAMPE 2003 ISTC*, SAMPE, Dayton, Ohio (2003).

J. H. Koo, H. Stretz, A. Bray, J. Weispfenning, Z. P. Luo, W. Wootan, *Proc. SAMPE 2003 ISSE*, SAMPE, Long Beach, California (2003).

J. H. Koo, H. Stretz, A. Bray, W. Wootan, S. Mulich, B. Powell, J. Weispfenning, T. Grupa, *Proc. SAMPE 2002 ISSE*, SAMPE, Long Beach, California (2002).

J. H. Koo, L. A. Pilato, G. Wissler, A. Abusafieh, J. Weispfenning, *Proc. SAMPE 2005 ISSE*, SAMPE, Long Beach, California (2005).

J. H. Koo, L. A. Pilato, P. Winzek, S. Shivakumar, C. U. Pittman, Z. P. Luo, *Proc. SAMPE 2004 ISSE*, SAMPE, Long Beach, California (2004).

J. H. Koo, *Polymer Nanocomposites – Processing, Characterization, and Applications*, McGraw-Hill: New York/Chicago/San Francisco (2006).

J. J. Sahlin, N. A. Peppas, *Ind. Eng. Chem. Res.*, **30**, 211 (1991).

J. Johnston, *Adhes. Age*, **26**, 34 (1983).

J. M. Barton, *Adv. Polym. Sci.*, **72**, 111, (1985).

J. M. Brown, D. Curliss, R. A. Vaia, *Chem. Mater.*, **12**, 3376 (1998).

J. M. Kenny, A. Trivisano, *Polym. Eng. Sci.*, **31**, 1426 (1991).

J. Massam, T. J. Pinnavaia, *Mater. Res. Soc. Symp. Proc.*, **520**, 223 (1998).

J. Njuguna, K. Pielichowski, *Adv. Eng. Mater.*, **5**, 769 (2003).

J. P. Pascault, R. J. J. Williams, *J. Polym. Sci. Part B: Polym. Phys.*, **28**, 85 (1990).

J. P. Pascault, R. J. J. Williams, *Polym. Bull*., **24**, 115 (1990).

J. Sandler, A. H. Windle, P. Werner, V. Altstadt, M. V. Es, M. S. P. Shaffer, *J. Mater. Sci.*, **38**, 2135 (2003).

J. Sandler, M. S. P. Shaffer, T. Prasse, W. Bauhofer, K. Schulte, A. H. Windle, *Polymer*, **40**, 5967 (1999).

J. Shen, X. Han, L. J. Lee, *J. Cellular Plastics*, **42**, 105 (2006).

J. W. Gilman, *Appl. Clay Sci.*, **15**, 31 (1999).

J. W. Gilman, C. L. Jackson, A. B. Morgan, R. Harris, Jr., E. Manias, E. P. Giannelis, M. Wuthenow, D. Hilton, S. H. Phillips, *Chem. Mater.*, **12**, 1866 (2000).

J. W. Gilman, T. Kashiwagi, J. E. T. Brown, S. Lomakin, E. P. Giannelis, E. Manias, *Proc. SAMPE 1998 ISSE*, SAMPE, Anaheim, California, **43**, 1053 (1998).

J. W. Mintmire, B. I. Dunlap, C. T. White, *Phys. Rev. Lett.*, **68**, 631 (1992).

J. Xu, J. P. Donohoe, C. U. Pittman Jr., *Compos. Part A,* **35A**, 693 (2004).

J. Xu, *Rheology of Polymeric Suspensions: Polymer Nanocomposites and Waterborne Coatings*, Doctorial Dissertation, The Ohio State University (2005).

J. Xu, S. Chatterjee, K. W. Koelling, Y. Wang, S. E. Bechtel, *Rheol. Acta*, **44**, 537 (2005).

J. Zeng, B. Saltysiak, W. S. Johnson, D. A. Schiraldi, S. Kumar, *Compos. Part B,* **35B**, 245 (2004).

J. Zhou, J. P. Lucas, *Polymer*, **40**, 5505 (1999).

J. Zhu, A. B. Morgan, F. J. Lamelas, C. A. Wilkie, *Chem. Mater.*, **13**, 3774 (2001).

J.-K. Kim, C. Hu, R. S. C. Woo, M.-L. Sham, *Compos. Sci. Technol.*, **65**, 805 (2005).

K. A. Mauritz, R. F. Storey, S. E. George, *Macromolecules*, **23**, 441 (1990).

K. Dusek, *Epoxy resins and composites,* Springer-Verlag: Berlin/New York (1986).

K. E. Strawhecker, E. Manias, *Chem. Mater.*, **12**, 2943 (2000).

K. G. Wagner, M. Maus, A. Kornherr, G. Zifferer, *Chem. Phys. Lett.*, **406**, 90 (2005).

K. H. Chen, S. M. Yang, *J. Appl. Polym. Sci.*, **86**, 414 (2001).

K. Han, S. Jiang, C. Zhang, B. Wang, *Composites Part A*, **31**, 79 (2000).

K. L. Loewenstein, *The Manufacturing Technology of Continuous Glass Fibers*, Elsevier Scientific: New York (1973).

K. Lozano, E. V. Barrera, *J. Appl. Polym. Sci.*, **79**, 125 (2001).

K. Lozano, J. Bonilla-Rios, E. V. Barrera, *J. Appl. Polym. Sci.*, **80**: 1162 (2001).

K. Lozano, S. Yang, R. E. Jones, *Carbon*, **42**, 2329 (2004).

K. P. De Jong, J. W. Geus, *Catal. Rev. Sci. Eng.*, **42**, 481 (2000).

K. Yano, A. Usuki, A. Okada, *J. Polym. Sci. Part A: Polym. Chem.*, **35**, 2289 (1997).

K. Yano, A. Usuki, A. Okada, T. Kurauchi, O. Kamigaito, *J. Polym. Sci. Part A: Polym. Chem.*, **31**, 2493 (1993).

K. D. Potter, *Composites Part A*, **30**, 619 (1996).

K. T. Hsiao, R. Mathur, S. G. Advani, J. W. Gillespie Jr, B. K. Fink, *J. Manuf. Sci. Eng.*, **122**, 463 (2000).

K.-T. Lau, M. Lu, C.-K. Lam, H.-Y. Cheung, F.-L. Sheng, H.-L. Li, *Compos. Sci. Technol.*, **65**, 719 (2005).

L. A. Utracki, *Polym. Eng. Sci.*, **35**, 2 (1995).

L. Aktas, Y. K. Hamidi, M. C. Altan, *Plast. Rubber Compos.*, **33**, 267 (2004).

L. E. Nielsen, *J. Macromol. Sci. Revs. Macromol. Chem.*, **C3**, 69 (1969).

L. Greenspan, *J. Res. Nat. Bur. Stand.*, **81A**, 89 (1977).

L. J. Lee, *Makromol. Chem., Macromol. Symp.*, **68**, 169 (1993).

L. Liu, Z. Qi, X. Zhu, *J. Appl. Polym. Sci.*, **71**, 1133 (1999).

L. S. Schadler, S. C. Giannaris, P. M. Ajayan, *Appl. Phys. Lett.*, **73**, 3842 (1998).

L. Skartsis, J. L. Kardos, B. Khomani, *Polym. Eng. Sci.*, **32**, 221 (1992).

L. V. Radushkevich, V. M. Lukyanovich, *Zurn. Fisic. Chim.*, **26**, 88 (1952).

L. Valentini, D. Puglia, E. Frulloni, I. Armentano, J. M. Kenny, S. Santucci, *Compos. Sci. Technol.*, **64**, 23 (2004).

L. X Benedict, S. G. Louie, M. L. Cohen, *Solid State Comm.*, **100**, 177 (1996).

L. Xu, *Integrated Analysis of Liquid Composite Molding (LCM) Process*, Doctorial Dissertation, The Ohio State University (2004).

L. Xu, L. J. Lee, *Polym. Eng. Sci.*, **45**, 496 (2005).

L. Xu, L. J. Lee, *Polymer*, **45**, 7325 (2004).

L. Zhi, T. Zhao, Y. Yu, *Scripta Mater.*, **47**, 875 (2002).

M. A. Scott, K. A. Carrodo, P. K. Dutta, *Handbook of Layered Materials*, Marcel Dekker: New York (2004).

M. Alexandre, P. Dubois, *Mater. Sci. Eng. R*, **28**, 1 (2000).

M. Biron, *Thermosets and Composites – Technical Information for Plastics Users*, Elsevier: Oxford/New York/Tokyo (2004).

M. F. Yu, O. Lourie, M. J. Dyer, K. Moloni, T. F. Kelly, R. S. Ruoff, *Science*, **287**, 637 (2000).

M. G. Lu, M. J. Shim, S. W. Kim, *J. Appl. Polym. Sci.*, **81**, 2253 (2001).

M. H. Choi, I. J. Chung, *J. Appl. Polym. Sci.*, **90**, 2316 (2003).

M. J. Yacaman, M. M. Yoshida, L. Rendon, J. G. Santiesteban, *Appl. Phys. Lett.*, **62**, 202 (1993).

M. Kato, A. Usuki, A. Okada., *J. Appl. Polym. Sci.*, **66**, 1781 (1997).

M. Kawasumi, N. Hasegawa, M. Kato, A. Usuki, A. Okada., *Macromolecules*, **30**, 6333 (1997).

M. L. Costa, S. F. M. Almeida, J. M. F. Paiva, M. C. Rezende, *Mater. Res.*, **8**, 335 (2005).

M. L. Costa, S. F. M. Almeida, M. C. Rezende, *Compos. Sci. Technol.*, **61**, 2101 (2001).

M. M. J. Treacy, T. W. Ebbesen, J. M. Gilson, *Nature*, **381**, 678 (1996).

M. M. Schwartz, *Composite Materials (II)*, Prentice Hall PTR: New Jersey (1996).

M. M. Schwartz, *Composite Materials Handbook*, McGraw-Hill: New York (1991).

M. Monthioux, V. L. Kuznetsov, *Carbon*, **44**, 1621 (2006).

M. R. Garnich, G. Karami, *J. Compos. Mater.*, **39**, 1225 (2005).

M. R. Kamal, S. Sourour, *Polym. Eng. Sci.*, **13**, 59 (1973).

M. R. Piggott, *Compos. Sci. Technol.*, **53**, 201 (1995).

M. R. Vanlandingham, R. F. Eduljee, J. W. Gillespie, J. Appl. Polym. Sci., 71, 699 (1999).

M. S. P. Shaffer, A. H. Windle, *Adv. Mater.*, **11**, 937 (1999).

M. S. P. Shaffer, K. Koziol, *Chem. Commun.*, (18), 2074 (2002).

M. Tian, F. Li, L. Chen, Z. Mao, *Phys. Rev. B*, **58**, 1166 (1998).

M. Zanetti, G. Camino, R. Thomann, R. Mulhaupt, *Polymer*, **42**, 4501 (2001).

Modern Plastics Encyclopedia, McGraw-Hill: New York (1998).

N. Hamada, S. Sawada, A. Oshiyama, *Phys. Rev. Lett.*, **68**, 1579 (1992).

N. Hasegawa, M. Kawasumi, M. Kato, A. Usuki, A. Okada., *J. Appl. Polym. Sci.*, **67**, 87 (1998).

N. M. Rodriguez, *J. Mater. Res.*, **8**, 3233 (1993).

N. Ogata, G. Jimenez, H. Kawai, T. Ogihara, *J. Polym. Sci. Part B: Polym. Phys.*, **35**, 389 (1997).

N. Ogata, S. Kawakage, T. Orgihara, *J. Appl. Polym. Sci.*, **66**, 573 (1997).

N. C. Correia, F. Robitaille, A. C. Long, C. D. Rudd, P. Simacek, S. G. Advani, *J. Fluid Eng.*, **126**, 201 (2004).

O. Becker, R. Varley, G. Simon, *Polymer*, **43**, 4365 (2002).

P. B. Messersmith, E. P. Giannelis, *Chem. Mater.*, **6**, 1719 (1994).

P. B. Messersmith, E. P. Giannelis, *J. Polym. Sci. Part A: Polym. Chem.*, **33**, 1047 (1995).

P. C. LeBaron, Z. Wang, T. J. Pinnavaia, *Appl. Clay Sci.*, **15**, 11 (1999).

P. Cortes, K. Lozano, E. V. Barrera, J. Bonilla-Rios, *J. Appl. Polym. Sci.*, **89**, 2527 (2003).

P. F. Bruins, *Unsaturated Polyester Technology*, Gordon and Breach Science Publishers: New York (1976).

P. H. Nam, P. Maiti, M. Okamoto, T. Kotaka, N. Hasegawa, A. Usuki, *Polymer*, **42**, 9633 (2001).

P. H. Nam, P. Maiti, M. Okamoto, T. Kotaka, *Proc. Nanocomposites*, Chicago, Illinois, USA (2001).

P. K. Mallick, *Fiber-Reinforced Composites*, Marcel Dekker: New York/Basel (1988).

P. K. Mallick, S. Newman, *Composite Materials Technology*, Hanser Publishers: Munich/ Vienna/New York (1990).

P. Svoboda, C. Zeng, H. Wang, L. J. Lee, D. L. Tomasko, *J. Appl. Polym. Sci.*, **85**, 1562 (2002).

R. A. Vaia, B. B. Sauer, O. K. Tse, E. P. Giannelis, *J. Polym. Sci. Part B: Polym. Phys.*, **35**, 59 (1997).

R. A. Vaia, E. P. Giannelis, *Macromolecules*, **30**, 7990 (1997).

R. A. Vaia, E. P. Giannelis, *Macromolecules*, **30**, 8000 (1997).

R. A. Vaia, G. Price, P. N. Ruth, H. T. Nguyen, J. Lichtenhan, *Appl. Clay Sci.*, **15**, 67 (1999).

R. A. Vaia, K. D. Jandt, E. J. Kramer, E. P. Giannelis, *Chem. Mater.*, **8**, 2628 (1996).

R. A. Vaia, K. D. Jandt, E. J. Kramer, E. P. Giannelis, *Macromolecules*, **28**, 8080 (1995).

R. A. Vaia, S. Vasudevan, W. Krawiec, E. P. Giannelis, *Adv. Mater.*, **7**, 154 (1995).

R. A. Venditti, J. K. Gillham, *J. Appl. Polym. Sci.*, **64**, 3 (1997).

R. Burns, *Polyester Molding Compound*, Marcel Dekkar: New York (1982).

R. D. Patton, C. U. Pittman Jr., L. Wang, J. R. Hill, *Compos. Part A,* **30A**, 1081 (1999).

R. Haggenmueller, H. H. Gommans, A. G. Rinzler, J. E. Fischer, K. I. Winey, *Chem. Phys. Lett.*, **330**, 219 (2000).

R. K. Bharadwaj, *Macromolecules*, **34**, 9189 (2001).

R. Krishnamoorti, R. A. Vaia, E. P. Giannelis, *Chem. Mater.*, **8**, 1728 (1996).

R. L. McCullough, *Concepts of Fiber-Resin Composites*, Marcel Dekker: New York (1971).

R. Levy, C. W. Francis, *J. Colloid Interface Sci.*, **50**, 442 (1975).

R. P. Sheldon, *Composite Polymeric Materials*, Applied Science Publishers: London/ New York (1982).

R. Sadeghiam, S. Gangireddy, B. Minaie, K.-T. Hsiao, *Composites Part A*, **37**, 1787 (2006).

S. A. Gordeyev, F. J. Macedo, J. A. Ferreira, F. W. J. Van Hattum, C. A. Bernardo, *Physica B*, **279**, 33 (2000).

S. Al-Malaika, A. Golovoy, C. A. Wilkie, *Chemistry and technology of polymer additives*, Blackwell Science: Oxford (1999).

S. F. M. Almeida, Z. D. Nougueira Neto, *Compos. Struct.*, **28**, 139 (1994).

S. Iijima, *Nature*, **354**, 56 (1991).

S. Iijima, P.M. Ajayan, T. Ichihashi, *Phys. Rev. Lett.*, **69**, 3100 (1992).

S. Iijima, T. Ichihashi, *Nature*, **363**, 603 (1993).

S. Nazaré, B. K. Kandola, A. R. Horrocks, *Polym. Adv. Technol.*, **17**, 294 (2006).

S. R. Ghiorse, *SAMPE Quarterly*, **24**, 54 (1993).

S. S. Ray, M. Okamoto, *Prog. Polym. Sci.*, **28**, 1539 (2003).

S. Sourour, M. R. Kamal, *Thermochim. Acta*, **14**, 41 (1976).

S. G. Advani, M. S. Sozer, *Process Molding in Composites Manufacturing*, Marcel Dekker: New York, (2003).

S.-J. Wang, C.-F. Long, X.-Y. Wang, Q. Li, Z.-N. Qi, *J. Appl. Polym. Sci.*, **69**, 1557 (1998).

S. V. Lomov, I. Verpoest, *J. Reinf. Plast. Compos.*, **19**, 1329 (2000).

T. D. Fornes, D. L. Hunter, D. R. Paul, *Macromolecules*, **37**, 1793 (2004).

T. D. Fornes, P. J. Yoon, H. Keskkula, D. R. Paul, *Polymer*, **42**, 9929 (2001).

T. G. Gutowski, *Advanced Composites Manufacturing*, John Wiley & Sons: New York (1997).

T. Gibson, B. Rice, W. Ragland, *Proc. SAMPE 2005 ISSE*, SAMPE, Long Beach, California (2005).

T. Guo, B. Nikolaev, A. G. Rinzler, D. Tomanek, D. T. Colbert, R. E. Smalley, *J. Phys. Chem.*, **99**, 10694 (1995).

T. J. Pinnavaia, *Science*, **220**, 365 (1983).

T. J. Pinnavaia, T. Lan, Z. Wang, H. Shi, P. D. Kaviratna, *ACS Sym. Ser.*, **622**, 250 (1996).

T. Kashiwagi, F. Du, J. F. Douglas, K. I. Winey, R. H. Harris Jr, J. R. Shields, *Nature Mater.*, **4**, 928 (2005).

T. Lan, P. D. Kaviratna, T. J. Pinnavaia, *Chem. Mater.*, **7**, 2144 (1995).

T. Lan, T. J. Pinnavaia, *Chem. Mater.*, **6**, 2216 (1994).

T. R. Cuadrado, J. F. Macgregor, A. E. Hamielec, *J. Appl. Polym. Sci.*, **40**, 867 (1990).

T.-Y. Tsai, C.-H. Li, C.-H. Chang, W.-H. Cheng, C.-L. Hwang, R.-J. Wu, *Adv. Mater.*, **17**, 1769 (2005).

V. L. Zvetkov, *Polymer*, **43**, 1069 (2002).

V. N. Popov, *Mater. Sci. Eng. R*, **43**, 61 (2004).

W. Feng, A. Ait-Kadi, B. Riedl, *Polym. Eng. Sci.*, **42**, 1827 (2002).

W. H. Seemann, *U.S. Patent 4,902,215* (1990).

W. H. Seemann, *U.S. Patent 5,052,906* (1991).

W. H. Seemann, *U.S. Patent 5,316,462* (1994).

W. J. Mikols, J. C. Seferis, A. Apicella, L. Nicolais, *Polym. Compos.*, **3**, 118 (1982).

W. Yi, L. Lu, D.-L. Zhang, Z.-W. Pan, S.-S. Xie, *Phys. Rev. B*, **59**, R9015 (1999).

W.-B. Xu, S.-P. Bao, P.-S. He, *J. Appl. Polym. Sci.*, **84**, 842 (2001).

X. Han, C. Zeng, L. J. Lee, K. W. Koelling, D. L. Tomasko, *Polym. Eng. Sci.*, **43**, 1261 (2003).

X. Kornmann, L. A. Berglund, J. Skerte, E. P. Giannelis, *Polym. Eng. Sci.*, **38**, 1351 (1998).

X. Sun, S. Li, L.J. Lee, *Polym. Compos.*, **19**, 807 (1998).

X. Wang, Z. Qi, F. Wang, *Eng. Plast. Appl.*, **27**, 1 (1998).

X. Zhao, K. Urano, S. Ogasawara, *Colloid Polym. Sci.*, **267**, 899 (1989).

X.-A. Fu, S. Qutubuddin, *Polym. Eng. Sci.*, **44**, 345 (2004).

Y. A. Dzenis, Y. K. Wen, *Mater. Res. Soc. Symp. Proc.*, **702**, 173 (2002).

Y. Ke, C. Long, Z. Qi, *J. Appl. Polym. Sci.*, **71**, 1139 (1999).

Y. Woo, *Inelastic Analysis of the Loop Tack Test for Pressure Sensitive Adhesives*, Doctorial Dissertation, Virginia Polytechnic Institute and State University (2002).

Y. Yang, Z. Zhu, J. Yin, X. Wang, Z. Qi, *Polymer*, **40**, 4407 (1999).

Y.-F. Chen, *American Helicopter Society 58th Annual Forum Proc.*, **56**, 391 (2002).

Y.-J. Juang, *Polymer Processing and Rheological Analysis Near the Glass Transition Temperature*, Doctorial Dissertation, The Ohio State University (2001).

Y.-K. Kwon, S. Saito, D. Tomanek, *Phys. Rev. B*, **58**, R13314 (1998).

Y.-X. Pan, Z.-Z. Yu, Y.-C. Ou, G.-H. Hu, *J. Polym. Sci. Part B: Polym. Phy.*, **38**, 1626 (2000).

Z. Fan, K.-T. Hsiao, S. G. Advani, *Carbon*, **42**, 871 (2004).

Z. Jia, Z. Wang, C. Xu, J. Liang, B. Wei, D. Wu, S. Zhu, *Mater. Sci. Eng. A*, **A271**, 395 (1999).

Z. Jin, K. P. Pramoda, G. Xu, S. H. Goh, *Chem. Phys. Lett.*, **337**, 43 (2001).

Z. N. Sanjana, W. H. Schaefer, J. R. Ray, *Polym. Eng. Sci.*, **21**, 474 (1981).

Z. Rappoport, *The Chemistry of Phenols*, John Wiley & Sons: New Jersey (2003).

Z. Wang, T. J. Pinnavaia, *Chem. Mater.*, **10**, 1820 (1998).

Z. Wang, T. J. Pinnavaia, *Chem. Mater.*, **10**, 3769 (1998).

Z. Wang, T. Lan, T. J. Pinnavaia, *Chem. Mater.*, **8**, 2200 (1996).

Z. Ying, J.-H. Du, S. Bai, F. Li, C. Liu, H.-M. Cheng, *Int. J. Nanoscience*, **1**, 425 (2002).